Università degli Studi di Ferrara

DOTTORATO DI RICERCA IN
BIOCHIMICA, BIOLOGIA MOLECOLARE E BIOTECNOLOGIE

CICLO XXVIII

COORDINATORE Prof. Francesco Bernardi

Mitochondria in Coronary Reperfusion Injury and Cancer: c subunit of F_oF_1-ATP synthase and Mcl-1 as potential therapeutic targets

Settore Scientifico Disciplinare **MED/04**

Dottorando	**Tutore**
Dott. Morciano Giampaolo	Prof. Pinton Paolo

Anni 2013/2015

Index

Abstract

Mitochondria are able to decode a variety of extracellular stimuli into greatly different intracellular actions, ranging from energy production to cell death. When mitochondrial Ca^{2+} homeostasis is compromised, very different pathological conditions can occur, from cancer to ischemia/reperfusion injury, depending on the cell type and pathway involved. During my Phd I tried to shed light on both mechanisms by which mitochondria are responsible for sensitizing cancer cells to Ca^{2+}-dependent apoptotic stimuli in HeLa cells and how they can influence cell death and infarct size (IS) in a STEMI-patients cohort. In the first case, performed experiments by using splice-switching antisense oligonucleotides (ASOs) specific for Mcl-1, allowed to increase the synthesis of Mcl-1S which induced a concurrent reduction of Mcl-1L, resulting in increased sensitivity of cancer cells to apoptotic stimuli. The Mcl-1 ASOs also induced mitochondrial hyperpolarization and a consequent increase in mitochondrial Ca^{2+} accumulation. The high Mcl-1S/L ratio correlated with significant hyperfusion of the entire mitochondrial network, which occurred in a dynamin-related protein (Drp1)–dependent manner. I propose that the Mcl-1L/S balance is a novel regulatory factor controlling the mitochondrial fusion and fission machinery. In the second part, the ongoing study on c subunit of FoF1-ATP synthase (Csub) in biological samples from STEMI patients showed that circulating Csub was strongly related to infarct size, ST-segment resolution and clinical outcome. Moreover, Csub expression found in fibroblasts from skin biopsy had a good correlation with mPTP activity values and myocardial salvage index (MSI) belonging to the same STEMI-patients.

Riassunto

I mitocondri sono in grado di decodificare una grande varietà di stimoli extracellulari dando origine a innumerevoli processi fisiopatologici: dalla produzione di energia alla morte cellulare. Quando l'omeostasi mitocondriale del calcio è compromessa, possono verificarsi condizioni patologiche anche gravi come il cancro e il cosiddetto danno da riperfusione coronarica. Durante il mio dottorato, ho cercato di far luce su meccanismi attraverso i quali i mitocondri sono responsabili della sensibilizzazione di cellule tumorali (HeLa) a stimoli apoptotici calcio-dipendenti e in che modo essi possano influenzare la morte cellulare e quindi l'area infartuata finale in pazienti affetti da infarto del miocardio di tipo STEMI. Nel primo caso, sono stati condotti esperimenti utilizzando metodiche di modulazione dell'espressione genica come quella degli oligonucleotidi antisenso. Il bersaglio, la proteina Mcl-1. Il suo utilizzo ha portato ad un aumento della sintesi del prodotto terapeutico Mcl-1S e una concomitante riduzione di Mcl-1L, con conseguente aumentata sensibilità delle cellule tumorali a stimoli apoptotici. L'oligonucleotide antisenso specifico per Mcl-1 ha anche indotto iperpolarizzazione mitocondriale con un conseguente accumulo di calcio nello stesso compartimento sub-cellulare. L'elevato rapporto Mcl-1S/Mcl-1L ha comportato un significativo stato di iperfusione dell'intera rete mitocondriale, verificatosi in maniera dependente dalla proteina di fissione mitocondriale Drp1. Ho proposto il rapporto intracellulare delle due isoforme proteiche Mcl-1L/S come un nuovo fattore di regolazione delle dinamiche mitocondriali di fusione e fissione. Nella seconda parte del lavoro, lo studio in corso di sviluppo sulla subunità c dell'ATP sintasi in campioni biologici di pazienti affetti da infarto di tipo STEMI, ha suggerito che i livelli sierici circolanti della proteina sono fortemente correlati a parametri clinici quali le dimensioni dell'infarto, la risoluzione del tratto ST e lo stato clinico del paziente. Inoltre, i livelli proteici di subunità c rilevati in fibroblasti provenienti da biospia cutanea, risultano essere correlati con l'attività del mPTP e l'indice MSI del relativo paziente.

Abbreviations

2OMePS: 2′-O-methyl phosphorothioate; AEQ: aequorin; AS: alternative splicing; AIF: apoptosis-inducing factor; ANT: adenine nucleotide translocase; ASO: antisense oligonucleotide; a.u.: arbitrary units; BH: Bcl-2 homology domain; $[Ca^{2+}]_c$: cytosolic Ca^{2+} concentration; $[Ca^{2+}]_m$: mitochondrial Ca^{2+} concentration; cADPR: cyclic ADP ribose; Csub: FoF1-ATP synthase C subunit; CsA: cyclosporine A; CYCLE: CYCLosporinE A in reperfused acute myocardial infarction; cyt: cytosolic; Drp1: Dynamin related protein 1; CyP-D: cyclophilin D; ER: endoplasmic reticulum; ESE: exonic splicing enhancer; FCCP: carbonyl cyanide 4-(trifluoromethoxy) phenylhydrazone; HF: heart failure; IHD: ischemic heart disease; IMM: inner mitochondrial membrane; IP_3: inositol 1,4,5 triphosphate; IP_3R: IP_3 receptor; IRI: ischemia reperfusion injury; IS: infarct size; LVEF: left ventricle ejection fraction; m: mitochondrial; Mcl-1: myeloid cell leukemia factor 1; Mcl-1S3: Mcl-1 ASO3; MCU: mitochondrial calcium uniporter; MOMP: mitochondrial outer membrane permeabilization; mPTP: mitochondrial permeability transition pore; MVO: microvascular obstruction; NAADP: nicotinic acid-adenine dinucleotide phosphate; OMM: outer mitochondrial membrane; PCI: percutaneous coronary intervention; PEST: sequence rich in proline (P), glutamic acid (E), serine (S), and threonine (T); PLC: phospholipase C; PMCA: Plasma membrane Ca^{2+}-ATPase; RI: reperfusion injury; PiC: mitochondrial phosphate carrier; PM: plasma membrane; RISK: reperfusion injury survival kinase; RYR: ryanodine receptors; SAFE: survivor-activating factor enhancement; SERCA: Sarco-Endoplasmic Reticulum Ca^{2+}-ATPase; SR: sarcoplasmic reticulum; STEMI: ST-segment elevation myocardial infarction; TM: transmembrane domain; TMRM: tetramethylrhodamine, methyl ester; TRO40303: 3,5-Seco- 4-nor-cholestan-5-one oxime-3-ol; TSPO: mitochondrial translocator protein; Ψ_m: mitochondrial membrane potential; WMSI: wall motion score index.

1. Introduction

1.1 The universality of Ca^{2+} signaling

Calcium (Ca^{2+}) is a ubiquitous intracellular signal responsible for monitoring various cellular processes. At first sight, its action is extremely simple: cells in resting condition have a Ca^{2+} concentration ([Ca^{2+}]) of 100 nM (in the cytosol) but are activated when this level increases to 1000 nM. The curiosty that arise from it is how can this Ca^{2+} elevation regulate so many processes. The answer can be found in the versatility of the Ca^{2+} signaling mechanism in speed, amplitude and spatio-temporal point of view [1].

This scenario can be summarized into four connected events:

- Signaling is triggered by a stimulus that generates various Ca^{2+}-mobilizing signals;
- These signals activate the mechanisms that promote Ca^{2+} entry into the cytoplasm;
- Ca^{2+} works as a messenger to stimulate many sensitive processes;
- Finally, mechanisms composed of pumps and exchangers, remove Ca^{2+} from the cytoplasm and restore the steady state.

Cells generate their Ca^{2+} signals by using both internal and external sources of Ca^{2+}. The internal stores are represented by the endoplasmic reticulum (ER) or the corresponding organelle, the sarcoplasmic reticulum (SR) in muscle cells and the Golgi apparatus where the Ca^{2+} concentration reaches about 500 μM [2]. The ER is an extensive network of cisternae and microtubules, which stretches from the nuclear envelope to the cell surface in all eukaryotic cells. It acts as an indispensable source for fast physiological signaling being a dynamic calcium ions reservoir, which can be activated by both electrical and chemical cell stimulation [3]. Release from these stores is controlled by various channels, of which the inositol-1,4,5-trisphosphate receptor (InsP3R) and ryanodine receptor (RYR) families are the mainly studied. Three types of RyRs and three types of IP3Rs are currently known. Ca^{2+} itself mobilizes second messengers as Ins(1,4,5)P3 which proceeds into the cell to interact with the InsP3R and release Ca^{2+} from the ER [4]. InsP3 is produced by the enzyme phospholipase C (PLC), which becomes activated when hormones or growth factors bind to their receptors on the surface of cells. PLC actually catalyses the hydrolysis of a lipid on the inner leaflet of the plasma membrane (PM), giving rise to both InsP3 and diacylglycerol, which can also act as an intracellular messenger. Although it is produced at the PM, InsP3 is highly diffusible, and can rapidly traverse the cytoplasm of cells. However, an InsP3 molecule has a lifetime only on the order of seconds inside cells, since it is metabolized by enzymes that either add or remove a phosphate group to terminate the Ca^{2+}-releasing potential of InsP3. The rapid

metabolism of InsP3 by these enzymes means that InsP3 may have a spatially-restricted action even though it can freely diffuse inside cells. Others second messengers are Cyclic ADP ribose (cADPR), Nicotinic acid-adenine dinucleotide phosphate (NAADP).

In addition to these release channels, there is also a leak pathway, some of which seems to occur through an aqueous pore in the translocon that is responsible for threading newly synthesized proteins into the ER. Both the release and the leak of Ca^{2+} are counteracted by the Sarco-Endoplasmic Reticulum Ca^{2+}-ATPase (SERCA) that operates to maintain the internal store of Ca^{2+} [5]. SERCA mobilizes Ca^{2+} from the cytosol of the cell to the lumen of the ER at the expense of ATP hydrolysis.

So calcium entry into the cytosol depends on those channels that lead the uptake of the external ion or its release from internal stores. In the first case, exist families of Ca^{2+} entry channels defined by the way in which they are activated:

- VOLTAGE-OPERATED CHANNELS (VOCs) are opened in response to cellular depolarization to mediate selective entry of calcium. Exist different subtypes (L, T P/Q, R) with different kinetics;
- RECEPTOR-OPERATED CHANNELS (ROCs) are opened by external stimuli;
- STORE-OPERATED CHANNELS (SOCs) are activated when intracellular stores are depleted;
- SECOND MESSENGER OPERATED CHANNELS (SMOC) activated by G protein after the activation of G coupled receptors with the binding of a specific agonist.

In the second one, Ca^{2+} is derived from the internal stores using the previously mentioned channels InsP3Rs and the RYRs. They are regulated by several factors, among these Ca^{2+} itself, that regulates Ca^{2+} release by acting from either the lumenal or cytoplasmic sides of the channel. The cytosolic pathway is the most complex between the two. Upon cell stimulation, $[Ca^{2+}]_c$ changes and exhibits sophisticated spatio-temporal patterns (oscillations with different frequencies, localized increases, Ca^{2+} waves diffusing inside the cell, see the next paragraph for further considerations) caused by the activity of channels with different regulatory mechanisms, intracellular distribution and allow the cell to differentially decode Ca^{2+}-mediated signals into radically different intracellular effects [6]. Briefly, when activated, Ca^{2+}-release channels introduce the ion into the cytoplasm. However, since these channels have short open-times, they introduce only brief spikes of Ca^{2+} that form a small plume around the mouth of the channel before diffusing into the cytoplasm. Calcium signals have only a limited spatial spread (usually 1−6 μm), and its concentration declines sharply with distance from the site of origin. Regulation of cellular activities relies on close localization of the Ca^{2+} channels and their targets, thus allowing to have a highly specific effect. In addition, by this way

signals can have a rapid action with low energy cost to the cells, in contrast to massive Ca^{2+} changes.

On the other hand, since an uncontrolled rise in cytoplasmic Ca^{2+} concentration will very rapidly produce a deleterious effect in cells, it need to mantain low the ion concentration in the cytosol. So once Ca^{2+} has exerted its function, it has to be rapidly removed by the following systems, reintegrating it in the intracellular stores or outside the cell:

- Plasma membrane Ca^{2+}-ATPase (PMCA). It is one of two primary active transporters universally distributed throughout cells and is embedded in the PM and it switches from the E1 state with high affinity for the ion (exposed on the intracellular side), to the E2 state with low affinity on the extracellular side where it releases calcium;
- SERCAs that can traslocate two divalent ions by consuming one ATP molecule. Their activity is calmodulin-independent;
- Na^+/Ca^{2+} exchanger. In resting conditions the PMCA activity is sufficient to mantain the ionic equilibrium; after stimulation when Ca^{2+} has reached high concentration, the exchanger activity is required. The Na^+ gradient (directed into the cell) is used to drive Ca^{2+} out of the cell. Sodium/Calcium exchange has a higher capacity for Ca^{2+} transport than the Ca^{2+} pump and it will also operate at a much faster rate than the Ca^{2+} pump. In other words it can move more Ca^{2+} more quickly than the Ca^{2+} pump. What Na^+/Ca^{2+} exchange cannot do is to drive the Ca^{2+} concentration to the very low levels required by most cells at rest. It is mainly expressed in excitable cells;
- Ca^{2+} buffers. Cells contain large amount of Ca^{2+} binding proteins both in the cytosol and in other stores such us calreticulin, calmodulin, calretinin and parvalbumin.

1.2 Mitochondria as sensors of Ca^{2+} signaling and wizards of Ca^{2+} handling

Since Ca^{2+}-based signaling was a crucial mechanism through which extracellular messengers modify the activity of target cells, eukaryotic cells have evolved a complex Ca^{2+} toolkit that encompasses proteins capable of detecting changes in Ca^{2+} levels, complex homeostatic mechanisms based on the intracellular $[Ca^{2+}]$ changes and generation of outputs as diverse as proliferation or death [7]. A central role in this intriguing signaling is represented by the mitochondrion (Figure 1). Mitochondria are an autonomous and dynamic cellular organelles that are intimately involved in orchestrating a wide range of cellular activities among these the Ca^{2+} homeostasis. A healthy population of this essential organelle during the lifetime of the organism is of particular importance, indeed they are required for fertility and for early

development. Moreover they have a pivotal role in regulating cellular metabolism, hormonal signaling and finally apoptosis cell death [8].

Mitochondria are known to be endowed with the capacity of accumulating Ca^{2+}. While the mitochondrial outer membrane (OMM) is believed to be freely permeable to ions and molecules up to 1000 Da, the inner membrane (IMM) is tightly sealed to all ions, but for the presence of specific transporters. The uptake of Ca^{2+} into the mitochondrial matrix under physiological conditions does not depend on ATP hydrolysis, but rather on the presence of a so called mitochondrial Ca^{2+} uniporter (MCU) and the driving force is provided by the negative membrane potential generated by the respiratory chain [9]. When the respiratory chain is inhibited, the membrane potential can be maintained by a reversal of the H^+ ATPase. If mitochondria accumulate large amounts of Ca^{2+} they store it in the matrix as insoluble phosphate salts and the release occurs very slowly. If accumulation is limited, the release is faster [10]. Under steady state conditions the Ca^{2+} concentration in the matrix ($[Ca^{2+}]_m$) depends on its uptake via MCU and release via the antiporters, referred as the mitochondrial Ca^{2+} cycle. To export Ca^{2+} from the mitochondrial matrix, mitochondria release Ca^{2+} via an antiporter by exchanging Ca^{2+} with Na^+ (in excitable tissues, such as the brain and heart as mentioned before) or H^+ (in the liver and many other tissues) [11], with what is considered an electroneutral stoichiometry for Ca^{2+} efflux (Ca^{2+}–$2H^+$ antiport). However, the identification of leucine zipper-EF-hand containing transmembrane protein 1 (Letm1) as the Ca^{2+}–H^+ antiporter suggests a different stoichiometry [12]. Letm1 seems to act as a Ca^{2+} extrusion mechanism when the $[Ca^{2+}]$ is elevated in the matrix, whereas it may contribute to non-linear Ca^{2+} uptake at low mitochondrial Ca^{2+} levels. Letm1 has also been proposed to act as a mitochondrial K^+–H^+ exchanger [13]. Consequently, the role of Letm1 awaits further confirmation.

At the resting $[Ca^{2+}]_c$ values, the uptake rate is very slow and the consumption of energy reduced to a minimum. The low Ca^{2+} affinity of MCU and the existence of electroneutral exchangers are essential to prevent the attainment of electrochemical equilibrium. The $[Ca^{2+}]_c$ increases induced by physiological stimuli hardly ever exceed 1–2 µM, values at which the uniporter is still very inefficient at transporting Ca^{2+}. Even if indirect evidence exist, especially based on the use of mitochondrial inhibitors and suggesting that a significant mitochondrial Ca^{2+} accumulation occurs also under physiological conditions, these observations failed to change the general view that mitochondria participate in calcium handling under pathological conditions.

Surprisingly, selective monitoring of $[Ca^{2+}]_m$ revealed that the $[Ca^{2+}]_c$ increases triggered by agonist-dependent Ins$P$3 generation were paralleled by rapid, transient elevations of $[Ca^{2+}]_m$,

the amplitude of which largely exceeded the $[Ca^{2+}]_c$ rises. This could be explained by the fact that mitochondria are somehow located close to InsP3 gated channels and transiently exposed to local high $[Ca^{2+}]$ microdomains induced by release from the ER, rather than the bulk changes in $[Ca^{2+}]_c$ [14,15]. Given that in the ER the $[Ca^{2+}]$ is around 500 µM, it is likely that in the close proximity of those channels the local Ca^{2+} concentration would be much higher than in the rest of the cytoplasm. It has been calculated that the $[Ca^{2+}]$ in the localized hot spots should be around 20–30 µM [16]. In fact the local high $[Ca^{2+}]$ at the mouth of the channels is rapidly dissipated by diffusion that thus serves the function of an automatic shut off mechanism for the rapid mitochondrial Ca^{2+} uptake. Using an ultra-fast image acquisition system and high resolution 3D reconstruction algorithms, close appositions between the two organelles (less than 100 nm distance) could be directly visualized in intact living cells expressing organelle-targeted mutants of GFP [10]. The contacts between the ER and mitochondria may imply specific interactions between the two membranes (Figure 1). Cisternae of ER particularly enriched in InsP3 receptors are very often apposed to the mitochondria. Conversely, in cells characterized by a relative sparse ER with very few contacts with mitochondria the uptake of Ca^{2+} in the latter organelle is slow and limited, as expected of mitochondria exposed to the bulk increases in $[Ca^{2+}]_c$. The emerging scenario is that of two reticular organelles, the ER and the mitochondria, closely connected at some selective sites. The release of Ca^{2+} from the ER occurs at clusters of InsP3 receptors facing a mitochondrial loop located at close distance. The rapid Ca^{2+} uptake in the latter thus occurs at discrete sites, and Ca^{2+} then diffuses within the mitochondrial matrix intralumenally to induce the activation of Ca^{2+} dependent enzymes therein localized.

Rapid accumulation of Ca^{2+} is not the only feature of the system. Indeed, $[Ca^{2+}]_m$ after the agonist-dependent increase, rapidly returns towards basal level, also if a sustained cytosolic plateau is maintained. This decrease is due on the one hand to the dramatic drop in the uptake rate (because of the dissipation of the high Ca^{2+} microdomains), on the other to Ca^{2+} extrusion via the antiporters, activated by the rise in $[Ca^{2+}]_m$. Indeed, specific inhibitors of mitochondrial antiporters drastically delay the return of $[Ca^{2+}]_m$ to basal.
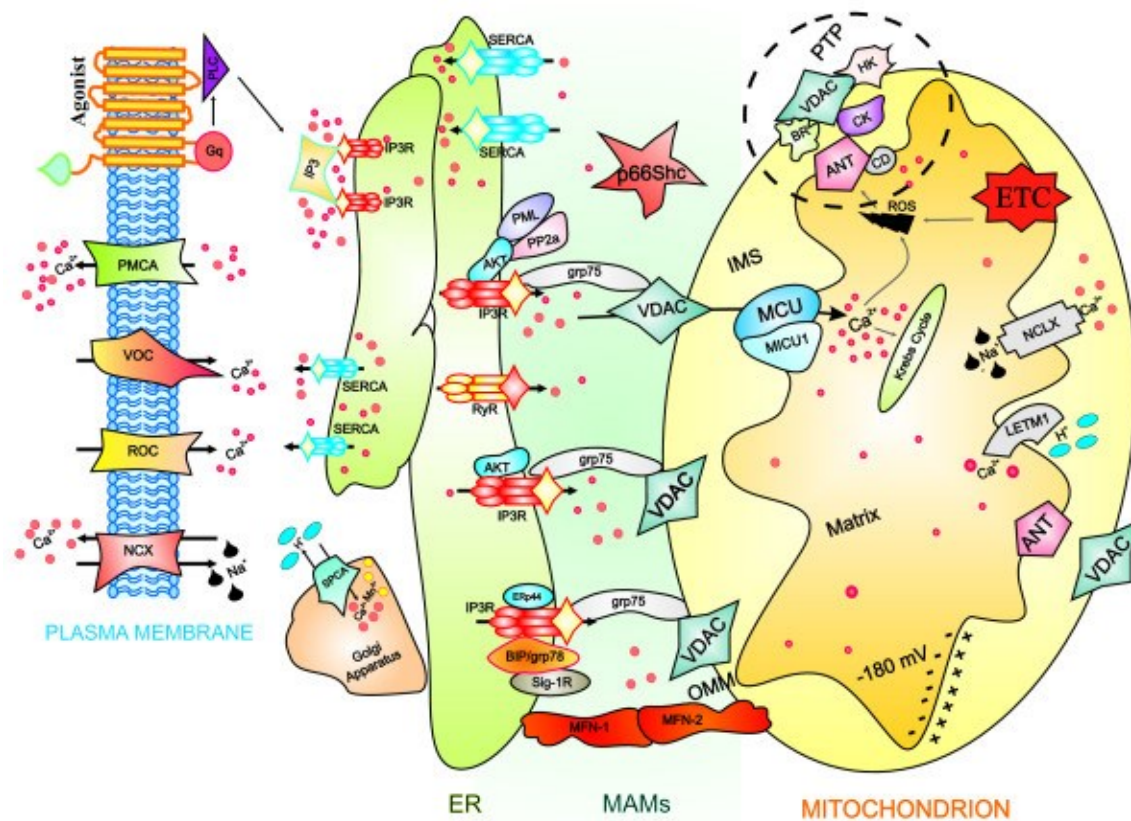
Figure 1 – Representation of intracellular Ca^{2+} dynamics, especially the ER-mitochondria Ca^{2+} cross-talk [17].
A series of protein localized between ER and mitochondria regulate Ca^{2+} release from the ER and an efficient mitochondrial Ca^{2+} uptake, resulting in different functional outcomes. Cells generate Ca^{2+} signal through two mechanism that use internal and external sources of Ca^{2+}. Calcium enters into the cell through channels and pumps situated on the PM; these are gated by VOCs or ROCs. A series of stimuli that act on cell surface receptors triggers the activation of PLC that catalyses the hydrolysis of phosphatidylinositol 4,5-biphosphate to IP3 and DAG. The binding of IP3 to its receptor IP3R stimulates ER Ca^{2+} release and consequently the transfer of Ca^{2+} (red dots) from ER to mitochondria. Mitochondrial surface directly interacts with the ER through contact sites defining hotspot Ca^{2+} signalling units. Mitochondrial Ca^{2+} import occurs through the MCU and LETM1; conversely, NCLX, mitochondrial Na^+/Ca^{2+} exchanger, together with the PTP, export Ca^{2+} from the matrix. Ca^{2+} levels return to resting conditions through a series of channels and pumps: PMCA, NCX and SERCA.

1.2.1 Physiological implications

Based on the Ca^{2+}-sensitivity of the matrix dehydrogenases, the first consequence of the $[Ca^{2+}]_m$ rise is the activation of mitochondrial metabolism. It has long-term been demonstrated the correlation between $[Ca^{2+}]_m$ increases and enzyme activation, increases in NADH levels, mitochondrial ATP production and O_2 consumption. It is also known that during Ca^{2+} accumulation the mitochondrial membrane potential drops and ATP synthesis is suppressed. This happens only for a very short period of time. Recent data demonstrate that mitochondrial Ca^{2+} uptake not only serves the function of controlling organelle function, but plays an unexpected role in the control of important, often apparently unrelated events which occur in the cytosol of a living cell.

The first of these events is the complex spatio-temporal patterning of Ca^{2+} signals. Jouaville *et al*. demonstrated that mitochondrial Ca^{2+} uptake can modulate the shape and velocity of Ins*P*3 induced Ca^{2+} waves [18]. The interpretation of the authors, that is consistent with the microdomain model described above, was that the local Ca^{2+} buffering effect of mitochondria can modulate the kinetics of Ins*P*3 channel gating with ensuing modification of the cytoplasmic Ca^{2+} waves. Recently, the speed and extent of Ca^{2+} release from the ER has been shown to be modulated by the local Ca^{2+} buffering of mitochondria also in mammalian cells. The role of mitochondria in modulating the activity of Ca^{2+} channels is not limited, however, to the ER. Evidence has recently been provided for a role of mitochondria in modulating the activity of plasma membrane channels, such as store-operated Ca^{2+} channels.

For pathological implications and the description of other involved channels, please refer to section 2.

2. Mitochondrial dysfunctions

2.1 Cancer

Mitochondria malfunctioning was claimed by Otto Warburg to explain his observation that tumor cells undergo increased aerobic glycolysis (Warburg effect) compared to normal cells [19]. Mutations in key Krebs cycle enzymes demonstrated that mitochondrial metabolism is defective in at least a few human cancers [20]. Increased glucose metabolism and the Warburg effect promote tumor cell survival through redox regulation of cytochrome *c* and inhibition of apoptosis [21]. This may explain the Warburg effect and tumor growth without necessarily invoking defective mitochondria. While mitochondrial dysfunction does not necessarily explain the Warburg effect, there is significant evidence that tumors do indeed accumulate defective mitochondria [22,23]. These mitochondrial-dependent bugs are not only represented by genome mutations [24] and linked to both increased primary tumor growth and metastasis, but also by increased ROS levels attributed to inefficiencies in electron transport at the respiratory chain, increased metabolic demand, reduced ROS scavenging, oncogene-induced replicative stress [25,26] and altered mitochondrial dynamics [27].

2.1.1 Mitochondrial dynamics

Mitochondria are highly dynamic organelles responding to cellular stress through changes in overall mass, interconnections and sub-cellular localization [27-29]. The extent to which mitochondria are interconnected to each other as a single continuous mitochondrial network is determined by fusion process while conversely, mitochondrial fission results in fragmented mitochondria shaped point (Figure 2). Mitochondria are also dynamic in terms of where they are located in the cell with increased perinuclear localization under hypoxia compared to normoxia [30], at axonal termini in neurons [31], and movement along microtubules toward lysosomes under conditions that promote mitophagy [32]. All these characteristics are deregulated in cancer even though less frequently studied and reviewed than Warburg, ROS, and mitochondrial genome DNA mutations.

Mitochondrial fusion is promoted by interactions of the Mitofusin 1 (Mfn1) and Mitofusin 2 (Mfn2) dynamin-related GTPases at the OMM of adjacent mitochondria and by Opa1, also a dynamin-related GTPase, at the IMM [33]. Inhibition or downregulation of any one of these proteins promotes mitochondrial fragmentation and is associated with diseases. Mitochondrial fission requires the recruitment of a different dynamin-related GTPase such as Drp1 to the OMM where it forms ring-like oligomers that cut mitochondria into smaller fragments [34,35].

Translocation of cytosolic Drp1 to the mitochondria during fission is a regulated process involving post-translational modification of the protein [36] and its interaction with putative receptors at the OMM such as Mff, Fis1, MiD49, MiD51, and possibly other proteins with which Drp1 interacts [27]. Beyond the actual mode of mitochondrial fission and fusion, the signaling pathways that regulate these processes are attracting the attention of many scientists since they appear to be disrupted in cancer. These signaling pathways respond to specific stresses and serve to coordinate mitochondrial dynamics with other aspects of cellular physiology. In the original article presented in the chapter 3, will be shown how a protein involved in mitochondrial dynamics also participates in mechanisms of cell death together to a Bcl-2 family protein: Mcl-1. Indeed, both mitochondrial fission and fusion proteins appear to modulate apoptosis through activities that are distinct from their roles in mitochondrial dynamics but which involve members of the Bcl-2 family. Members of the Bcl-2 family of cell death regulators are extensively characterized for their key role in regulating apoptosis [29,37] but they also have an emerging role in mitochondrial dynamics [27,38,39]. It has been demonstrated that Bak/Bax double knockout cells are resistant to apoptosis so these proteins are essential for cell death [40,41]. Bak and Bax once activated by pro-apoptotic signals undergo oligomerization to form a channel in the OMM through which cytochrome *c* is released resulting in the formation of the apoptosome and activation of caspases [42]. A link with mitochondrial dynamics was established when apoptosis-resistant Bax/Bak null cells exhibited extensive mitochondrial fragmentation rescued by over-expression of Bak in the absence of apoptotic signaling suggesting that Bak and Bax can promote mitochondrial fusion [38]. Indeed, Bax is able to interact with Mfn2 to promote its GTPase activity while both Bak and Bax can interact with Mfn1 [43]. On the other hand, the anti-apoptotic Bcl-XL has been shown to promote mitochondrial fission through interactions with Drp1 that promote synapse formation in neurons [44]. More recently, Mcl-1 has been implicated in modulating mitochondrial dynamics through an amino-terminal truncated form that localizes to the mitochondrial matrix, in contrast to full-length Mcl-1 at the OMM [45]. Thus there is regulation of the apoptotic activity of Bcl-2 related proteins by fusion/fission proteins and conversely regulation of fission/fusion protein activity by Bcl-2 related proteins.

The dark side of this topic is if the altered mitochondrial dynamics contributes to the oncogenic activity of key Bcl-2 family members, such as Bcl-2, Bcl-XL and Mcl-1 that are both over-expressed in certain human tumors.
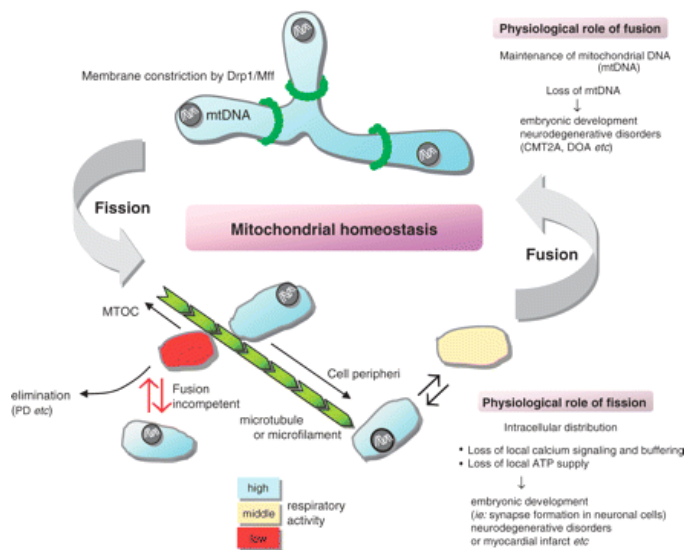
Figure 2 – Overview of mitochondrial dynamics and homeostasis [33].
Mitochondrial morphology is maintained by fusion and fission. Excessive mitochondrial fission often causes the generation of depolarized (respiratory inactive) mitochondria. Although the mildly depolarized mitochondrial fragments fuse back with the active mitochondria and recover the respiratory activity, severely depolarized mitochondrial fragments cannot fuse back with the reticulum. Therefore, mitochondrial fusion prevents the loss of mtDNA nucleoids and contributes to maintain mitochondrial respiratory activity. Dysfunctional mitochondria return to the cell soma and are eliminated by the autophagy system, named mitophagy. Disruption of the mitochondrial dynamics or mitochondrial quality control system leads to the accumulation of dysfunctional mitochondria and causes a collapse of the cellular environment followed by cell death.

2.2 Myocardial Infarction

Mitochondria play a pivotal role in both the life and death of cardiac myocytes. In healthy cells, their primary function is to meet the high energy demand of the beating heart by providing ATP through oxidative phosphorylation. Mitochondria occupy a large portion of each myocyte and are located between the myofibrils and just below the sarcolemma. The strategic positioning and abundance of mitochondria ensure a highly efficient localized ATP delivery system to support contraction, metabolism, and ion homeostasis. However, mitochondria are also important regulators of cell death. The switch to a cell death program can be mediated by opening of the mitochondrial permeability transition pore (mPTP) in the IMM, causing collapse of the membrane potential and swelling of the mitochondria, often culminating in necrotic cell death, or permeabilization of the OMM with release of proapoptotic proteins such as cytochrome c, Smac/Diablo, and apoptosis-inducing factor (AIF) to activate an energy-dependent apoptosis.

Both processes have been implicated in loss of myocardial cells in pathologies such as ischemia/reperfusion (I/R), cardiomyopathy, and congestive heart failure.

13

2.2.1 Necrosis and apoptosis, mitochondria and the mPTP

Mitochondria are important dynamic organelles that function as the gatekeepers of life and death. In cardiac myocytes, mitochondria occupy up to 30% of the total volume, as these cells have a large energy requirement in the form of ATP via oxidative phosphorylation (OXPHOS) to maintain their functional integrity [46]. Mitochondria, the powerhouses of the cell, are sensitive to alterations in the cellular environment and can quickly switch from a sustainer of cell survival to a promoter of cell death via the necrotic or apoptotic pathways [47]. Therefore, it is not surprising that mitochondrial dysfunction is associated with the loss of myocytes and the subsequent development of HF. Necrosis and apoptosis differentially contribute to MI. Both processes are regulated by many of the same biochemical intermediates, including alterations in the levels of high-energy phosphates, intracellular Ca^{2+} and ROS.

2.2.1.1 Necrosis

Necrosis is generally considered to be initiated by non-cellular mechanisms, such as ischemia, trauma and thrombosis, which ultimately lead to irreversible cell death (Fig. 3). This cell death is characterized by cell swelling, depletion of high-energy stores and disruption of the cellular membrane, which involves alterations in fluid levels, alterations in electrolyte levels, loss of potassium ions (K^+), loss of Mg^{2+} ions and the intracellular accumulation of water, sodium ions (Na^+), chloride ions (Cl^-), protons (H^+) and Ca^{2+} ions [48,49]. During ischemia, anaerobic metabolism is predominant due to energy failure, thus producing a decrease in intracellular pH. To buffer this accumulation of hydrogen ions, the Na^+/H^+ exchanger excretes excess hydrogen ions, which produces a large influx of Na^+ [50]. Indeed, ischemia depletes cellular ATP, which inactivates ATPases (e.g., Na^+/K^+ ATPase), reduces active Ca^{2+} efflux, and limits the reuptake of Ca^{2+} by the SR, thereby producing intracellular Ca^{2+} overload. In the heart, these cellular changes are accompanied by the activation of intracellular proteases (e.g., calpains) that damage myofibrils and induce hypercontracture and contracture band necrosis. This type of cell death is also referred to as passive necrosis.

In the 1980s, Crompton et al. were the first to propose a pivotal role for MPT in cardiac ischemia reperfusion injury (IRI) [51]; as a working hypothesis, they proposed that the changes in Ca^{2+}, P_i and adenine nucleotide levels during ischemia trigger mPTP opening [51,52]. Griffiths and Halestrap subsequently demonstrated that MPT occurs upon reperfusion of the ischemic heart. In 1995, using the mitochondrial "Hot DOG" entrapment technique, they showed that some mitochondria can undergo mPTP opening and closure in the ischemic-reperfused heart [53]. Their data confirm that pore opening occurs during reperfusion of the heart after ischemia, but not in the ischemic priming period. Their experimental procedures tell us that the extent of

DOG uptake increases until the period of ischemia that precedes reperfusion increases to an empirical maximum of 30–40 min [53]. Opening of the mPTP facilitates the free passage of protons across the IMM, leading to a dissipation of the mitochondrial membrane potential and pH gradient, which comprise the proton motive force. Not only does this process prevent ATP generation, but reversal of the ATPase also occurs, thus causing the breakdown of cytosolic ATP that is generated via glycolysis. Energy metabolism is further impaired, thereby resulting in a continuous cycle of increasing Ca^{2+} deregulation and mPTP opening. These changes activate phospholipases, nucleases and proteases. The importance of the mPTP in the necrotic death of cardiomyocytes under such conditions was initially detected in experiments using mPTP inhibitors, such as cyclosporin A (CsA) [48,52]. Recently, further evidence for a critical role of mPTP opening in necrotic cell death has been provided by the use of mice in which the target of CsA, mitochondrial cyclophilin D (mtCypD), was knocked out [49,50]. These animals exhibit substantial protection from IRI-induced damage (infarct size) to the heart. In addition, using these mice, it has been shown that cardiac failure associated with chronic Ca^{2+} overload involves the mPTP-dependent death of cardiomyocytes [54]. Finally, in 2014, a study of sixty-one patients that was directed by Ovize showed that cyclosporine administration at the time of reperfusion protects against reperfusion injury in patients undergoing aortic valve surgery by reducing the levels of cardiac troponin I in the cyclosporine group compared with the control group [55]. Most of these concepts have been widely reviewed [56,57]. Today, MI, bypass surgery and organ transplantation provide dramatic examples of this mechanism of cardiac failure. This step in cell death involves the mPTP and a complex network of cellular signals. Because the severity of the insult in most infarction cases in the heart is heterogeneous, there is often no clear boundary between apoptosis and necrosis. However, if the stress experienced by the cell is a severe insult, the extent of mPTP opening is catastrophic, and necrotic cell death is inevitable, as occurs in the core of vessel obstruction. In this region, most mitochondria undergo massive matrix swelling and OMM rupture.

2.2.1.2 Apoptosis
In addition, reperfusion can lead to an enhancement in apoptosis [54], which is an evolutionarily conserved mode of cell death that can be initiated via two different pathways in mammals: the death receptor pathway (extrinsic apoptotic pathway) and the mitochondrial pathway (intrinsic apoptotic pathway). Furthermore, the apoptosis pathway that is activated depends on the nature of the death signal (Figure 3). Apoptosis, similarly to necrosis, can be induced by mPTP opening. For apoptosis, the stress is often a milder insult than that for necrosis, which could explain the apoptotic ring around the necrotic core of a coronary infarct [58]. mPTP opening might be transient or maintained in some mitochondria undergoing matrix swelling,

where all small molecular mass solutes equilibrate across the IMM, and proteins remain at a high concentration in the matrix and exert colloidal osmotic pressure that unfolds the IMM cristae and induces OMM rupture [59,60]. Mitochondrial membrane permeabilization does not play a crucial role in the extrinsic pathway. Instead, it is most likely activated in response to inflammation, which is required for healing and scar formation in the infarct. PM receptors are activated by pro-inflammatory ligands, including Fas, TNF-α and TNF-related apoptosis-inducing ligand (TRAIL).

Fas and Fas ligands are expressed in the heart and enhanced expression of Fas is associated with increased apoptosis in experimental models of MI [61,62]. Simulated IRI in a cell culture model increases the sensitivity of myocytes to Fas-mediated death. Therefore, it has been suggested that IRI might down-regulate inhibitors of the Fas pathway, such as cellular FLICE-inhibitory protein (cFLIP). cFLIP is highly expressed in the heart under normal physiological conditions but is degraded after IRI. Thus, the loss of cFLIP expression may be important for enhancing the sensitivity of cardiomyocytes to apoptosis after IRI. These results suggest that the Fas-mediated cell death pathway exists in cardiomyocytes but that under normal conditions, this pathway is down-regulated by inhibitors. However, after stress, such as ischemia, cFLIP becomes inactivated, thus rendering the cells susceptible to death via the Fas pathway. Recent studies have revealed that TNF plays a role in the progression of myocardial disease. Increased TNF-α and TNF receptor 1 (TNFR1) expression levels are associated with HF [63]. As TNF-α induces apoptosis in cardiomyocytes [64], it is thought that at least part of its pathogenic effect in the heart is due to its induction of cell death.

In contrast, there is also evidence supporting a prosurvival role of TNF in the heart, including the involvement of TNF in the regulation of adaptive responses to biomechanical stress. Examples of these adaptive responses include the induction of cellular hypertrophy in response to pressure overload and the modulation of contractile function following ischemia. The role of inflammation in MI as a target for cardioprotection has not been completely addressed. A small number of studies have investigated the effects of reducing the inflammatory response to myocardial reperfusion injury. Experimental animal studies have reported significant reductions in MI size with several interventions administered at the time of myocardial reperfusion, such as the inhibition of neutrophil aggregation and attenuation of leukocyte infiltration into the infarcted myocardium [65,66]. On the other hand, more recently, clinical studies targeting the inflammatory components of MI have failed to show a significant improvement in reperfused–STEMI patients [67]. Further studies on the role of inflammation in MI are required.

Ca^{2+} is a critical sensitizing signal for the pro-apoptotic transition of mitochondria that plays a key role in the regulation of cell death [68]. Mitochondrial Ca^{2+} overload is a pro-apoptotic inducer of mitochondrial swelling, and OMM perturbation or OMM rupture leads to mitochondrial apoptotic factor (cytochrome c, Smac/DIABLO, AIF and Omi/HtrA2) release into the cytosol [69] (Figure 3). Cytochrome c-mediated apoptosis is important in cardiomyocytes. Serum and glucose deprivation induce cytochrome c release in vitro, thereby resulting in the activation of caspase-9, caspase-3 and apoptosis [70]. As serum and glucose deprivation are components of ischemia in vivo, these results indicate that this pathway may be involved in heart disease-related cell death.

Most reperfusion-induced apoptotic death of cardiomyocytes occurs during the initial minutes of reperfusion due to increased ROS production, intracellular Ca^{2+} overload and mPTP opening [54]. The role of apoptosis in reperfusion injury has recently been addressed using rat and rabbit animal models in which reperfusion accelerates the occurrence of apoptosis in cardiomyocytes [54,71]. In the infarcted region of the ventricular wall, myocytes containing DNA strand breaks are detected 2 hours after coronary artery occlusion, and approximately 2.7 million myocytes are apoptotic at this time point. Moreover, 6.6 million cells are apoptotic at 4.5 hours, indicating that there is a 2.4-fold increase in the absolute number of apoptotic myocytes in the left ventricular free wall from 2 to 4.5 hours after coronary artery occlusion. The magnitude of apoptosis progressively decreases at later time intervals. Necrosis of myocytes also appears 2 hours after coronary artery occlusion and continuously increases until one day following coronary artery ligation. These findings demonstrate that myocyte apoptosis and necrosis are independent variables contributing to IS, although apoptosis accounts for 86% of the total loss of myocytes, and necrosis accounts for only 14% of the total loss [71]. In contrast, findings from other laboratories that support these experimental data indicate that MI results from a significant increase in necrosis rather than apoptosis, where pro-apoptotic factors are evident only early during ischemia but do not significantly contribute to IS [72,73]. Others have found that apoptosis and necrosis occurred simultaneously in all instances in hearts from cases of fatal MI [74]. One likely hypothesis that could explain the coexistence of apoptosis and necrosis after IRI is that damage produced by ischemia is capable of initiating apoptosis, but if ischemia is prolonged, necrosis ensues.
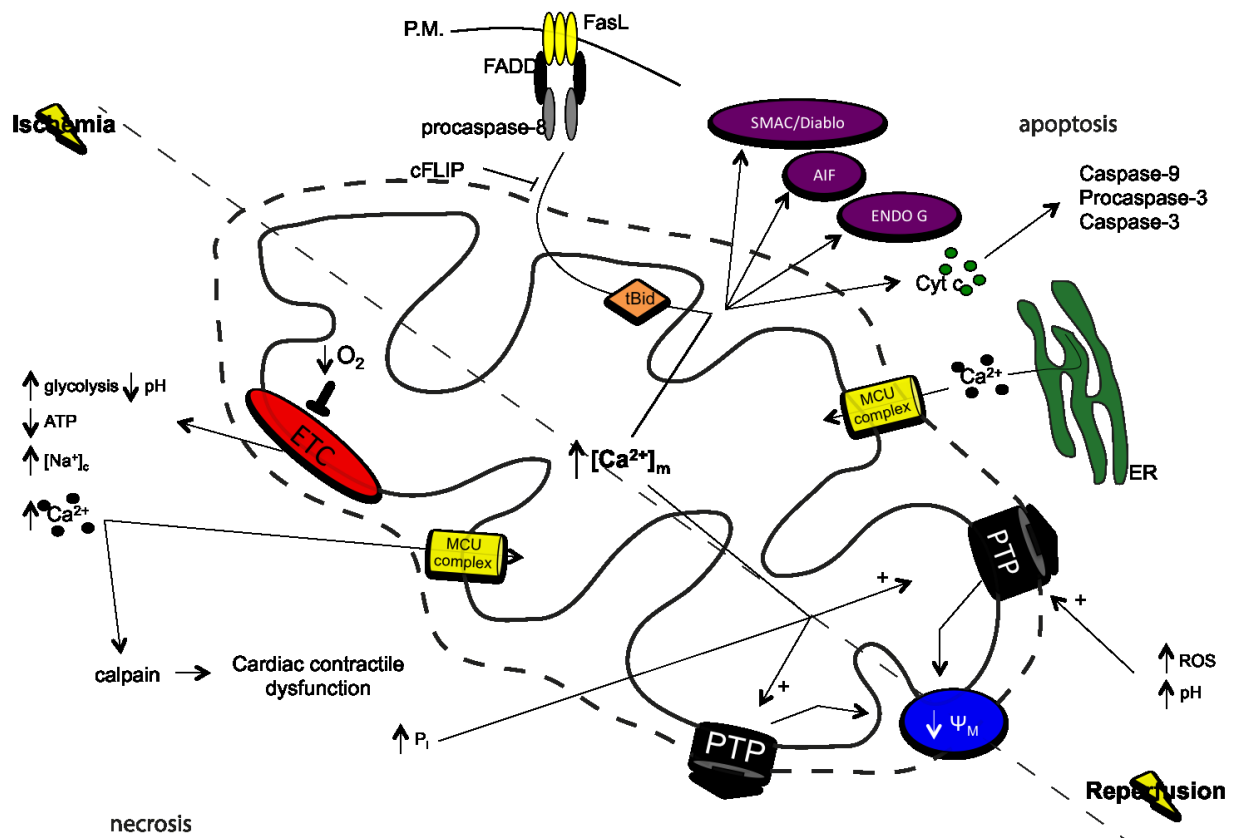
Figure 3 – Mitochondrial involvement in cell death during ischemia/reperfusion injury in MI.
Ischemia is on the left side; reperfusion is on the right side. The dashed line that divides the mitochondrion reveals that both events share similar pathways that lead to different pathological effects. Ischemia: insufficient blood supply to the heart. Ischemia leads to alterations in the mitochondrial electron transport chain (ETC) complexes, anaerobic metabolism prevails as a consequence of energy failure, lactic acid accumulates, and cellular pH decreases. This accumulation of hydrogen ions causes alterations in intracellular calcium homeostasis that lead to cell death. In the heart, these cellular changes are accompanied by activation of intracellular proteases, which damage myofibrils and result in cardiac contractile dysfunction. Reperfusion: restoring blood flow. Depending on its severity, reperfusion is characterized by the increased formation of ROS, increased pH, decreased ATP production, and cell death. Some of the main pathways that occur, such as intrinsic and extrinsic apoptosis, permeability transition pore opening and lastly dissipation of the mitochondrial potential and membrane swelling, are represented in the figure.

2.2.2 Role of ROS and Ca^{2+} in IRI-induced damage

A wide range of mitochondrial ROS-induced damage has been described, including protein carbonylation, lipid peroxidation and mitochondrial DNA damage [75]. These modifications are important factors in the progression of myocardial IRI-induced damage. The reintroduction of abundant oxygen at the onset of reperfusion evokes a burst of toxic oxygen derivatives within the first few minutes of reperfusion. Moreover, oxidative stress also reduces the bioavailability of nitric oxide (NO, a vasodilator) during reperfusion [76]. Cytosolic Ca^{2+} accumulation plays major roles in the initiation of programmed cell death during acute MI. A prolonged increase in cytosolic Ca^{2+} induces mitochondrial Ca^{2+} overload, which leads to mPTP opening and the activation of Ca^{2+}-dependent proteases [77]. Increased cytosolic Ca^{2+} plays a pivotal role in activating the serine threonine Ca^{2+}/calmodulin-regulated phosphatase,

calcineurin. This phosphatase is a critical transducer of Ca^{2+} signals in most cell types, particularly in the heart, due to its specific responsiveness to sustained, low-frequency Ca^{2+} signals [78].

3. Mcl-1 involvement in mitochondrial dynamics is associated with apoptotic cell death

3.1 Introduction

More than 20 years ago, the identification and cloning of Bcl-2 marked the discovery of an entirely new class of genes with crucial roles in cancer [79]. The Bcl-2 family of proteins includes a great variety of members with proapoptotic (Bax, Bak, Bok, Bid, Bim, Noxa, Puma, myeloid cell leukemia factor 1 [Mcl-1] variant S) or antiapoptotic (B-cell lymphoma-2 [Bcl-2], Bcl-xL, Bcl-w, Mcl-1L) functions. They form homodimers and heterodimers through Bcl-2 homology (BH) domains. The relationships and relative ratios among the Bcl-2 family proteins are critical in cell fate determination [80].

Mcl-1 was discovered based on its increased expression during cell commitment toward differentiation in a human myeloid leukemia cell line [81]. In humans, the Mcl-1 pre-mRNA undergoes alternative splicing (AS) to produce two isoforms with opposite functions. The first isoform, Mcl-1L, is primarily anchored by its transmembrane (TM) domain [82] to the OMM, where it inhibits the release of cytochrome c [83]. Mcl-1L consists of 350 amino acids (aa) encoded by three exons. Bcl-2 and Mcl-1 share high similarity, especially in their carboxyl termini (C-ter), which terminate in a hydrophobic domain with membrane-spanning potential [81]. The similarities between these two genes are highly significant, although Mcl-1L and Bcl-2 are clearly distinguishable, except for two nearly identical stretches (7 aa each). The amino terminus (N-ter) of Mcl-1L differs from that of Bcl-2 in that it contains regions of low sequence complexity and sequences rich in proline, glutamic acid, serine, and threonine residues, which are often found in proteins that are rapidly turned over by the proteasome [84]. As a result, unlike other Bcl-2 family members, the Mcl-1L protein is extremely unstable and has a very short half-life (1–3 h; [85]). The rapid induction and destruction of Mcl-1L has been proposed as a molecular mechanism for cells to switch between survival and apoptotic pathways in response to various stresses [86]. Sequence analysis shows that Mcl-1L contains three putative BH domains: BH1–3. The BH2 domain allows Mcl-1 to heterodimerize with other Bcl-2 family members and is critical for antiapoptotic pathways [87]. In contrast, the BH3 motif has a prominent proapoptotic role [88], especially in the presence of a direct activator of Bax or Bak.

The second major splicing product of Mcl-1 arises from exon 2 skipping and encodes a 271-aa protein isoform called Mcl-1S. Compared with the longer variant, Mcl-1L, Mcl-1S lacks the BH1, BH2, and TM domains [89,90] and is primarily localized to the cytosol. Although it occurs with low efficiency, Mcl-1 may undergo an additional AS event to produce an

extrashort Mcl-1 form (Mcl-1ES) that interacts with Mcl-1L and induces the mitochondrial cell death pathway [91].

Given the clear association between defective apoptosis and cancer and because Mcl-1 is often overexpressed in several types of human tumors [92-95], many attempts have been made to reestablish cellular sensitivity to apoptosis by modulating Mcl-1 expression.

Developments in the study of apoptosis have also uncovered a central role for mitochondrial morphology. Its influence has been observed for bioenergetic and redox homeostasis [96], Ca^{2+} regulation [69], and cell life and death decisions [97], with mitochondrial shape influencing function and vice versa. A number of components of the fission and fusion machinery, including optic atrophy 1 (OPA1), Fis1, dynamin-related protein 1 (Drp1), Mfn1, and Mfn2, have been directly implicated in the alteration of mitochondrial shape and thus in the regulation of apoptosis [98,99], although often with apparently contradictory results. In this scenario, Drp1 has been suggested to be both a fundamental inducer of apoptosis [100] and an inhibitor of Ca^{2+}-dependent apoptosis [101] by fragmenting the mitochondrial network into punctate units. Although mitochondrial fusion has been associated with a healthy cell state because of matrix content exchanges [102], it has recently been shown that fusion can also favor cell death [103]. Additional evidence for this arises from the mitochondrial protein 18 kDa (MTP18), for which a reduction impairs mitochondrial morphology, increasing the interconnections among mitochondria and increasing the response to apoptotic stimuli [104].

Antisense oligonucleotides represent powerful tools for manipulating gene expression for therapeutic purposes and have been extensively exploited to knock down genes involved in cancer progression and therapeutic resistance [105] and in a wide range of genetic disorders [106]. In particular, the therapeutic potential of ASO–mediated Mcl-1L silencing has been shown in a variety of cancer cells, including blood cancer, melanoma [107], gastric cancer [108], hepatocellular carcinoma [109] and squamous cell carcinoma [110] cells, making Mcl-1L an important target in both liquid and solid tumors.

In addition, ASOs are emerging as promising tools to finely modulate gene expression by disrupting pre-mRNA splicing. In this case, the strategy consists in using ASOs to mask splicing regulatory elements in the nascent pre-mRNA to alter exon inclusion or exclusion [111]. This strategy has been extensively explored to induce exon skipping as a therapy for human genetic disorders [112], and it also represents a valid option for cancer treatment [113].

Mcl-1 has features that suggest that it is an ideal target for therapeutic splicing modulation. For example, an sc-ASO-mediated shift of the isoform ratio toward proapoptotic Mcl-1S triggers cancer cell apoptosis and inhibits tumor development in mouse models [91,114]. However, the sc-ASOs tested thus far were designed to target Mcl-1L exon–intron junctions

that are moderately conserved among human genes, thus potentially leading to off-target effects.

Driven by these considerations, we designed a novel Mcl-1-specific sc-ASO that could significantly reduce the Mcl-1L/S ratio and sensitize cells to apoptosis. For the first time, we demonstrated that the Mcl1S-mediated mechanism involves mitochondrial physiology, thus suggesting that the Mcl-1L/S balance is a critical regulator of mitochondrial morphology and dynamics.

3.2 Results

3.2.1 Mcl-1 mRNA splicing pattern and protein expression

In view of the importance of Mcl-1 in determining apoptosis sensitivity, we measured the expression levels of both Mcl-1L and Mcl-1S in tumor cells. HeLa cells have a significantly high level of Mcl-1L mRNA, as illustrated by the 689–base pair fragment from a reverse transcription (RT) PCR analysis (Figure 4A). As expected, the shorter isoform Mcl-1S (441 base pairs) is weakly expressed compared with the long variant. Western blot (WB) revealed that the protein counterparts of the two isoforms were expressed at comparable levels (Figure 4B). The discrepancy between mRNA and protein patterns may be due to the higher rate of proteasome-mediated turnover of the long form compared with that of the short form, which can be blocked by carbobenzoxy-Leu-Leu-leucinal (MG132) treatment (Figure 4C). To promote a shift toward the proapoptotic form of Mcl-1 and investigate the underlying mechanism, we designed a panel of novel 2′-O-methyl phosphorothioate–based oligonucleotides targeting the putative exonic splicing enhancers (ESEs) of Mcl-1L exon 2 (Figure 4D). Treatment of HeLa cells with sc-ASO and subsequent RT-PCR analysis showed that only Mcl-1 sc-ASO3 (Mcl-1S3) induced an appreciable and dose-dependent effect with a shift toward the Mcl-1S form (Figure 4E). The capacity of Mcl-1S3 to decrease Mcl-1L protein production was then assessed by WB using protein lysates of HeLa cells 24 h after treatment (Figure 4F), which demonstrated a significantly lower level of Mcl-1L (40 kDa) compared with the untreated cells. The expression of the smaller protein (32 kDa) did not vary appreciably. This could be due to the labile nature and high instability of Mcl-1 [115], which make its detection difficult. Taken together, these results showed that steric interference of the ESE elements in the Mcl-1 exon 2 pre-mRNA by the newly designed Mcl-1S3 leads to exon skipping and a consequent increase in the expression of the short Mcl-1S protein isoform.
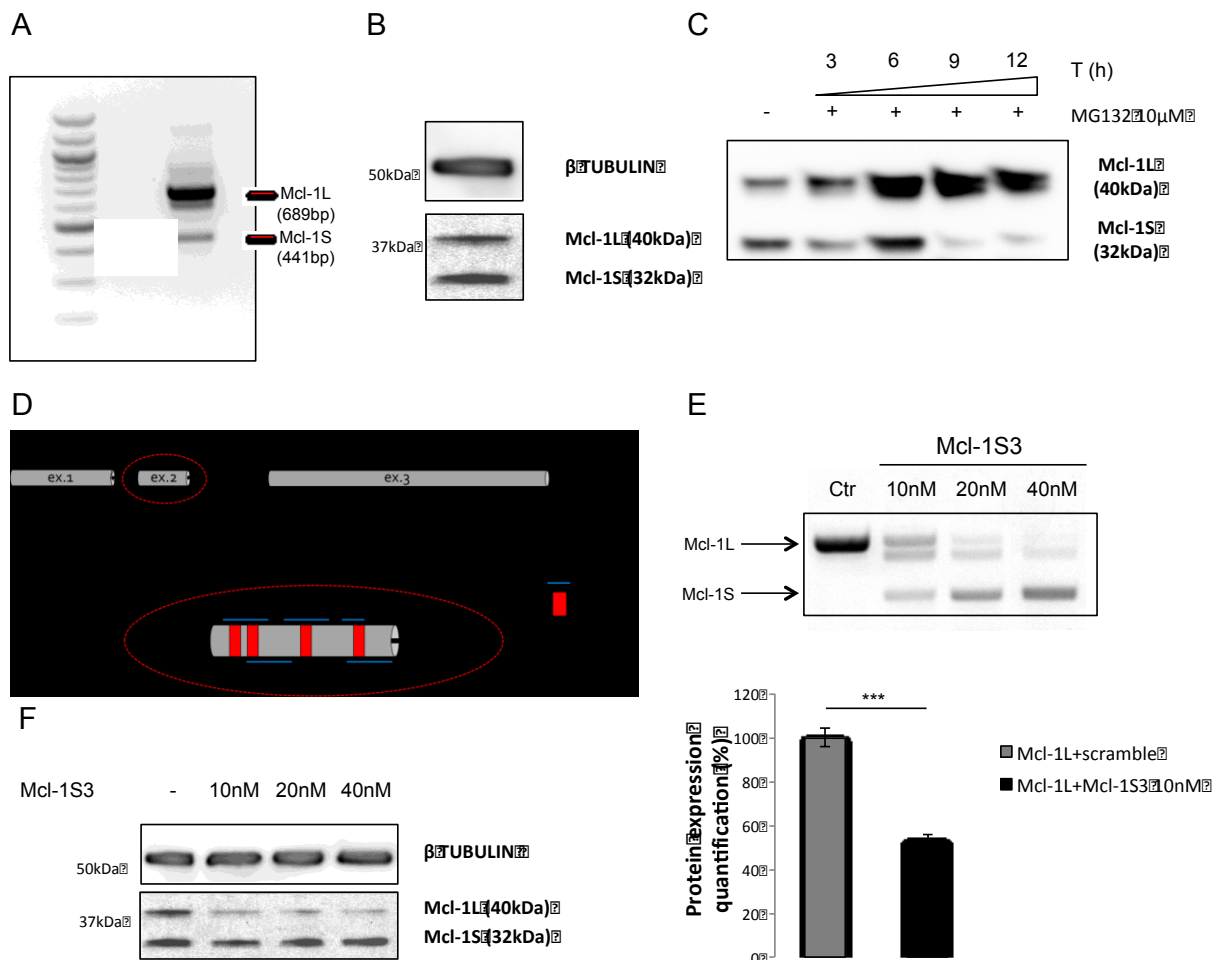
Figure 4 – Mcl-1 mRNA splicing pattern and protein expression in control and experimentally treated HeLa cells.

The figure depicts the splicing pattern (A) and protein expression (B) of Mcl-1 in control HeLa cells. MG132 treatment from 3 to 12 hours shows that Mcl-1L has a rapid turnover via proteasomal degradation (C). Schematic illustration of the ASO dsRNAs complementary to the ESEs of exon 2 (D). Splicing shifting from Mcl-1L to Mcl-1S after ASO transfection is dose dependent (E), and relative protein expression levels are shown (F). ***: p<0.001.

3.2.2 Shifting the dominant Mcl-1 variant from L to S reestablished sensitivity to apoptosis in HeLa cells

Next we evaluated whether modifying Mcl-1L pre-mRNA splicing with Mcl-1S3 could lead to an increase in apoptosis upon treatment with Ca^{2+}-dependent apoptotic stimuli. To test this hypothesis, we analyzed apoptosis by both WB analysis of two apoptotic markers, including cleaved poly(ADP)ribose polymerase (PARP) and caspase 3, and annexin V staining. Treatment with Mcl-1S3 resulted in increased apoptotic cell death [116], as indicated by apoptosis markers (Figure 5A) and an increase in the number of annexin V–positive cells (Figure 5C). HeLa cells had increased susceptibility to menadione, ceramide, hydrogen peroxide, and thapsigargin when the Mcl-1S isoform was dominant. Of importance, Mcl-1S3 did not promote apoptosis with Ca^{2+}-independent stimuli, such as etoposide (Figure 5B). These results indicated that the shift in splicing from Mcl-1L to Mcl-1S by Mcl-1S3 is a

priming stimulus for extensive cell death through the mitochondrial intrinsic apoptotic pathway. The absence of appreciable cell death in untreated cells (Figures 5C and later discussion) upon Mcl-1S3 transfection is not likely due to a balancing mechanism activated by other antiapoptotic proteins, such as Bcl-2 and Bcl-XL, upon the loss of Mcl-1L protein (Figure 5D).
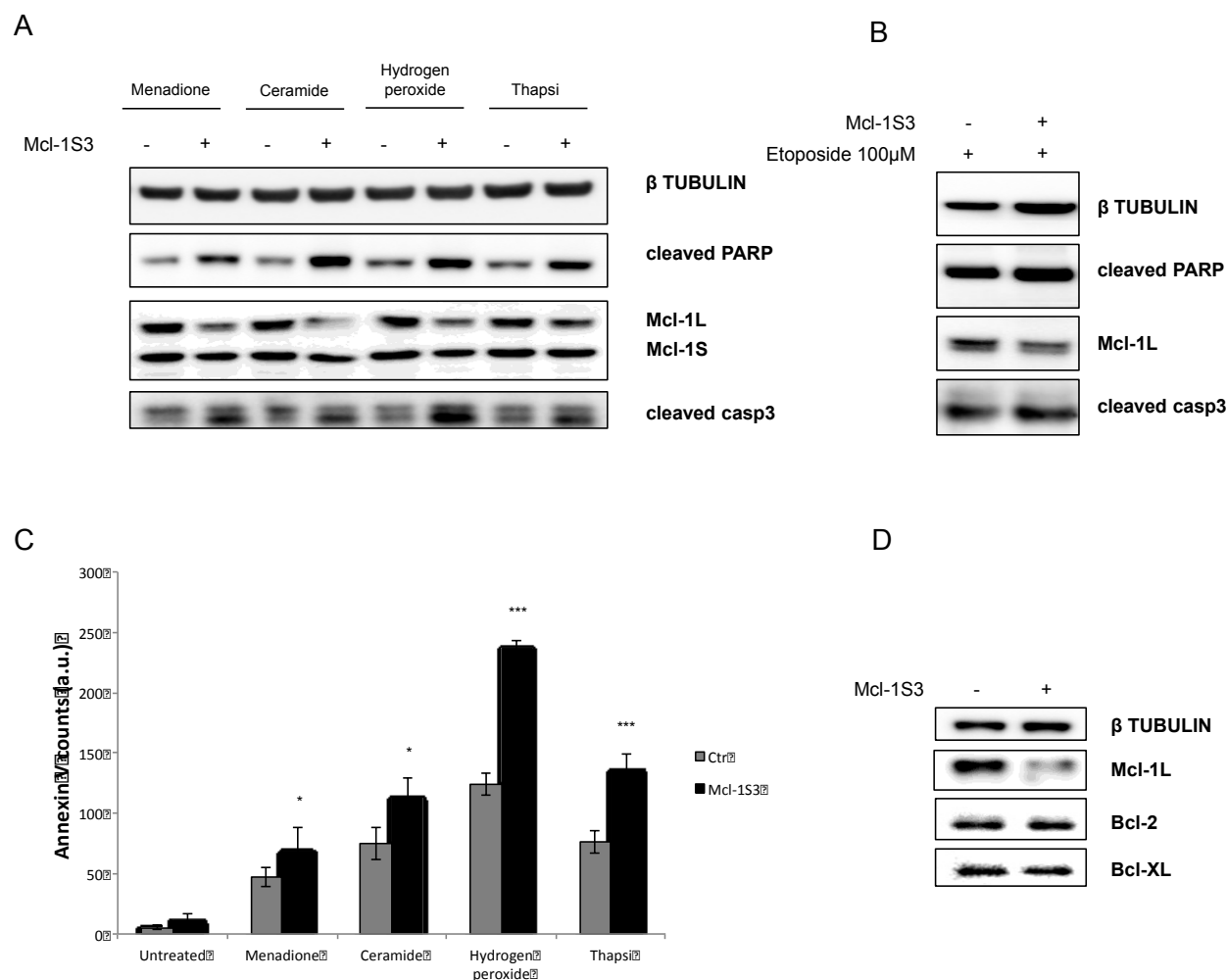
Figure 5 – Apoptosis in control and experimentally treated HeLa cells.
Apoptosis assessment in control and Mcl-1S3-transfected HeLa cells upon treatment with Ca^{2+}-dependent (A) and Ca^{2+}-independent (B) apoptotic stimuli. Western blot analysis of the apoptotic markers cleaved PARP and cleaved caspase 3 are shown as is the quantification of annexin V-stained cells (C), where significant differences are starred (*: $p<0.05$; ***: $p<0.001$). a.u.: arbitrary units. Treatments: menadione 20 μM for 2 h; ceramide 10 μM for 2 h; H_2O_2 1 mM for 1 h, thapsigargin 4 μM for 2 h; etoposide 100 μM for 3 h. The expression of major anti-apoptotic proteins Bcl-2 (26 kDa) and Bcl-XL (26 kDa) upon altering the L/S isoform ratio (D). N=3 (for each experiment).

3.2.3 Mcl-1S3–induced imbalance in the Mcl-1L/S ratio altered mitochondrial Ca^{2+} homeostasis in HeLa cells

Given that Mcl-1L is primarily located on the outer mitochondrial membrane and Ca^{2+} is an important second messenger molecule involved in life and death decision pathways, we evaluated whether intracellular Ca^{2+} homeostasis was affected by the Mcl-1L/S imbalance.

For this purpose, we monitored Ca^{2+} homeostasis using specific organelle-targeted aequorin (AEQ) probes, including those that were targeted to the cytosol (cytAEQ), mitochondria (mtAEQ), and endoplasmic reticulum (erAEQ; [117]). Specifically, we cotransfected each aequorin probe with a scrambled oligonucleotide or different concentrations of Mcl-1S3 (Figure 6A). Under all conditions, we investigated the Ca^{2+} response to histamine (His), which signals through Gq-coupled receptors to produce inositol 1,4,5 triphosphate (IP3; Figure 6A). Mcl-1S3–expressing cells displayed increased mitochondrial Ca^{2+} uptake after agonist addition (Figure 6A, top). This effect of Mcl-1S3 was dose dependent. We observed a significant increment in $[Ca^{2+}]$ exclusively at the mitochondrial level, which suggested a specific mitochondrial effect (Figure 6A, middle and bottom). Of importance, Mcl-1S3 did not alter the basal mitochondrial Ca^{2+} levels measured by a plasmid encoding the mitochondrial-targeted GCaMP6m (Figure 6B). These findings indicated that the Mcl-1S3 ASO caused an imbalance in the Mcl-1L/S ratio, which altered mitochondrial Ca^{2+} homeostasis without perturbing other organelles. These data also explained the increased susceptibility to cell death upon the treatment of Mcl-1S3–transfected cells with Ca^{2+}-dependent apoptotic stimuli (as observed in Figure 5, A and C). Of note, pharmacological inhibition of Ca^{2+} uptake with the thiourea derivative KB-R7943 (permeable mitochondrial Ca^{2+} uniporter blocker) in Mcl-1S3-transfected cells decreased mitochondrial Ca^{2+} concentration by ∼50% (Figure 6C) and protected cells from the ASO-induced effects (Figure 6D). Thus these results suggest that the mitochondrial Ca^{2+} level plays a pivotal role in determining susceptibility to cell death when Mcl-1 levels are unbalanced. We further explored whether the decrease in the Mcl-1L/S ratio could modify other mitochondrial parameters, such as organelle morphology and membrane potential.
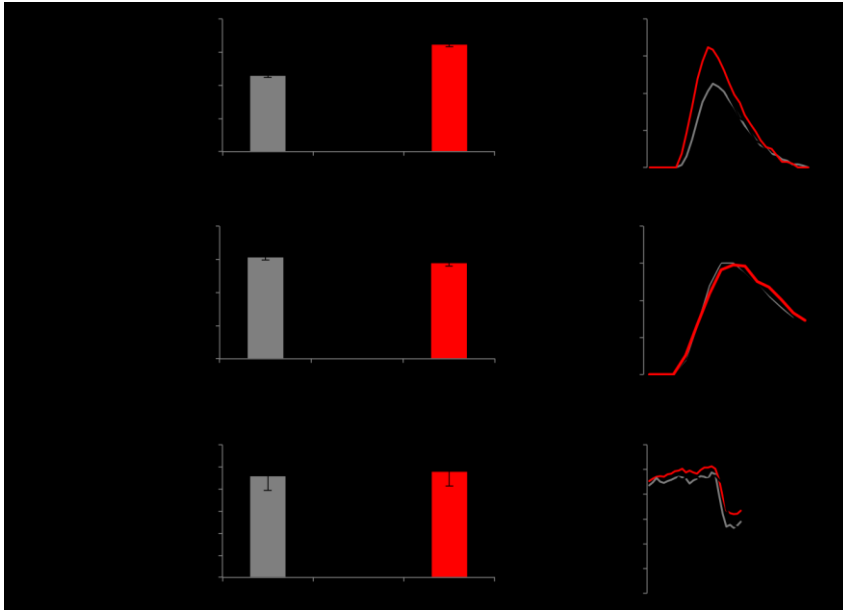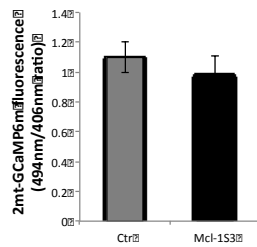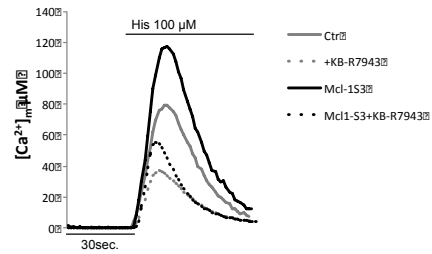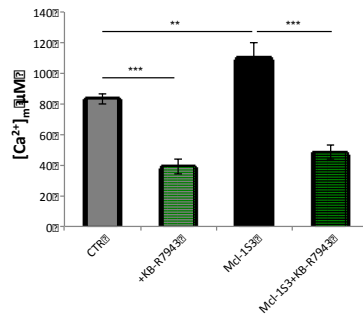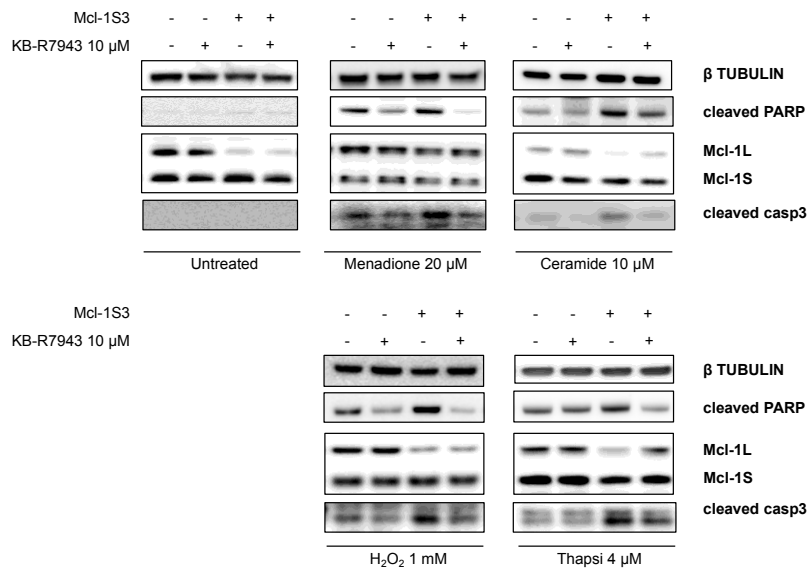
Figure 6 – Ca^{2+} homeostasis and its role in the death of experimentally treated HeLa cells.
Ca^{2+} homeostasis was monitored via aequorin in mitochondria (top), cytosol (middle), and ER (bottom) in control and Mcl-1S3-transfected HeLa cells. The ASO had a specific, dose-dependent mitochondrial effect, as indicated by the black (10 nM of Mcl-1S3) and red (20 nM of Mcl-1S3) bars (A). Basal mitochondrial Ca^{2+} concentrations were further assessed by imaging 2mt-GCaMP6m-expressing cells (B). [Ca^{2+}] concentration (µM) upon the pharmacological inhibition of mitochondrial Ca^{2+} uptake by the permeable MCU blocker KB-R7943 in control and Mcl-1S3-transfected HeLa cells. KB-R7943 (as confirmed by aequorin measurements) promoted ~50% of the ion concentration in mitochondria (C). Western blot analysis of the apoptotic markers cleaved PARP and caspase 3 in MCU inhibitor-treated cells. The inhibition of Ca^{2+} uptake protected cells from

Ca²⁺-dependent apoptosis (D). Where indicated, the cells were challenged with 100 μM histamine. Significant differences are starred (**: $p<0.01$; ***: $p<0.001$). N=6 (for each experiment).

3.2.4 A greater mitochondrial membrane potential promoted Ca²⁺ uptake in Mcl-1S3– treated HeLa cells

The mitochondrial membrane potential Ψm is a critical regulator of Ca²⁺ accumulation [118-121]: depolarization reduces the driving force for Ca²⁺ uptake by mitochondria and thereby prevents Ca²⁺ overload. Conversely, hyperpolarization increases Ca²⁺ uptake. To measure $\Delta\Psi$m changes, we stained mitochondria with a fluorescent cationic probe, tetramethylrhodamine methyl ester (TMRM), and analyzed the cells by confocal microscopy. To allow for nonspecific TMRM binding, we corrected measurements for residual TMRM fluorescence after full $\Delta\Psi$m collapse with the mitochondrial uncoupler carbonyl cyanide 4-(trifluoromethoxy) phenylhydrazone (FCCP). Mcl-1S3–transfected cells had a significant increase in Ψm compared with the controls (Figure 7A). Of importance, the mitochondrial hyperpolarization that was observed upon reduction of the Mcl-1L/S ratio could explain the previously described increase in mitochondrial Ca²⁺ accumulation (Figure 6A). Subsequently we assessed whether Mcl-1S3 could modify the expression level of the MCU, which facilitates Ca²⁺ uptake into the mitochondrial matrix. No difference in MCU expression was observed upon Mcl-1S3 transfection (Figure 7B). Similarly, the expression levels of other mitochondrial proteins (TIM23 for inner mitochondrial membrane [IMM], ATP5A and HSP60 for matrix, and VDAC and TOM20 for OMM) were also unchanged (Figure 7B; β-tubulin was used as a loading marker). These data suggested that no changes in mitochondrial mass occurred. Thus variation in Ψm appears to be the main cause of increased mitochondrial Ca²⁺ uptake in Mcl-1S3–transfected HeLa cells, which do not exhibit changes in MCU expression, total mitochondrial mass, or mitochondrial biogenesis (as evaluated in Figure 7B by PGC1α detection).

3.2.5 Reduced Mcl-1L/S ratio induced mitochondrial fusion in HeLa cells

Mitochondria are dynamic organelles that fuse and divide to form constantly changing tubular networks [122-124]. This evolutionarily conserved activity affects membrane composition (e.g., IMM and OMM) and is mediated by the combined effects of several large GTPases, potentially with other mitochondrial proteins [125]. To assess changes in mitochondrial morphology in our experimental model, we used the mitochondria-targeted red fluorescence protein mtDsRed. Specifically, we cotransfected HeLa cells with either the scrambled oligonucleotide and mtDsRed (control) or Mcl-1S3 and mtDsRed. The fluorescent dye calcein was used as a marker of cell volume to identify living cells and normalize the

quantification of the mitochondrial network to cell volume (see Materials and Methods). Confocal images revealed a decreased number of mitochondria in Mcl-1S3–transfected cells (designated as n° of objects by the analysis software) compared with the control. Moreover, Mcl-1-S3–transfected cells showed a higher mean mitochondrial volume (Figure 7C). Analyses of the total mitochondrial network and cell volumes revealed no significant differences. The same results were confirmed in the SH-SY5Y cell line, which displayed a less filamentous network than did HeLa cells (Figure 7D). Taken together, these findings indicated that 24 h after Mcl-1S3 transfection, a shift from Mcl-1L to Mcl-1S promoted mitochondrial fusion without altering the total mitochondrial volume. Of interest, the increased hyperfusion was not linked to enhanced expression of fusion proteins, such as Mfn1/2 and OPA1 (Figure 7E).

These data indicated that shifting from antiapoptotic to proapoptotic Mcl-1 isoforms promoted mitochondrial hyperpolarization and increased mitochondrial fusion in HeLa and SH-SY5Y cells.
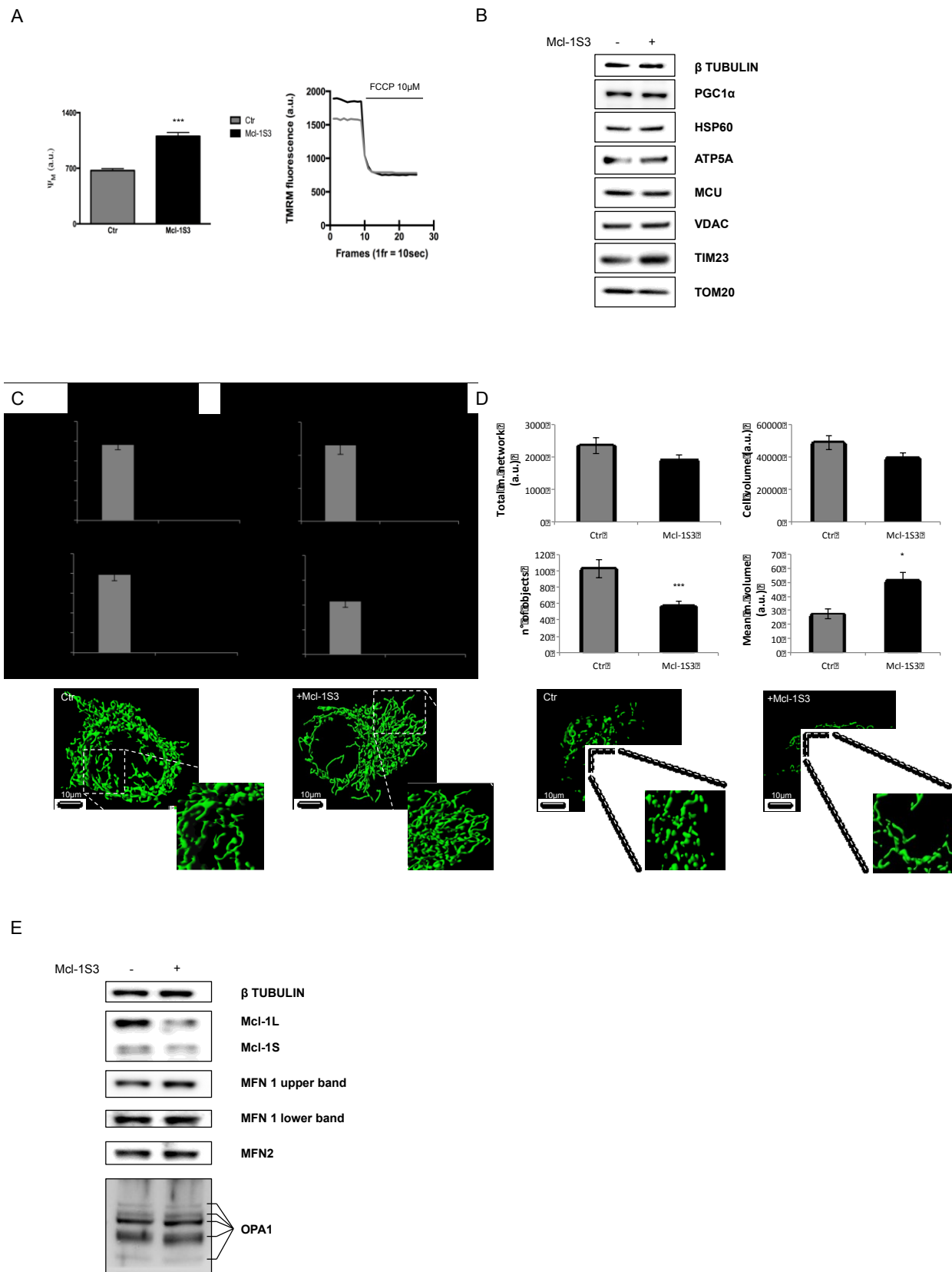
Figure 7 – Ψ_M and morphological changes in the mitochondria of ASO-transfected HeLa cells.
Mcl-1S3-treated HeLa cells had a greater mitochondrial membrane potential than the untreated cells (A).
Western Blot analysis to monitor changes in the expression of proteins involved in Ca^{2+} uptake (MCU),
mitochondrial mass (HSP60, ATP5A, VDAC, TIM23, TOM20), and biogenesis (PGC1α) (B). Different
parameters describing the mitochondrial network dynamics are shown in histograms (top) and confocal images
(bottom). Black bars indicate Mcl-1S3-transfected HeLa (C) and SH-SY5Y (D) cells; a decrease in n° of objects

and an increase in mean mitochondrial volume are evidence of hyperfused mitochondria. Significant differences are starred (*: p<0.05; **: p<0.01; ***: p<0.001). a.u.=arbitrary units. Mitochondrial fusion proteins were investigated by Western Blot with MFN1/2 and OPA1 antibodies (E) in both experimental conditions. N=3 (for each experiment).

3.2.6 A lower Mcl-1L/S ratio induced mitochondrial hyperfusion in a Drp1-dependent manner

In humans, mitochondrial fission is highly regulated by Fis1 and Drp1. Drp1 is a member of the dynamin superfamily of proteins; it consists of a GTPase and a GTPase effector domain and has a predominantly cytosolic localization. Drp1 overexpression induces extensive mitochondrial fragmentation, whereas its depletion promotes fusion [126]. Thus mitochondrial fusion can originate from either lack of fragmentation or up-regulation of fusion proteins. Accordingly, after excluding a possible role for Mfn1/2 and OPA1 proteins, we investigated whether the augmented mitochondrial fusion that was observed upon Mcl-1S3 transfection occurs in a Drp1-dependent manner (Figure 8). To induce mitochondrial fission, we overexpressed wild-type Drp1. Drp1 overexpression promoted mitochondrial fission (Figure 5A, bottom, white bars with gray stripes), which was quantitatively expressed as an increased number of mitochondrial objects and a reduction of the mean volume of a single mitochondrial object. Surprisingly, cotransfection of Mcl-1S3 and Drp1 abolished the fragmentation of the mitochondrial network, reestablishing a mitochondrial shape that resembled the control condition.

These data suggested that Drp1 and Mcl-1 are functionally related in the regulation of mitochondrial morphology through a balance between fusion and fission events.
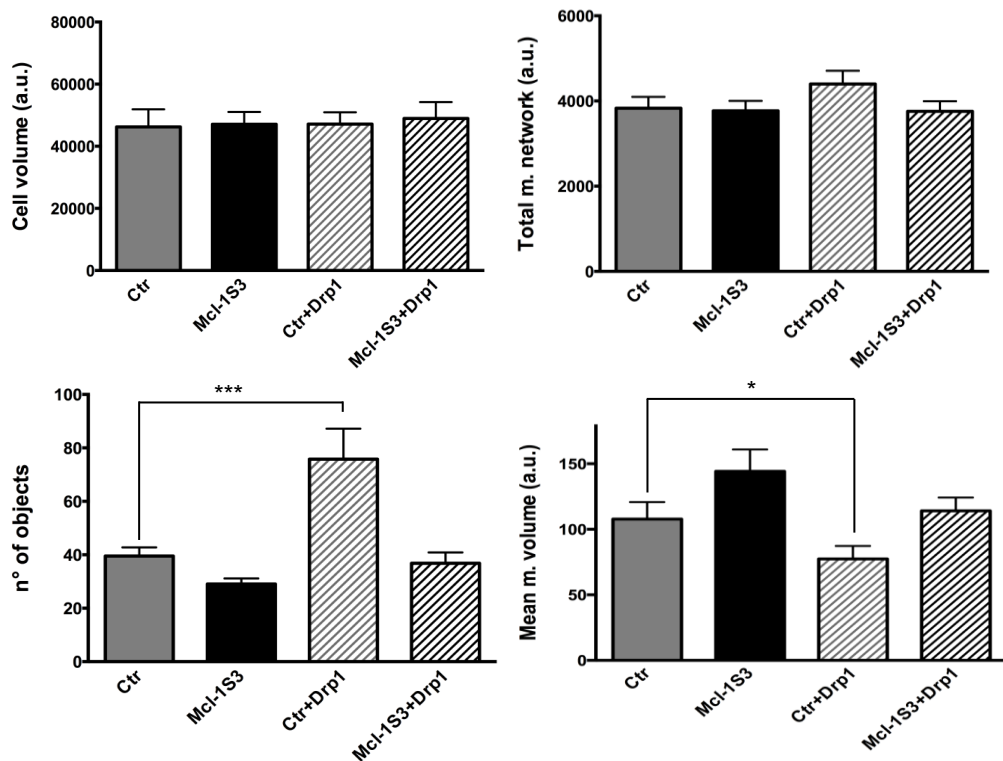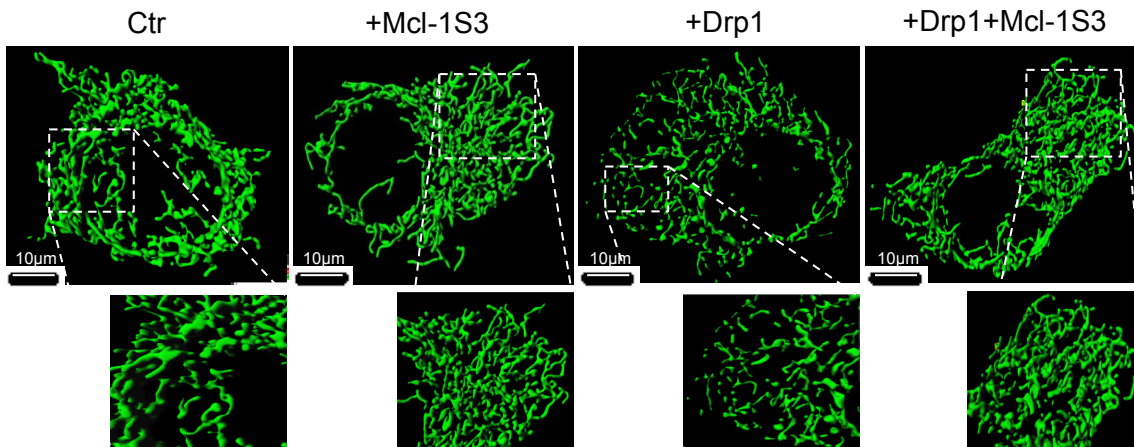
Figure 8 – Mcl-1L involvement in mitochondrial dynamics is Drp1 dependent.
Analysis of mitochondrial morphology under four experimental conditions. No significant differences were detected in cell volume or the total mitochondrial network (top). Drp1 overexpression promoted extensive fragmentation as shown by the increased number of objects and the reduction of mean mitochondrial volume (bottom: white bars with grey stripes). Co-transfection of Mcl-1S3 and Drp1 reverted the effect of Drp1 overexpression alone, suggesting an association between Mcl-1L and Drp1 in the regulation of mitochondrial dynamics (A). Significant differences are starred (*: $p<0.05$; ***: $p<0.001$). a.u.=arbitrary units. Representative confocal images of mitochondrial networks (green fluorescence) under each condition (B). N=3 (for each experiment).

3.2.7 Inhibiting Drp1 activity in the mitochondria promoted apoptotic cell death

To investigate the link between cell death and Drp1/Mcl-1L–driven changes in morphology in our experimental model, we monitored the activation of apoptosis in control and Mcl-1S3–

transfected HeLa cells by WB analysis. We subjected these cells to forced fission (by the transfection of wild-type Drp1) and then treated them with apoptotic Ca^{2+}-dependent and Ca^{2+}-independent stimuli as previously described. As in Figure 5, there was a higher percentage of apoptotic cells after Mcl-1S3 transfection than with the control upon Ca^{2+}-dependent treatments, whereas no apoptosis was detected for any of the conditions lacking apoptotic stimuli (Figure 9A). Of note, fragmentation of the mitochondrial network of control cells by Drp1 overexpression provided protection from cell death, whereas apoptosis occurred at levels between those of the control and ASO groups when fission was inhibited by down-regulation of Mcl-1L (Figure 9A, lane Mcl-1S3+Drp1). In all conditions concerning down-regulation of Mcl-1L and experimental treatments, no significant changes in Mcl-1S expression were detected. These observations were not seen with etoposide treatment. In contrast, when the functionality of Drp1 was abolished by the use of its dominant-negative Drp1-K38A, cells with a persistent mitochondrial hyperfusion state died, based on PARP and caspase 3 cleavage (Figure 9B).

These final experiments indicated a strong link between changes in mitochondrial morphology driven by Mcl-1L and Drp1 and the intrinsic apoptotic pathway previously described.
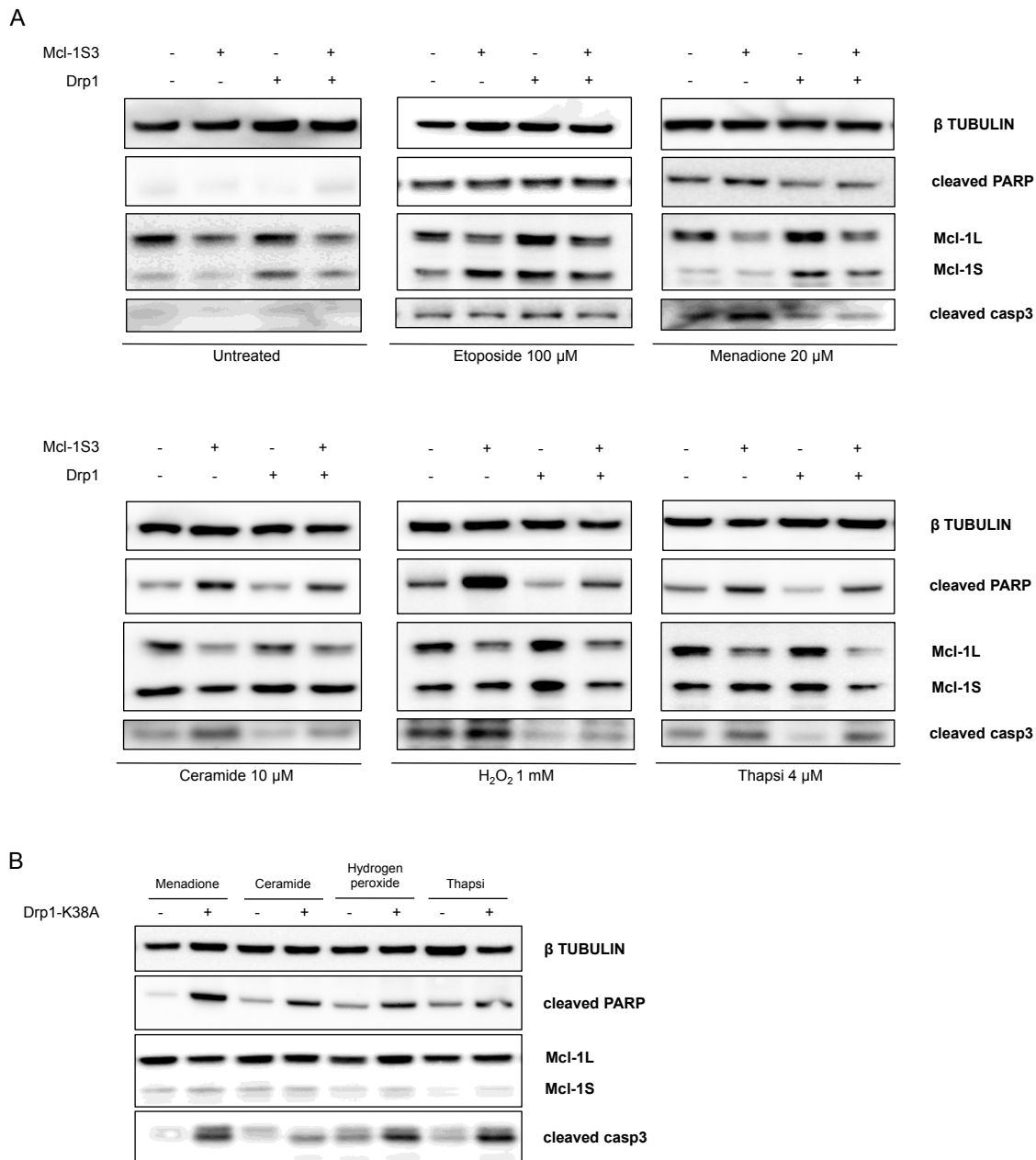
Figure 9 – Inhibition of Drp1 activity in the mitochondria restored apoptotic cell death.
Apoptosis assessment upon treatment with Ca^{2+}-dependent and Ca^{2+}-independent apoptotic stimuli detected by Western blot analysis of cleaved PARP and cleaved caspase 3. Control and Mcl-1S3-transfected HeLa cells were first co-transfected with a wt Drp1 construct (as described in morphology experiments) and then divided into six conditions: untreated (with culture medium exchange), 100 μM etoposide for 3h, 20 μM menadione for 2h, 10 μM ceramide for 2h, 1 mM hydrogen peroxide for 1h, and 4 μM thapsigargin for 2h (A). Overexpression of the dominant negative Drp1-K38A promotes mitochondrial fusion and widespread cell death (B). N=3 (for each experiment).

3.2.8 Mcl-1: a link between cell cycle and mitochondrial dynamics

In a study focused on the link between mitochondrial morphology and cell cycle progression, Mitra et al. [127] described a greater membrane potential and a massive, hyperfused network state in mitochondria at the G1/S transition of the cell cycle. In light of our previous observations of Mcl-1 ASO transfection, which echoed their findings, we proceeded to

investigate the Mcl-1 expression pattern at the G1/S transition after the cells were synchronized with a double- thymidine block. Of interest, we observed a shift in the Mcl-1L/S ratio at the G1/S transition, with a greater amount of Mcl-1S than Mcl-1L (Figure 10).
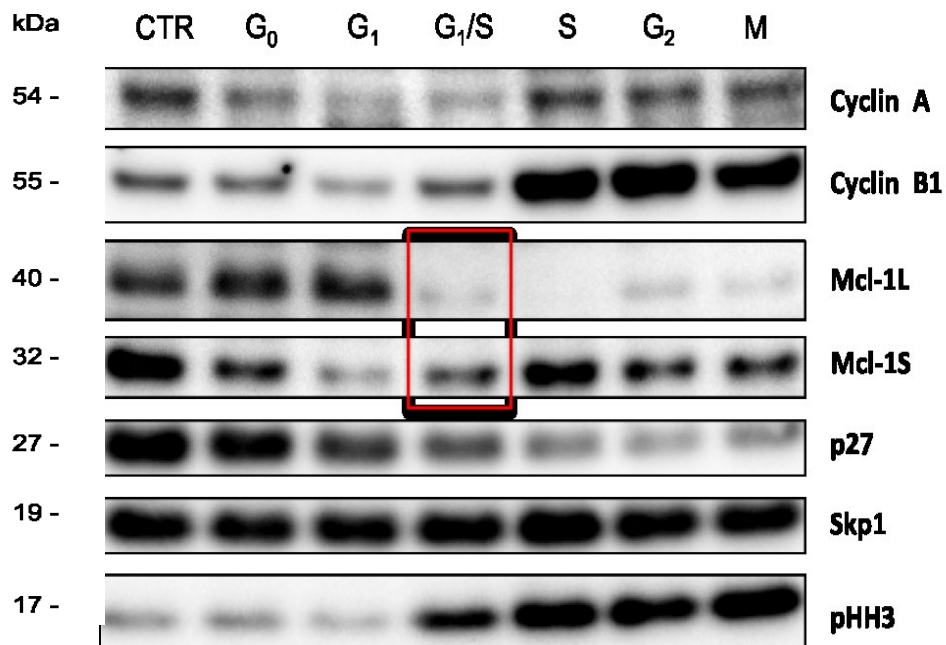
Figure 10 – Mcl-1 links cell cycle regulation and mitochondrial dynamics.
Mcl-1L and Mcl-1S expression levels are shown in different phases of the T98G cell cycle. Cells were synchronized by double thymidine block and were assayed at each phase of the cell cycle (top). The proteins of interest are shown on the right. Skp1 was used as a loading control. Other markers: Cyclin A for S and M phases; Cyclin B for the G_2/M checkpoint; p27 for quiescent cells; and pHH3 for mitotic activity. The red rectangle indicates Mcl-1L and Mcl-1S expression in G_1/S phase. N=2.

3.2.9 Drp1 interacted with Mcl-1L to regulate mitochondrial dynamics

Next, to further support our model, we investigated whether Drp1 could be coimmunoprecipitated with Mcl-1L. As shown in Figure 11A, Mcl-1L formed immune complexes with Drp1 in control HeLa cells, whereas Mcl-1S remained in the supernatant. The same result was obtained by performing the experiment in reverse; immunoprecipitation of overexpressed Drp1 and antibody cross-linking to protein A agarose revealed a preferential binding to Mcl-1L. These data suggested that the two proteins specifically interacted with each other to regulate the hyperfused mitochondrial state detected in previous experiments.

3.2.10 Lowering the Mcl-1L/S ratio inhibited Drp1 translocation from the cytosol to mitochondria

Drp1 localizes primarily in the soluble fraction of the cell [128]. Although Drp1 can be found in membrane compartments, membrane localization occurs only under certain environmental conditions and depends on the phase of the cell cycle [126]. In HeLa cells, we detected Drp1

predominantly in the cytosol, which is in agreement with current literature, and moderately at the mitochondrial membranes (Figure 11B), where it likely exerts physiological roles in maintaining a basal fission rate. In contrast, Mcl-1L was enriched at the mitochondria, whereas Mcl-1S was found in the cytosol and ER compartments. Drp1 translocates from the cytosol to mitochondria to exert its profission functions. To evaluate Mcl-1L function at the OMM during the fission/fusion processes, we assessed the amount of mitochondrial Drp1 after overexpressing Drp1 and after altering the Mcl-1L/S ratio. As shown in Figure 8C, upon Drp1 overexpression, the level of mitochondrial Drp1 increased compared with mock-transfected cells. On Mcl-1S3 transfection, which consequently depleted Mcl-1L, Drp1 accumulation at mitochondria was less efficient (Figure 11C).

These findings suggested that Mcl-1L acts as a molecular anchor for mitochondrial Drp1 and further validated the pivotal role of Mcl-1L/S balance in the regulation of the fusion and fission machinery.
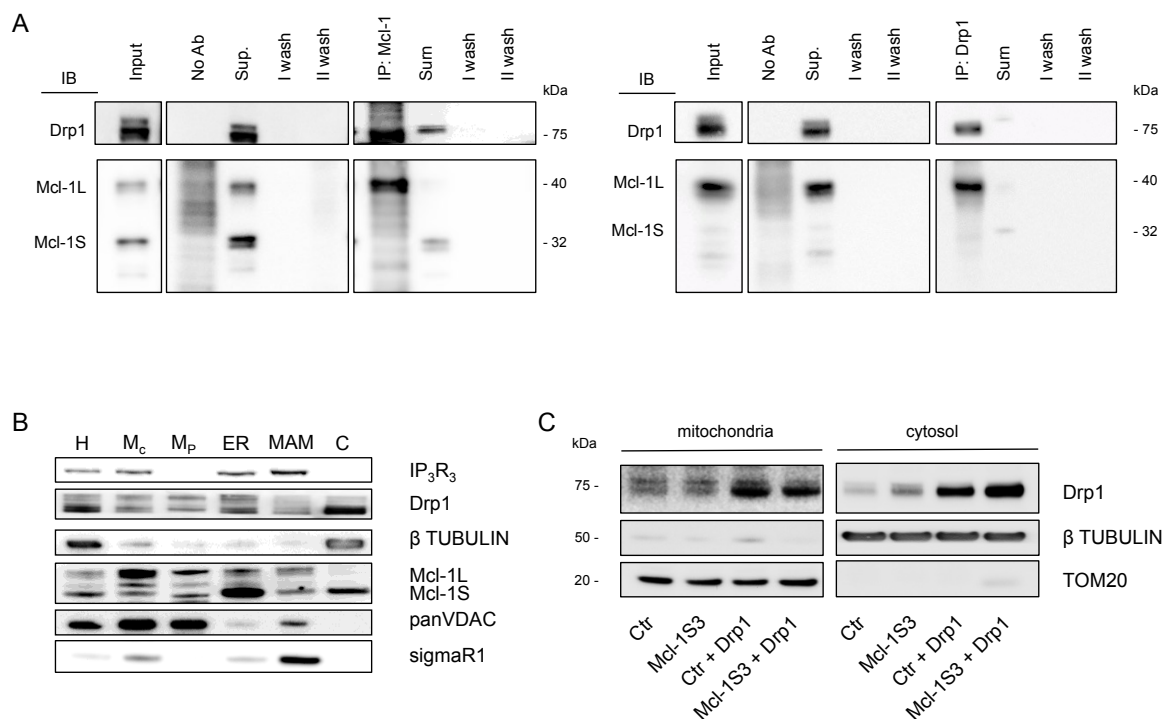
Figure 11 – Subcellular localization of Drp1, Mcl-1L/Mcl-1S, and their interactions.
Co-immunoprecipitation (Co-IP) of Mcl-1L and Drp1 in HeLa cells. IP was performed in control (in absence of antibody), with rabbit anti-Mcl-1 antibody, and in a reverse IP mode with rabbit anti-Drp1 antibody followed by immunoblotting with anti-Mcl-1 and anti-Drp1 antibodies. Input lysates as well as flow-through after the IPs are shown (A). Subcellular localization of Drp1, Mcl-1L, and Mcl-1S as determined by fine fractionation. IP$_3$R$_3$, β-tubulin, panVDAC, and sigmaR1 were used as markers of ER, cytosol, mitochondria, and MAM, respectively. H: homogenate; M$_c$: crude mitochondria; M$_P$: pure mitochondria; ER: endoplasmic reticulum; MAM: mitochondria-associated membranes; C: cytosol (B). Induction of Drp1 translocation from cytosol to mitochondria upon Drp1 overexpression in control and Mcl-1S3-transfected cells. Protein localization and

expression were evaluated under each condition by WB after digitonin-based fractionation (C). N=3 (for each experiment).

3.3 Discussion

Dysregulation of apoptosis contributes to numerous pathological conditions, including cancer. Indeed, one of the hallmarks of cancer cells is their capacity to evade apoptosis, prompting research for drugs that can restore cell death susceptibility in tumor cells [129]. The mitochondrial apoptotic pathway is regulated by interactions between members of the Bcl-2 protein family, which contain up to four BH domains (BH1–4; [130,131]). Protein factors possessing all four BH domains, including Mcl-1L, antagonize apoptosis by preventing mitochondrial outer membrane permeabilization (MOMP), thus sequestering proapoptotic factors in mitochondria. Factors lacking one or more BH domains, including Mcl-1S, are proapoptotic and promote MOMP. Mcl-1L is highly expressed in human malignancies, and its cellular localization is consistent with a role in controlling key mitochondrial events during apoptosis [115]. Mitochondrial Ca^{2+} also plays a critical role in the regulation of cell death [69,132]. Two requisite events during the early stages of apoptosis are the ER release of Ca^{2+} into the cytosol and the mitochondrial release of cytochrome c. The Ca^{2+} uptake by the mitochondria determines cell susceptibility to apoptotic stimuli. For example, reduced ER Ca^{2+} flux toward mitochondria results in resistance to apoptosis, inhibiting the mitochondrial Ca^{2+} overload required for permeability transition pore opening [133]. Several earlier studies described the role of Mcl-1 in Ca^{2+} homeostasis. Minagawa et al. [134] showed that Mcl-1 overexpression did not affect IP3R expression or the amount of Ca^{2+} contained in ER stores. However, mitochondrial Ca^{2+} signals were decreased in cells overexpressing Mcl-1. Conversely, Eckenrode et al. [135] proposed a different activity for Mcl-1 that is quite similar to the molecular mechanism of Bcl-2 function. They reported that Mcl-1 bound with comparable affinity to the C-ter of different IP3R isoforms, with the cells consequently displaying low ER Ca^{2+} content and an enhanced rate of IP3-mediated Ca^{2+} release. Moreover, Mcl-1 expression enhanced spontaneous IP3R-dependent Ca^{2+} oscillations and spiking in intact cells in the absence of agonist stimulation.

The data presented here support a mitochondria-specific function for Mcl-1, with no effect on ER Ca^{2+} homeostasis (Figure 6A). In contrast to previous studies [136], we used an antisense oligonucleotide approach to modulate mRNA splicing rather than direct overexpression, silencing, or antagonism of the protein to investigate Mcl-1 functional features. Because of the high therapeutic potential of ASOs, especially in combination with cytotoxic agents [108,110], we opted for splice-switching antisense technology to modulate the balance between the different variants of Mcl-1. To guarantee high gene specificity for Mcl-1 pre-mRNA and

reduce potential off-target toxic effects, we designed a novel Mcl-1S3 sc-ASO that targets an ESE within exon 2 (Figure 4D) and were able to successfully induce exon skipping, which permitted an appreciable and dose-dependent increase in Mcl-1S expression (Figure 4E). Of most importance, this effect was associated with an extensive induction of cell death through the mitochondrial intrinsic apoptotic pathway (Figure 5), which further supports the role of Mcl-1 pre-mRNA AS as a target for the development of anticancer therapies. It is worth noting that intervention at the pre-mRNA level would maintain the transcriptional regulation and absolute levels of Mcl-1 premRNA, thus selectively decreasing the long/short isoform ratio, which has proapoptotic effects. In cells overexpressing the Mcl-1L pre-mRNA in a manner similar to tumors, the splice-switching strategy would result in a marked increase in the Mcl-1S form, thus magnifying the proapoptotic effect compared with the generic silencing of Mcl-1L expression.

Using Mcl-1S3, we showed that the shift in the Mcl-1L/S ratio resulted in increased mitochondrial Ca^{2+} levels after agonist addition without affecting its baseline content (Figure 6B) or the Ca^{2+} homeostasis of other subcellular organelles. These data suggest that the lower Mcl-1L/S ratio affects mitochondrial Ca^{2+} uptake only when the cytosolic $[Ca^{2+}]$ rapidly increases (i.e., upon Ca^{2+}-dependent apoptotic stimuli). Under our experimental conditions, the higher mitochondrial Ca^{2+} uptake observed on Mcl-1S3 transfection was certainly due to a significant increment in the mitochondrial membrane potential (Figure 7A). Variation in $\Delta\Psi m$ is a highly sensitive indicator of the energetic state of mitochondria and is strictly associated with the morphology of the mitochondrial network. Of interest, when mitochondrial potential was monitored at different cell cycle stages, it appeared to be the greatest at G1/S. Nevertheless, mitochondria form a giant tubular network in G1/S [127]. Accordingly, we observed a shift in the Mcl-1L/S ratio during G1/S phase, with a greater amount of Mcl-1S present compared with the L variant (Figure 10). A higher level of Mcl-1L was detected at G0, which coincides with greater mitochondrial fragmentation. Moreover, we also detected a low Mcl-1L/S ratio during mitosis, which is characterized by a high number of tubular mitochondria.

These findings suggest a pivotal role of Mcl-1 in the regulation of the fusion and fission dynamics, which occurs in a Drp1-dependent manner. Mcl-1 interacts with Drp1 (Figure 11A). On Mcl-1S3 transfection, Drp1 was unable to induce extensive fragmentation (Figure 11).

This finding suggests that the reduction of Mcl-1L at the OMM may prevent the normal physiologic functions of Drp1, producing a persistent hyperfused mitochondrial state (Figure 7, C and D) without changes in fusion protein expression (Figure 7E).

Recently a pivotal role for Mcl-1 in regulating fusion/fission dynamics was proposed [45,136], based on extensive mitochondrial fragmentation upon Mcl-1 down-regulation, which occurred independently of Mcl-1–related apoptosis. These studies used either Mcl-1 deficient MEFs [45] or pharmacological inhibition (BH3 mimetics) of Mcl-1 expression [136]. Conversely, our approach was to decrease the Mcl-1L/S ratio, resulting in a hyperfused mitochondrial network and increased sensitivity to apoptosis. Thus, if the inefficient mitochondrial fusion caused by total Mcl-1 inhibition/depletion is not related to altered susceptibility to cell death, the hyperfused state induced by decreasing the Mcl-1L/S ratio might represent a crucial event for sensitizing mitochondria to a wide range of apoptotic stimuli. Of note, we observed a reduced level of mitochondrial Drp1 upon Mcl-1S3 transfection (Figure 11C) without any modification in the total endogenous Drp1 level. These data suggested the putative involvement of the fission factor in Mcl-1–dependent mitochondria remodeling, most likely by regulating Drp1 translocation from the cytosol to the OMM. We also observed the interaction between Drp1 and Mcl-1, although Drp1 overexpression was required. Of interest, Drp1 seems to coimmunoprecipitate with the long form of Mcl-1, but further work is required to clarify the exact relationship between Mcl-1 and Drp1 shuttling/localization.

Another key conclusion from the present study is the link between mitochondrial morphology and apoptosis. Despite the large quantity of literature available on the topic, the relationship between the two events has not been fully elucidated. In particular, Drp1 is described as both a fundamental inducer of apoptosis [100] and an inhibitor of Ca^{2+}-dependent apoptosis [101]. The model presented here is more consistent with the latter functionality, and our findings are further supported by a recent study [103] showing that persistent mitochondrial fusion leads to robust caspase-dependent cell death. In contrast to the current opinion that mitochondrial fragmentation is associated with apoptosis, our data indicate that apoptosis can also occur when mitochondria are hyperfused, as shown in Figure 9A, upon the inhibition of Drp1 activity in the mitochondria by Mcl-1S3 transfection and as shown with regard to BAX-dependent MOMP failure when mitochondria are fragmented. The same effect was also confirmed with the dominant negative form Drp1-K38A in all experimental conditions (Figure 9B). An intact mitochondrial network could ensure rapid propagation of Ca^{2+} through the mitochondrial matrix to promptly trigger apoptosis. Of note, we obtained a similar result when Mcl-1L was down-regulated by Mcl-1S3, thus avoiding Drp1 activity at the OMM. However, if Drp1 is free to act at the mitochondria, fragmentation could inhibit the propagation of the apoptotic wave, limiting the harmful effects caused by treatment.

In this scenario, Ca^{2+} signaling behaves as the primary initiator of cell death, and accordingly, the pharmacological inhibition of MCU by KB-R7943 (Figure 6C) protected cells from the therapeutic effects of Mcl-1S3 (Figure 6D).

Taken together, these data suggest that redirecting Mcl-1 synthesis from the antiapoptotic L variant to the proapoptotic S variant might represent a novel strategy for anticancer therapies.

4. The c subunit of F_oF_1-ATP synthase and the mPTP in the I/R injury

4.1 Introduction

Ischemic heart disease (IHD) is the leading cause of death in Western countries. Each year, approximately 17 million people worldwide suffer from myocardial infarction (MI), and in 40% of cases, an ST segment elevation MI (STEMI) is presented [137]. Recent developments in myocardial reperfusion technique (e.g., primary percutaneous coronary intervention (PCI)) and in antithrombotic therapies permitted a significant improvement in the long-term outcome of STEMI patients [137]. Nevertheless, the mortality and disability associated with STEMI remain high [138] for several reasons, including a lack of therapy compliance and the under-use of specific cardiovascular drugs. Contemporaneously, the effectiveness of myocardial reperfusion remains a principal issue. It is estimated that approximately 50% of the final infarcted area is related to IRI [139], which consists of cardiomyocyte death following the restoration of blood flow in the related infarcted artery. IRI is strongly related to IS and to left ventricular (LV) remodeling. Both of these processes are known in daily clinical practice as strong and independent predictors of prognosis, heart failure (HF) and mortality [140]. Several clinical, cellular and molecular events occur during IRI (Figure 12). The most relevant clinical events are as follows: reperfusion-induced arrhythmia, myocardial stunning, microvascular obstruction (MVO) and myocardial necrosis secondary to reperfusion (Figure 12). The latter two entities are particularly well understood and are associated with increased IS and LV dysfunction severity. MVO is a phenomenon that occurs due to the following changes: capillary damage induced by vasodilatation, external compression caused by endothelial cell and cardiomyocyte swelling, micro-embolization of friable material released from the atherosclerotic plaque and infiltration of inflammatory cells [141]. The myocardial necrosis that occurs secondary to reperfusion includes apoptosis and necrosis of cardiomyocytes and endothelial cells at a higher percentage than expected, resulting in a complete loss of the benefits of myocardial reperfusion via PCI [139]. In recent years, the complex mechanism that promotes the onset of IRI has been extensively studied but is currently only partially understood. This field of research is commonly referred to as "cardioprotection," and various drugs and strategies have been initially evaluated using animal models and subsequently evaluated via clinical studies in humans in an attempt to reduce IS and thereby improve long-term prognosis. Recently, new advancements and discoveries in "cardioprotection" research have been reported. In particular, these advancements involve the role, function and structure of the mPTP. Indeed, the mPTP

(specifically, its opening) plays a key role in the development of myocardial necrosis that occurs secondary to reperfusion.
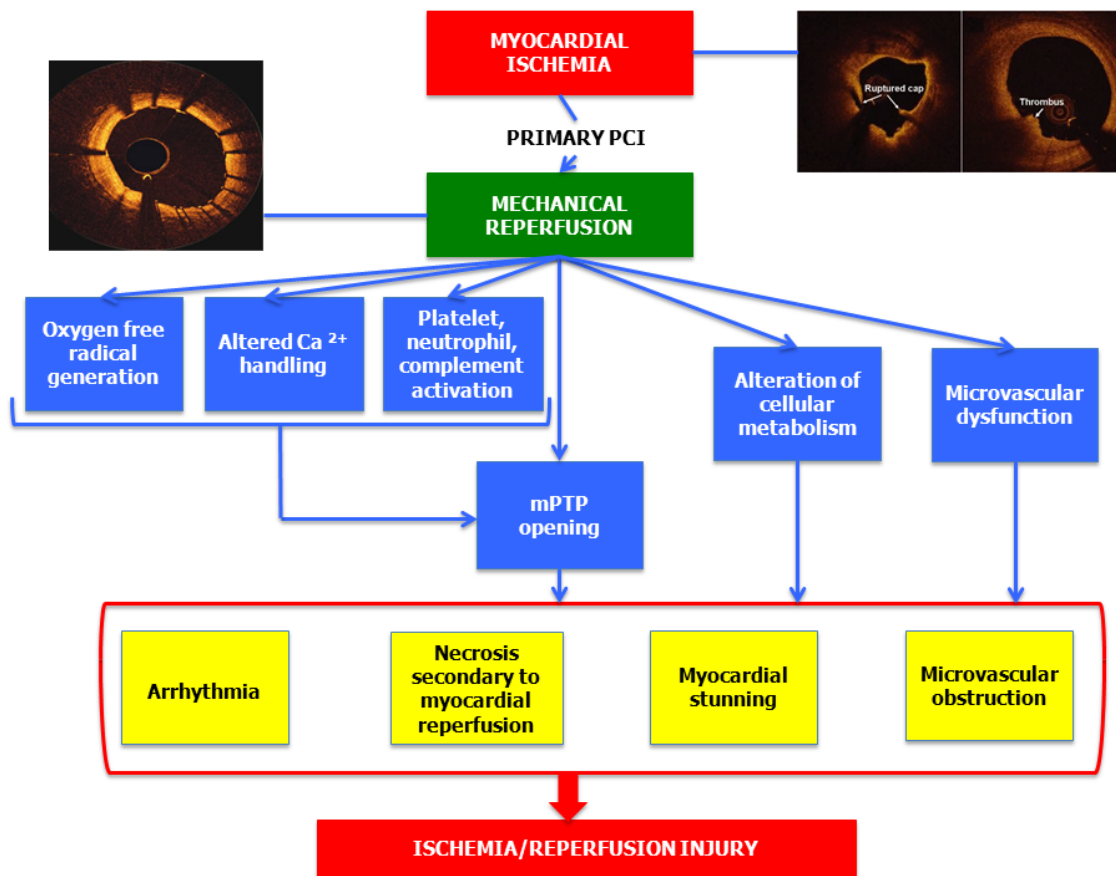
Figure 12 – Ischemia-reperfusion injury during acute myocardial infarction [142].

4.1.1 mPTP structure

4.1.1.1 Core components of the mPTP (Figure 13)

It has been widely accepted that the permeability of the mitochondrial inner membrane is extremely low; thus, the discovery of a nonspecific permeability transition with a threshold of 1.5 kDa suggested the existence of a pore that was responsible for this transition [143].

The initial clue for the existence of the mPTP came from the very early studies of Haworth and Hunter, which suggested that a hydrophilic channel was responsible for the permeability transition induced by polyethylene glycol (PEG) polymers of size up to 1.5 kDa [144]. This idea was confirmed by Crompton and Costi in 1988, who showed how, in its opened state, the mPTP channel should obtain a diameter of 2–2.6 nm [145]. Later electrophysiological studies performed by Zoratti's group identified the putative mPTP as the giant channel that, at that time, was known as the mitochondrial megachannel [146,147].

The initial evidence about the sensitivity of the mPTP to ADP and to the adenine nucleotide transporter (ANT) inhibitor atractyloside suggested a role for the ANT in the regulation of mPTP, and this finding was further supported by several other studies that involved identifying MPT sensitivity to other ANT ligands such as bongkrekic acid, palmitoyl-CoA and carboxy-atractyloside [148].

This idea was confirmed in a study by Halestrap and Davidson, who clearly displayed the correlation between ADP, ATP, bongkrekic acid and carboxy-atractyloside with Ca^{2+}-induced MPT induction or in combination with cyclosporine A, an already well-known MPT inhibitor at that time [52]. Furthermore, in this initial study, Halestrap and Davidson proposed for the first time, a model for the mPTP structure that involved the conformational state of the ANT and its interaction with the CsA target mtCypD. This model was supported by observations indicating that reconstituted ANT generates oligomers with properties analogous to the mPTP in artificial membranes [149].

Shortly thereafter, electrophysiological studies proposed that two molecules of the voltage-dependent anion channel (VDAC) were components of the mPTP. The involvement of the VDAC in the mPTP structure suggested that it might not be a common pore but rather a more complex and highly organized structure that included contact sites between the inner mitochondrial membrane (IMM, where the MPT actually occurs) and the outer mitochondrial membrane (OMM, where the VDAC is located).

This concept was demonstrated in 1996 by Brdiczka's group, who observed the existence of a protein complex that included the VDAC, ANT, hexokinase I (HK) and creatine kinase (CK, in its octameric form), and that displayed MPT activities when reconstituted in liposomal vesicles [150].

Due to its pharmacological properties, a protein of particular relevance for solving the molecular identity of the mPTP was mtCypD. mtCypD can be inhibited by CsA, which has similar but opposite binding sensitivities to Ca^{2+} and ADP. Additionally, mtCypD was shown to bind both the VDAC and the ANT [151]. The generation of transgenic mice lacking the peptidylprolyl isomerase f (ppif) gene confirmed that mtCypD is the protein element of mPTP that confers sensitivity to CsA [152]. Nonetheless, mtCypD is a mitochondrial matrix protein; thus, it is unable to generate a pore, and its depletion does not deny the existence of an MPT but rather dramatically increases the threshold for Ca^{2+} induction [153].

However, two different studies based on knockout animal models challenged this model. The first study was performed using ANT1 and ANT2 double-knockout mice, and it demonstrated that the MPT occurs despite the loss of the ANT, even though these mice exhibit a loss of sensitivity to ANT inhibitors (bongkrekic acid or atractyloside) and a reduction in the Ca^{2+}

threshold for mPTP opening [154]. The second study performed by Molkentin's group was based on a triple VDAC knockout model, which did not display any significant differences in either the Ca^{2+} threshold for mPTP induction or in cell death in response to various types of stimuli [155]. These findings prompted a reconstruction of the structural mPTP model. It has long been known that inorganic phosphate sensitizes the MPT pore, suggesting that the mPTP could possess a Pi-binding site. Inorganic phosphate is transported to the mitochondrial matrix by the mitochondrial phosphate inorganic carrier (PiC). In support of this concept, Leung and colleagues determined that the PiC interacts with mtCypD and the ANT [156]. Furthermore, this interaction is strengthened by MPT-inducing agents, whereas MPT-blocking compounds diminish this interaction. In the same year, based on a genetic screen, another group determined that PiC overexpression induces mitochondrial dysfunction and apoptosis [157]. These results, together with the earlier finding that a nonspecific pore is generated in liposomes by reconstituting the PiC, identified PiC as a strong candidate for the core-forming element of the mPTP. This idea was well accepted until last year, when the same group performed PiC silencing experiments and found that knockdown of up to 70% of this carrier does not lead to any significant alteration in the Ca^{2+} threshold for the MPT, suggesting that either a small amount of PiC is required in the mPTP structure or that PiC is not a component of this structure [158]. Identifying what variables could generate the differences observed by these studies could be difficult, but overall, they confirm that PiC should not be considered a structural component but rather a minor regulator of the mPTP.

4.1.1.2 mPTP regulatory elements

Although the minimal structure required for mPTP activity is uncertain, a plethora of mPTP regulators have been identified. One of the first regulators to be discovered was the mitochondrial translocator protein (TSPO), an 18-kDa protein that is localized in the OMM. The interactions of TSPO with the VDAC and the ANT indicate that it is a possible component of the mPTP, and this hypothesis was supported by Sileikyte and co-workers in 2011 [159]. The effects of TSPO on mPTP activity remain controversial because opposite outcomes have been observed for some of its ligands (as RO5-4864 and PK11195) in different studies [160,161]. Of note, TSPO ligands have been shown to display pro-apoptotic effects, even during TSPO silencing, which likely results from the expression of other benzodiazepine receptors. Recently, Sileikyte and co-workers updated their findings in mouse liver through the use of a conditional TSPO KO. In this study, they indicated that TSPO is not a requirement for the OMM to regulate the MPT, but can exert only minor regulatory effects [162].

The crucial importance of the MPT in cell death is indicated by the participation of Bcl-2 family members in the formation of the mPTP. Bax and Bak are well known pro-apoptotic members of the Bcl-2 family that translocate to the OMM to induce mitochondrial depolarization and cytochrome c release, even in isolated mitochondria, which implicates the involvement of Bax and Bak in the formation of the mPTP. In 1998, two independent groups demonstrated that both proteins interact with the mPTP to induce the MPT and release of cytochrome c, and these studies indicated that this process requires cooperation with the ANT [163,164]. These data were confirmed by Molkentin's group, who used genetic background knockout models for Bax and Bak [165]. Molkentin's group proposed that regulation of the MPT by Bak and Bax is dependent on their ability to permeate the OMM, representing a minimal requirement for the induction of mitochondrial swelling and occurs independent of the ANT. In the future, this model should be validated using an ANT knockdown model. During their stimulation, Bax and Bak can also increase the amount of free Ca^{2+} in the mitochondrial matrix (by promoting Ca^{2+} flux into the mitochondrial matrix) to trigger the MPT. Furthermore, Bad, which is a pro-apoptotic member of the Bcl-2 family, has been shown to induce the MPT in isolated mitochondria in a Bax- and Bak-independent manner [166]. In addition to these findings, anti- apoptotic members of the Bcl-2 family have been shown to modify MPT activity. For example, Bcl-2 and Bcl-XL have been shown to interact with the ANT and the VDAC, respectively [167,168].
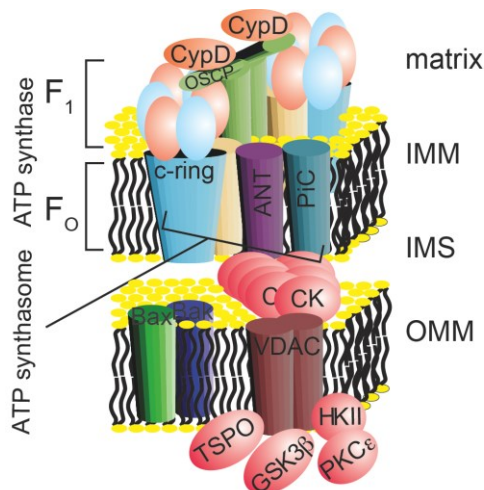
Figure 13 – Novel model of mPTP structure [142].
The present model for mPTP is built around F1/FO ATP synthase superstructures (involving the ANT and PiC) that directly interact with the main mPTP regulator CypD. The c-ring of the ATP synthase acts as the pore of the mPTP. The model spans from the inner mitochondrial membrane (IMM) to the outer mitochondrial membrane (OMM) by interactions with the VDAC, Bax and Bak, and CK oligomers in the intermembrane space (IMS). Finally, the complex is surrounded by regulatory elements, as protein kinase C epsilon (PKCε), glycogen synthase kinase 3-beta (GSK3-β) and mitochondrial translocator protein (TSPO) are involved.

4.1.2 The critical role of the ATP synthase c-subunit in mPTP function

ATP synthase displays a series of characteristics upstream of its regulation that resemble those of the mPTP. First, the hydrolytic activity of ATP synthase is strongly inhibited by the concurrent binding of two mPTP inhibitors, namely, ADP and Mg^{2+}, to its catalytic site, the so called Mg-ADP block, but the mPTP inducer Pi has been proposed to abolish this block. Second, two different cysteine residues (C294 in the alpha subunit and C103 in the gamma subunit) may be linked by a disulfide bridge during oxidative stress, thereby impeding ATP synthase activity [169]. Furthermore, the ATP synthase complex forms a supercomplex with the ANT and PiC, both of which have been proposed as components of the mPTP, and this complex is referred to as the ATP synthasome [170]. In 2009, mtCypD, another regulatory component of the mPTP, was shown to interact with the peripheral stalk of ATP syn- thase, particularly the oligomycin sensitivity conferring protein (OSCP) and d subunits. These interactions result in reduced catalytic activity (both hydrolase and synthase) that can be restored by displacing mtCypD with CsA [171]. Finally, anti-apoptotic Bcl-XL, a known MPT inhibitor, interacts with ATP synthase and promotes its synthetase activity [172]. Physiological studies also suggest a correlation between ATP synthase and the mPTP. The c-ring-selective inhibitor, oligomycin, prevents both tumor necrosis factor alpha (TNFα) and Bax-induced MPT and cell death. Recently, we identified the c subunit of the mitochondrial ATPase as a fundamental regulator of mPTP activity [133,173]. Of all the subunits that compose the Fo complex, the a, b and c subunits are sufficient to facilitate the translocation of protons across lipid bilayers, and these subunits are highly evolutionarily conserved. It has recently been shown that Rho0 cells, which lack mitochondrial DNA, are equipped with a functional mPTP [174]. This finding excludes a role for the a subunit of the mitochondrial ATP synthase in the mPTP. Furthermore, conductive properties have only been ascribed to the c subunit [175], and a peptide displaying a consistent degree of similarity to the c subunit has been proposed as a putative regulator of the mPTP, thus indicating that the c subunit is the best candidate for a pore component. Furthermore, we found that silencing c subunit expression completely blocks MPT induction by Ca^{2+} and oxidants, whereas c subunit over-expression dramatically enhances MPT induction. Silencing the c subunit does not affect ATP synthesis, suggesting that MPT inhibition is not due to the accumulation of ADP in the mitochondrial matrix. Furthermore, silencing α subunit expression does not lead to any significant alteration in MPT activity, suggesting that the c subunit of the mitochondrial ATP synthase is a central component of the mPTP. In support of our results, it has been recently reported that the isolated c subunit induces the MPT in isolated mitochondria and forms ion channels in artificial bilayer membranes. Furthermore, this activity is stimulated by Ca^{2+}, inhibited by

CsA and dependent on the phosphorylation state of the c subunit [176]. Nonetheless, it has yet to be validated that c-rings exist on the outside of ATP synthase, leaving the c-ring unoccupied by the central stalk and thus available to generate currents in vivo.

4.1.3 Biochemical events leading to mPTP opening during ischemia and reperfusion

The effects of ROS and Ca^{2+} on MPT have been widely reported as key players during ischemia and reperfusion damage [56,177]. During ischemia (the MPT-priming phase), the accumulation of factors, including Ca^{2+}, long-chain fatty acids and ROS, progressively increases the susceptibility to MPT, thus increasing the likelihood that MPT will occur upon reperfusion (the MPT-activating phase) [178]. Indeed, the conditions that occur during ischemia and reperfusion are identical to those that induce mPTP opening. During ischemia, increased glycolysis causes the accumulation of lactic acid and the reduction of pH. To restore the pH, the Na^+/H^+ antiporter is activated, but it acts inefficiently because Na^+ cannot be pumped out of the cell, as the Na^+/K^+ ATPase is inhibited by the absence of intracellular ATP. Consequently, the cytosolic Ca^{2+} concentration increases because the activity of the Na^+/Ca^{2+} antiporter is reduced or reversed. In addition, during ischemia, there is a decrease in the adenine nucleotide concentration, which is associated with an increased phosphate concentration, thereby sensitizing mPTP opening in response to Ca^{2+}; however, low pH inhibits mPTP opening. If the period of ischemia is prolonged, the heart becomes irreversibly damaged due to the activity of degradative enzymes, such as phospholipases and proteases, which also compromise mitochondrial function [179].

Upon reperfusion, the mitochondria recover their ability to respire and rescue the sustained mitochondrial membrane potential, which is required for ATP synthesis. However, the mitochondrial membrane potential is the driving force for mitochondrial Ca^{2+} uptake, thus leading to Ca^{2+} overload. In addition, rapid and extensive production of ROS occurs when the inhibited respiratory chain is re-exposed to oxygen. Thus, the following resulting conditions are nearly optimal for mPTP opening: high Ca^{2+} levels within the mitochondrial matrix, increased levels of phosphate and oxidative stress, depletion of adenine nucleotide concentration, and rapid return of the pH to a physiological value [180,181].

After ischemia and reperfusion, the fate of the cell is determined by the severity of the damage as follows: if the damage is minimal, the cell may recover; if the damage is moderate, the cell may undergo apoptosis; and if the damage is severe, the cell may die from necrosis due to inadequate energy production. Thus, mitochondria serve as an arbiter of cell fate in response to stress [77].

4.1.4 Clinical studies examining pharmacological agents to reduce IRI

Considering the pivotal role of the mPTP in IRI during STEMI, many studies have focused their attention on pharmacological agents that modulate mPTP opening. Currently, a limited number of these agents act directly on mPTP and/or its components. Contrarily, the majority of these agents are able to influence biological parameters (e.g., ROS, pH and PI signaling pathways) that indirectly modulate the final stage of mPTP opening. Finally, several strategies of ischemic pre- and post- conditioning have been developed and studied to reduce IRI during STEMI [182].

4.1.4.1 Agents directly targeting mPTP

One of the most promising results in cardioprotection has been reported by Piot et al. using CsA [183]. Since the 1990s, it has been known that CsA inhibits mPTP opening by binding to mtCypD, a mitochondrial isomerase that binds to subunits b, d and O in the lateral stalk of the F1-Fo ATPase. Studying 58 patients, Piot el al. examined the effect of administration of an intravenous bolus of 2.5 mg/kg CsA to patients experiencing STEMI immediately before undergoing PCI by measuring the release of myocardial-specific enzymes and performing magnetic resonance imaging (MRI) on the infarcted heart within the fifth day after reperfusion. The results confirmed the cardioprotective effect of CsA and showed a significantly reduced overall infarcted area in the group treated with CsA compared with the control group [183]. Despite the hopeful findings from previous study and in vivo animal research, more recently, two randomized trials based on the investigation whether CsA improve ST-segment resolution and prevent adverse left ventricular remodeling at 1 year, failed: the CYCLosporinE A in reperfused acute myocardial infarction (CYCLE) phase III clinical trial and CIRCUS phase II study [184,185] (for details see [186-190]). The role of CsA in cardioprotection has also been tested in cardiac surgery and after coronary artery bypass graft and after aortic valve surgery. In the first study, Haunseloy et al. demonstrated that a single intravenous bolus of CsA (2.5 mg/kg) administered prior to CABG surgery reduced the extent of perioperative myocardial injury, with a reduced postoperative cardiac troponin T rise by 0.03 ng/ml for every 10 min, when compared with the control (p=0.049) [191]. Additionally, in the setting of aortic valve surgery, the administration of CsA demonstrated a beneficial effect in reducing RI that was expressed as a 35% reduction in the area under the curve of cardiac troponin I compared with the control group (p=0.03) [55]. 3,5-Seco- 4-nor-cholestan-5-one oxime-3-ol (TRO40303) is an mPTP modulator that binds to the mitochondrial translocator protein at its cholesterol site, which results in reduced release of apoptosis-inducing factors into the cytosol after ischemia and reperfusion [192]. This new drug was under evaluation in the MITOCARE trial to test whether its injection reduces IS, as measured via both cardiac

biomarker release and MRI within the fifth day after primary PCI [193], but in 2015 it failed [194] (see discussion section for further considerations).

4.1.4.2 Agents indirectly targeting the mPTP

Many other substances that indirectly target the mPTP have been tested. Among the most interesting drugs that have been studied are exenatide, atrial natriuretic peptide, and glucose-insulin-potassium (GIK). Exenatide is an analog of glucagon-like peptide 1 (GLP-1), and a post hoc study has demonstrated that this substance reduces the final IS by 30% in patients experiencing STEMI and thrombolysis in MI (TIMI) flow grades of 0 or 1 based on angiogram [195]. However, this benefit was limited to patients with a rapid symptom onset to balloon time (≤132 min). The beneficial effect of atrial natriuretic peptide has been evaluated in a small, randomized trial [196]. This study enrolled patients experiencing acute MI who received PCI, and the atrial natriuretic peptide was administered as an adjunctive treatment (compared to placebo). The authors showed that the patients receiving atrial natriuretic peptide exhibited a 14.7% reduction in the IS (95% CI, 3.0%–24.9%) and a significant increase in the LV ejection fraction after 6–12 months. The effect of atrial natriuretic peptide on mPTP is most likely due to inactivation of GSK3-β [196]. Despite promising preliminary results (generally using animal models), randomized studies using other pharmacological agents have failed to demonstrate a clear benefit in reducing IRI or mortality (Table 1). Yellon et al. described the cardioprotective role of reperfusion injury survival kinase (RISK) and survivor-activating factor enhancement (SAFE), which are two pro-survival kinase pathways that converge on the mitochondria to reduce mPTP opening [197]. Accordingly, some authors have speculated that a GIK solution exerts a cardioprotective effect by modulating pro-survival kinase pathways via the GIK receptor, which is a G protein-coupled receptor [198]. Nevertheless, no clinical benefit has been observed in a confirmatory randomized clinical trial (Table 1) [199]. Finally, a new substance, namely Bendavia was under evaluation until a few months ago. Bendavia is a peptide that interacts with cardiolipin in the IMM to reduce ROS production and maintain the efficiency of the electron transport chain during reperfusion [200]. The principal aim of the EMBRACE trial was to demonstrate that Bendavia injection reduce infarct size, as assessed by analyzing cardiac biomarker release and MRI [200]. Among subjects with first-time anterior STEMI who undergo successful PCI, administration of MTP-131 was safe and well tolerated, but treatment with MTP-131 was not associated with a decrease in myocardial IS [201].

Overall, the current available data regarding pharmacological agents acting directly or indirectly on the mPTP and IRI are limited. Few trials have demonstrated a net clinical benefit

but have been limited by a small sample size, the use of surrogate endpoints and extensive exclusion criteria.

As mentioned above, to evaluate the reduction in IS, all trials measured the biomarker levels, and the ejection fraction was determined based on echocardiography and magnetic resonance imaging. In the majority of cases, all patients underwent two MRI scans as follows: the first scan was performed within a week after primary PCI, and the second scan was performed at a follow-up visit. The measured parameters include the area at risk based on T2-weighted images, the final IS based on late-enhancement MRI sequences and the myocardial salvage index [(area at risk minus infarcted size)/area at risk] [202,203].

4.2 Results

Starting from several recent papers that claimed Csub to be the FoF1-ATP synthase and although assays in cell cultures from our and other groups prompted that the long-sought molecular pore of the mPTP could be the Csub [133,142,176,204,205], this protein has never been evaluated in humans and its presence and role in STEMI patients is unknown.

Thus, the first aim of this study was to investigate whether serum levels of Csub are detectable in STEMI patients and whether they are associated with surrogate endpoints of reperfusion. Secondly, to investigate whether Csub expression in fibroblasts from skin biopsy of STEMI patients is associated to mitochondrial parameters [220] and magnetic resonance index of IRI. Results were obtained in strictly collaboration with Prof. Gianluca Campo (U.O. Cardiologia, Cardiovascular Institute, Azienda Ospedaliero-Universitaria di Ferrara, University of Ferrara) and collaborators.

4.2.1 Csub values in controls and STEMI patients

Table 2 shows baseline characteristics and Csub serum levels in the study groups. These were properly matched for age, sex and cardiovascular risk factors. Csub levels were detectable in the serum. Csub was significantly higher in controls as compared to STEMI patients (p=0.008). On the contrary, TIM 14 serum levels were higher in STEMI patients than in controls (p=0.01) (Table 2). As a consequence, Csub/TIM 14 ratio is significantly lower in STEMI patients vs. controls (p=0.002) (Table 2).

Variables	Controls (n=31)	STEMI (n=32)	p
Age, (years)	62±10	63±9	0.3
Men, no. (%)	22 (71)	23 (72)	0.8
BMI, (kg/m2)	27.2±5	27.3±4	0.9
Cardiovascular risk factors, no (%)			
Diabetes,	5 (16)	6 (18)	0.7
Hypertension,	22 (71)	21 (65)	0.4
Current Smoker,	17 (54)	16 (50)	0.5
Hyperlipidemia,	18 (58)	18 (56)	0.9
Family History for IHD,	8 (25)	7 (22)	0.6
Laboratory			
WBC, (u/mm3)	6±3	9.3±4	0.01
Haemoglobin, (g/dl)	13.6±2	13.2±2	0.5
Platelets, (u/mm3)	230 [180-260]	225 [182-265]	0.8
Creatinine, (mg/dl)	1±0.2	1±0.3	0.9
CrCl, (ml/min)	77±10	76±13	0.8

CK-MB at peak, (ng/ml)	2.2 [1-3.1]	97 [48-227]	<0.0001
Troponin T at peak, (ng/ml)	0.008 [0.006-0.009]	1.8 [0.6-4.6]	<0.0001
C subunit, (%)	10.3 [7.2-15]	6.5 [3.9-10]	0.008
TIM 14, (%)	21 [18-25.5]	31 [23-43.1]	0.01
Ratio C subunit/TIM 14,	0.468 [0.28-0.57]	0.165 [0.13-0.32]	0.002

Table 2 – Characteristics and Csub levels of study population groups.
BMI: body mass index. WBC: white blood cells. CrCl: creatinine clearance.

4.2.2 Csub values in STEMI patients and relationship with cardiac markers release

From June 2013 to January 2015, 625 patients were admitted to our centre with STEMI and treated with primary PCI (see Materials and Methods). Overall, 158 (25%) respected all criteria and were enrolled (Table 3). Circulating Csub was not normally distributed (mean: 7.5±5.7%; median 6.3% [4-9.3%]; range 1.1-47.5%). Out of all variables reported in Table 3, there was only a weak inverse correlation between age and Csub serum levels (R=-0.16, p=0.04). None of the variables of Table 3 was related to TIM 14 values (mean: 32±22%; median 29.5% [18.3-42%]; range 9.5-134%). The Csub/TIM 14 ratio was not normally distributed (median: 0.221 [0.149-0.34]; range 0.014-1.059), and it was related only to age (R=-0.21, p=0.006). There was a significant relationship between Csub and troponin and CK-MB at peak (R=0.64, p<0.001; R=0.62, p<0.001, respectively). Patients with Csub levels above the median value, as compared to those below, showed significantly higher troponin T and CK-MB values (Figure 14A and Table 4). This was confirmed also after the stratification of study population according to median value of ratio Csub/TIM 14 (Figure 14B and Table 4). The median values of troponin T and CK-MB AUC were 6.4 [2.4-19] and 279 [100-682], respectively. At univariate analysis, only symptom-balloon time and first medical contact-balloon time together with Csub predicted troponin T AUC above the median value. After multivariable analysis, Csub emerged as independent determinant (HR 1.53, 95%CI 1.26-1.86 as single change unit, p=0.0005). Repeating similar analysis with CK-MB AUC, Csub confirmed its predictive role (HR 1.65, 95%CI 1.35-2 as single change unit, p<0.0001).

Variables	All (n=158)	C subunit below median value (n=79)	C subunit above median value (n=79)	p
Age, (years)	63±11	65±11	62±10	0.3
Men, no. (%)	119 (75)	61 (77)	58 (74)	0.3
BMI, (kg/m2)	27±4	27±4	27.5±4	0.7

Cardiovascular risk factors, no. (%)				
Diabetes,	22 (14)	9 (11)	13 (16)	0.2
Hypertension,	112 (71)	54 (68)	58 (73)	0.5
Current Smoker,	86 (55)	41 (52)	45 (57)	0.6
Hyperlipidemia,	89 (56)	46 (58)	43 (54)	0.7
Family History for IHD,	36 (23)	20 (25)	16 (20)	0.2
Laboratory,				
WBC, (u/mm3)	9.3±4	9.2±4	9.4±4	0.8
Haemoglobin, (g/dl)	13±2	13±2	13.1±2	0.9
Platelets, (u/mm3)	225 [182-270]	225 [180-268]	225 [185-270]	0.8
Creatinine, (mg/dl)	1±0.2	1±0.3	1±0.3	0.9
CrCl, (ml/min)	78±15	77±14	79±13	0.7
Angiographic data,				
Multivessel disease, no. (%)	82 (52)	44 (55)	38 (48)	0.1
Proximal LAD, no. (%)	81(51)	41 (52)	40 (50)	0.9
Mid LAD, no. (%)	77 (49)	38 (48)	39 (50)	0.9
Pre-dilatation, no. (%)	79 (50)	39 (50)	40 (50)	0.6
Manual thrombectomy, no. (%)	65 (41)	33 (42)	32 (40)	0.5
DES, no. (%)	129 (81)	64 (81)	65 (82)	0.9
Stent diameter, (mm)	3 [3-3.5]	3 [3-3.5]	3 [3-3.5]	0.9
Stent length, (mm)	24±8	24±8	25±8	0.8
Post-dilatation, no. (%)	34 (21)	18 (23)	16 (20)	0.5
Symptom-balloon time, (min)	128 [93-200]	130 [90-200]	125 [95-190]	0.6
FMC-balloon time, (min)	83±42	85±40	80±42	0.5
Procedural therapy, no. (%)				
Unfractioned heparin,	140 (88)	69 (87)	71 (89)	0.8
Bivalirubin,	18 (12)	10 (13)	8 (11)	0.7
GP IIb/IIIa inhibitors,	31 (19)	15 (19)	16 (20)	0.8
Morphine,	21 (13)	10 (12)	11 (14)	0,8
Nitrates,	15 (9)	8 (10)	7 (9)	0.8
Therapy at discharge, no. (%)				
Aspirin,	158 (100)	79 (100)	79 (100)	0.9
P2Y12 inhibitors,	158 (100)	79 (100)	79 (100)	0.9
- clopidogrel	33 (21)	16 (20)	17 (21)	0.8
- prasugrel	21 (13)	11 (14)	10 (13)	0.8
- ticagrelor	104 (66)	52 (66)	52 (66)	0.9
ACE inhibitors,	131 (83)	64 (81)	67 (85)	0.6
β-blockers,	137 (87)	66 (83)	71 (89)	0.3
Statins,	155 (98)	78 (99)	77 (97)	0.8

Table 3 – Characteristics of STEMI patients stratified according Csub median value.

LAD: left anterior descending. DES: drug eleuting stent. FMC: first medical contact. ACE: angiotensin-converting enzyme.

A
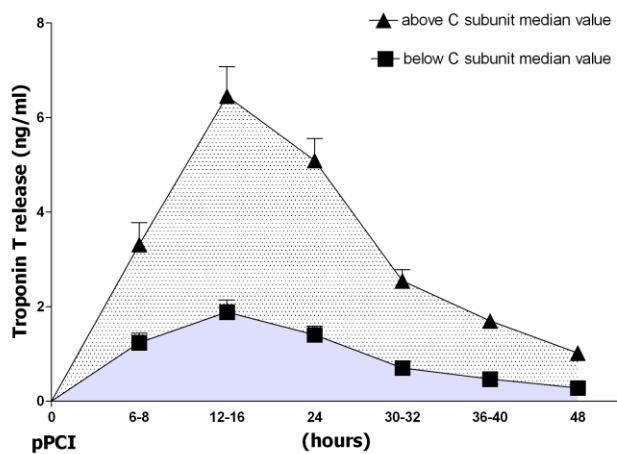
B
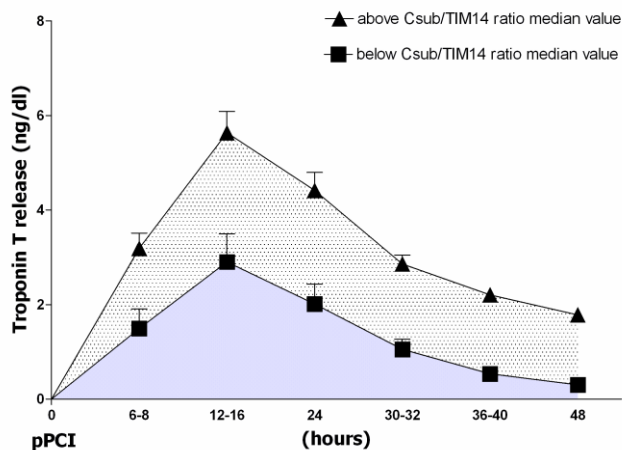
Figure 14 – Assessment of infarct size by troponin T release.
A: study population stratified according median value of Csub. B: study population stratified according median value of C subunit/TIM 14 ratio. TIM: translocase of inner membrane. pPCI: primary percutaneous coronary intervention. Squares and triangles denote mean values. T bars denote standard error.

4.2.3 Csub values in STEMI patients and relationship with ST-segment resolution

At the end of PCI, ST-segment resolution was classified as no/absent, partial, and complete in 47 (30%), 54 (34%) and 57 (36%) patients, respectively. Complete ST-segment resolution was significantly higher in patients with C subunit below the median value (p=0.008) (Table 4). After multivariable analysis, Csub emerged as independent determinant of complete ST-segment resolution (HR 0.8, 95%CI 0.69-0.94 as single change unit, p=0.007). Ninety minutes after the end of PCI, ST-segment resolution was no/absent, partial, and complete in 39 (25%), 54 (34%) and 65 (41%) patients, respectively. Even at this time, complete ST-

segment resolution was significantly higher in patients with C subunit below the median value (p=0.04) (Table 4) and Csub emerged as independent predictor (HR 0.83, 95%CI 0.72-0.98 as single change unit, p=0.03). Similar results were observed after stratification of C subunit serum levels in tertiles (Figure 15A and 15B). TIM 14 values were not related to ST-segment resolution, whereas Csub/TIM 14 ratio was (Table 4).

Variables	C subunit below median value (n=79)	C subunit above median value (n=79)	p	C subunit/TIM 14 below median value (n=79)	C subunit/TIM 14 above median value (n=79)	p
Cardiac markers, (ng/ml)						
CK-MB at peak,	48 [21-103]	245 [102-345]	<0.0001	70 [30-132]	159 [67-303]	<0.0001
CK-MB AUC,	129[58-279]	650 [294-900]	<0.0001	172 [88-379]	452[190-927]	<0.0001
Troponin T at peak,	1 [0.5-2.1]	5.2 [2.3-8.4]	<0.0001	1.5 [0.7-3.9]	3.8 [1.6-7.9]	<0.0001
Troponin T AUC,	2.7 [1.5-82]	15 [7.4-23]	<0.0001	3.8 [2-12]	12 [4.8-21]	<0.0001
ST-segment resolution, no. (%)						
-At the end of PCI						
No/absent,	19 (24)	28 (36)		19 (24)	28 (35)	
Partial,	21 (26)	33 (42)	0.001	27 (34)	27 (34)	0.05
Complete,	40 (50)	17 (22)		33 (42)	24 (30)	
-90' after PCI						
No/absent,	12 (15)	27 (35)		13 (16)	26 (33)	
Partial,	27 (34)	27 (34)	0.006	30 (38)	24 (30)	0.03
Complete,	41 (51)	24 (31)		36 (46)	29 (37)	
Echocardiography,						
-At hospital discharge						
LVEF, (%)	48±9	44±9	0.005	48±10	45±9	0.1
WMSI,	1.5 [1.25-1.75]	1.65 [1.3-1.9]	0.05	1.5 [1.25-1.75]	1.6 [1.25-1.8]	0.2
-At 6 months						
LVEF, (%)	53±10	43±6	0.001	51±10	43±10	0.05
WMSI,	1.3 [1.2-1.61]	1.7 [1.4-1.9]	0.03	1.4 [1.2-1.7]	1.6 [1.3-1.9]	0.1
Adverse events, no. (%)						
Death,	1 (1.2)	3 (3.7)	0.3	1 (1.2)	3 (3.7)	0.3
ACS,	2 (2.5)	2 (2.5)	0.9	1 (1.2)	3 (3.7)	0.4
HF,	1 (1.2)	5 (6.3)	0.1	1 (1.2)	5 (6.3)	0.1
Death and ACS,	2 (2.5)	4 (5)	0.3	1 (1.2)	6 (7.5)	0.08
Death and HF,	1 (1.2)	7 (8.8)	0.04	1 (1.2)	7 (8.8)	0.04

Table 4 − Endpoints of the study in STEMI patients.

WMSI: wall motion score index. ACS: hospital readmission for acute coronary syndromes. HF: hospital readmission for heart failure.

A

B
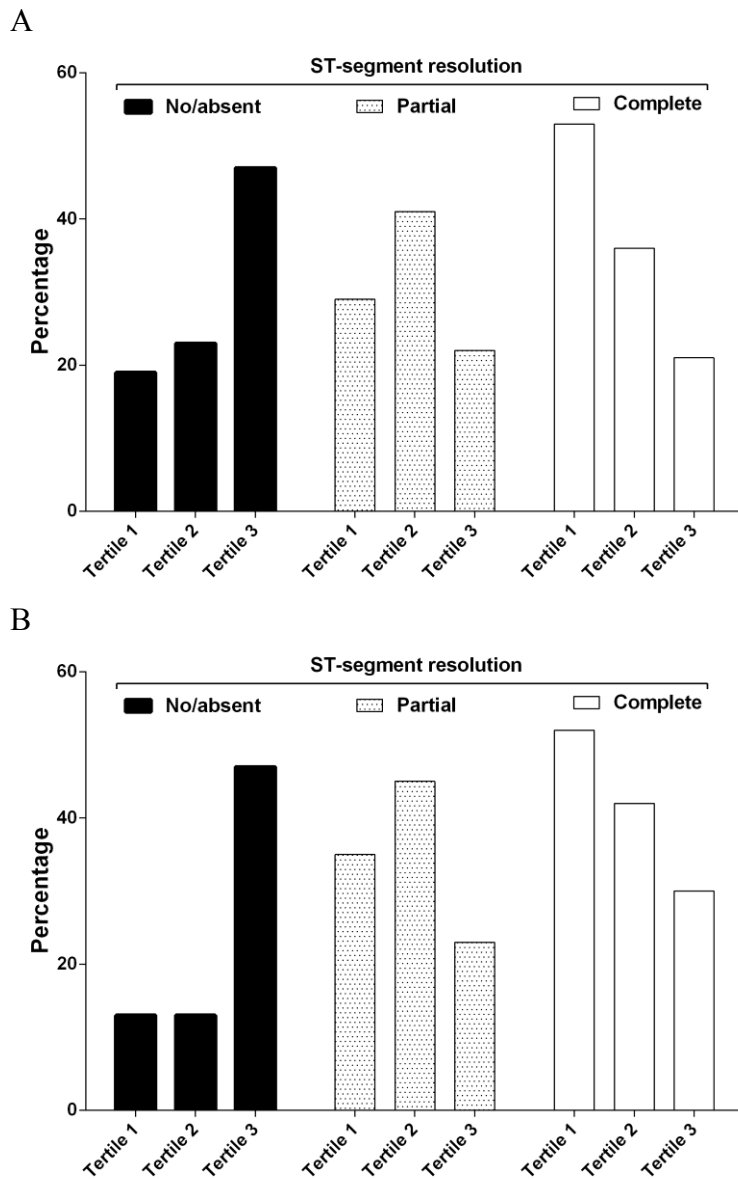
Figure 15 - ST-segment resolution.
A: as assessed at the end of the PCI. B: as assessed 90 minutes after the end of PCI. PCI: percutaneous coronary intervention.

4.2.4 Csub values in STEMI patients and relationship with echocardiographic data and clinical outcome

Table 4 also shows echocardiographic data. Both LVEF and WMSI were poor in patients with C subunit above the median value (Table 4). At 6 months, we observed 4 (2.5%) deaths, 4 (2.5%) and 6 (3.8%) hospital readmission for ACS and/or HF. The cumulative occurrence of death and HF was significantly higher in patients with C subunit or C subunit/TIM 14 ratio above the median value (Table 4).

4.2.5 Csub expression in fibroblasts and relationship with mPTP activity and MSI index

In addition, in a pilot study of 11 patients undergoing coronary revascularization we assessed Csub expression and the mPTP activity in skin fibroblasts. Preliminary data confirmed that there is a significant correlation between Csub cellular levels and mPTP activity (Pearson r=-0.71; p=0.0149) (Figure 16). Finally, the activity of mPTP resulted highly correlated with one of the most common clinical reperfusion end point such as the MSI (Pearson r=0.82; p=0.0021) (Figure 17).
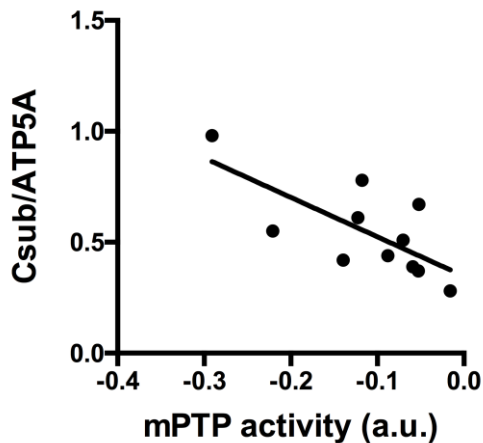
Figure 16 – Mitochondrial parameters measurements.
Analysis of correlation between Csub expression in cell lysates from skin fibroblasts and mPTP activity in those cells from the same patients. Pearson r=-0.71; p value=0.0149. ATP5A=mitochondrial loading control; a.u.=arbitrary units.
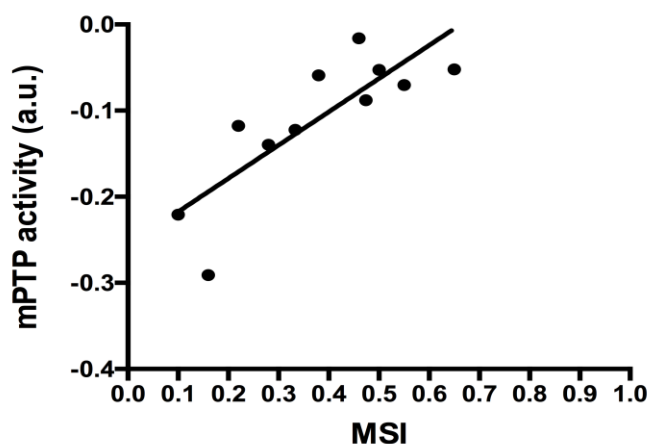
Figure 17 – Analysis of correlation between mPTP activity in fibroblast cells and MSI from magnetic resonance of the same patients.
Pearson r=0.82; p value=0.0021. MSI=myocardial salvage index; a.u.=arbitrary units.

4.3 Discussion

At the best of our knowledge, this is the first study showing that F_o-ATP synthase C subunit is: i) detectable in serum of both controls and MI patients; ii) lower in MI patients than in

controls; iii) highly related to surrogate markers of RI; iv) strongly related to mPTP activity in intact cells and v) in turn mPTP activity showed significant correlation with MSI. Despite a large number of cardioprotective strategies has been proposed to reduce RI in experimental animals, their translation and application into the clinical setting has been largely disappointing [140,206]. Recently, two randomized clinical trials targeting mPTP, the first with TRO40303 and the second with cyclosporine, failed [184,194]. The reasons for this failure are multiple [207,208]. The incomplete knowledge of mPTP could also be the cause of such fail. It has been suggested that mitochondrial ATP synthase arranges in a super-complex with ANT and PiC to form an ATP synthasome [142,205]. Under favorable circumstances, such as those occurring during reperfusion, the Csub ring is rearranged and becomes the pore of the mPTP [142,172,176]. Accordingly, Csub depletion considerably reduced mPTP opening by Ca^{2+} and ROS, whereas Csub over-expression enhanced mPTP opening [133]. We found that Csub is measurable in serum from subjects with cardiovascular risk factors, but not clinical manifestation of coronary artery disease. Consistent with a previous study in isolated perfused hearts from mice, Csub in humans correlates only with age [209]. Circulating Csub is present also in MI patients during the first hours after reperfusion, but its levels are lower. On the contrary, TIM 14 values are higher. TIM 14 is a constituent of the IMM and probably its increase reflects the ongoing myocardial necrosis. As consequence, Csub/TIM 14 ratio decreased from controls to STEMI patients. These results are unexpected and of difficult explanation. This is the first report of Csub in serum from humans. We are unable to explain where the measured Csub was generated from. Nevertheless, the differences in the serum values between controls and MI patients and the finding that Csub levels predicted IS suggest a possible link between acute event (myocardial infarction and reperfusion) in cardiomyocites and peripheral blood assessment. The lower levels in STEMI patients could reflect just a re-arranging of Csub to form mPTP in cardiomyocytes, or just a removal from the serum due to undefined mechanisms. Similarly, the dual opposite effects of Csub ATP production for cell life or mPTP generation for cell death is still not fully elucidated and could be involved in our observations. Csub is located at the centre of the energy-producing complex (mitochondrial respiration), but at the same time it may orchestrate the rapid onset of death through mPTP generation [204]. It is well known that macrophage cholesterol efflux is dependent on functionally respiring mitochondria and that ATP production and ATP availability for cholesterol efflux affect atherosclerosis development [210]. Increased Csub levels stimulate mitochondrial activity and ATP production [133]. We may speculate that individuals with higher Csub levels may show a slower insurgence of coronary atherosclerosis with a mechanism related to mitochondrial respiration, but independent on mPTP activity. On the contrary, at

the moment of acute event, high Csub levels are associated with an opposite effect, determining more mPTP generation, more RI and bigger IS. Clearly, these are speculations and further studies are needed to discover the significance of our findings. We found that circulating Csub is an independent predictor of IS, as measured by cardiac marker release. This finding is consistent with that of the other surrogate endpoints of RI. Csub levels in STEMI patients were significantly related to poor values of ST-segment resolution, LVEF and WMSI. Of course, our study is not powered for prognostic implication. Nevertheless, we observed a significant relationship with the occurrence of death and HF, being higher in patients with elevated Csub. This finding could be considered an indirect confirmation of experimental data suggesting that Csub is involved in RI and supports the hypothesis that Csub could be a good target for agents against RI (see Future perspectives). In-vitro/ex-vivo studies could help this point of view by clarifying the exact relationship between molecular events and the peculiarity of clinical outcomes in reperfusion injury upon PCI. In our pilot study of 11 patients we found that high Csub expression in fibroblasts was related to a greater open probability of the mPTP in that model (Figure 16). Moreover, the latter showed an intriguing link with myocardial salvage index (Figure 17). Indeed an increased activity of mitochondrial pore matches a poorer clinical outcome of the patient in term of MSI upon PCI as assessed by cardiac magnetic resonance (CMR). These data give consistency to the PTP as central player in reperfusion injury.

Study limitations.

This is the first attempt to validate in humans the possible relationship between Csub and RI. It follows that there are several limitations. First, the role of Csub in the mPTP has been previously investigated mainly in cell culture. Further validation in preclinical setting are clearly on demand [207,208]. Second, we assessed Csub at single time-point. Third, to minimize potential confounding factors, we applied restrictive inclusion and exclusion criteria selecting a highly homogenous study population. Finally, we are aware that CMR is the gold standard to assess IS [183]. On the other hand, CMR is expensive, time-consuming and its application on large number of patients may be difficult.

5. Future perspectives

5.1 Mcl-1 involvement in mitochondrial dynamics is associated with apoptotic cell death study

My first study entitled "*Mcl-1 involvement in mitochondrial dynamics is associated with apoptotic cell death*" was published online on November 4, 2015 in Molecular Biology of the Cell (MBoC). Mcl-1S ASO3 is now under trials in TT cell line (directly derived from the human medullary thyroid carcinoma) where Mcl-1L results over-expressed compared to control tissue (preliminary data not shown). Molecular aspects provided by this research could improve the reversion of the pathological phenotype of many cancers and the effectiveness in sensitizing cells to drugs currently in use without side effects. Moreover, we are creating a more stable form of Mcl-1S ASO3 in which its expression is able to be induced and with a tropism for a given organ.

5.2 The c subunit of F_oF_1-ATP synthase and the mPTP in the I/R injury study

My second study, started from the Csub analysis in blood samples from patients with STEMI is currently under review by a clinical journal, while the second part (Csub in cell samples) aims to confirm the roles of mitochondrial function and the Csub protein in IRI. The ultimate goal will be the definitively identification of the molecular mechanisms of reperfusion injury in man and discriminate new pharmacological targets for the development of cardioprotective drugs to be tested in future clinical trials. The failure of several studies, only recently [184,185], recommends that it is necessary to change the target of action. We believe this target could be represented by C subunit. For this purpose, our objectives can be summarized as follow:

- validation of cellular model: human cardiomyocytes will be tested for and compared to the experiments performed in Figures 16 and 17. This may enable the use of fibroblasts as a readily available cell source to study mitochondrial functions in patients enrolled. Cardiomyocytes will be collected from the atrium of patients undergoing surgical procedure (as approved by Ethics Committee in 2015) and skin biopsy;
- validation of the correlation between Csub expression and sensitivity to reperfusion injury. In order to identify the Csub levels as a new cardiovascular risk factor, preliminary data (Table 2 and Table 4) will be validated in a larger cohort of patients;
- identification of the Csub gene mutations that increase susceptibility to reperfusion injury. The evidence that the levels of Csub expression correlate with the damage of

the myocardium (see section 4.2) confirm the hypothesis that the genes coding for Csub can carry information relevant to the RI;

- demonstration of the advantages to use Csub as therapeutic target to inhibit mPTP by administering known selective inhibitors of the protein (particularly oligomycin, venturicidin A and DCCD). To convince the reader about this issue, in Figure 18A we report the PTP activity of living cells in control condition (black line) and upon Csub selective inhibitors Venturicidin A (red line) and DCCD (yellow line) pre-treatments. Both molecules desensitized mPTP opening as did the known inhibitor CsA (green line) upon stimulation with ionomycin. This results in a significant delay of mitochondrial depolarization if the pore is stimulated to open upon oxidative stress (Figure 18B);

- identification of new compounds capable of inhibiting the mPTP by targeting Csub. We will test a library of molecules designed against Csub and synthesized in collaboration with Dr. Claudio Trapella (Department of Chemical and Pharmaceutical Sciences of the University of Ferrara).

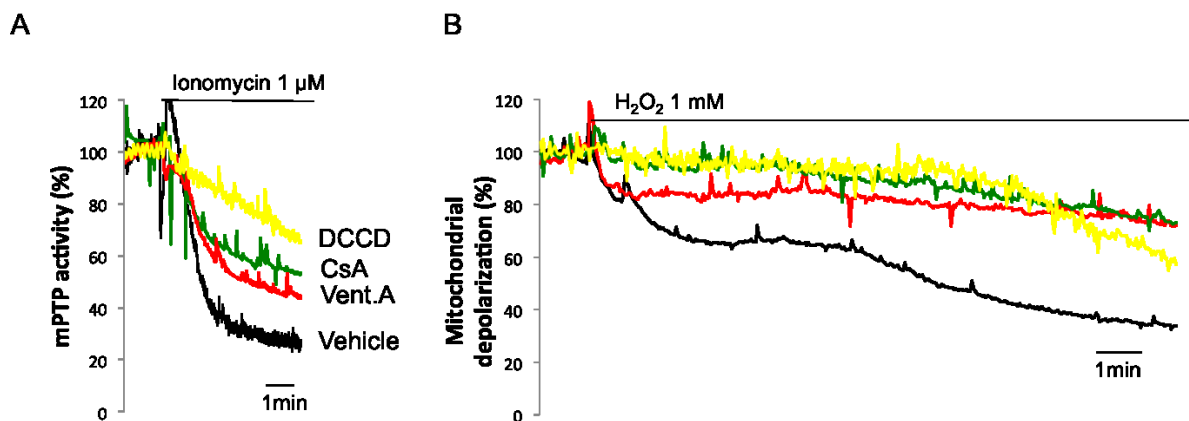**Figure 18** – Mitochondrial functions assessment in living cells upon Csub inhibition.
A: representative kinetics of mPTP activity in living cells pre-treated with vehicle (black line), Venturicidin A (red line), CsA (green line) and DCCD (yellow line) and stimulated with ionomycin. B: mitochondrial depolarization assay in the same conditions of the first panel and stimulated with hydrogen peroxide.

6. Materials and Methods

Mcl-1

6.1 Reagents and solutions

All reagents were purchased from Sigma-Aldrich, Life Technologies, and Santa Cruz Biotechnology.

6.2 Cell culture and transient transfection

HeLa cells were grown in Dulbecco's Modified Eagle Medium (DMEM) and SH-SY5Y cells in RPMI 1640, both supplemented with 10% fetal bovine serum (FBS), in 75-cm^2 Corning flasks. All cells were maintained at 37°C and 90% relative humidity in 5% CO_2. Before transfection, cells were seeded onto 13-mm glass coverslips for intracellular Ca^{2+} measurements and onto 24-mm glass coverslips for microscopic analysis. Next, plasmid transfections (see later) with Lipofectamine 2000 were performed. All experiments were performed 24 h after transfection.

In experiments involving KB-R7943, for Ca^{2+} measurements and apoptosis, cells were pre-treated for 15 min with 10 µM KB-R7943 in complete medium.

6.3 Primers for RT-PCR

Oligonucleotides for reverse transcriptase-polymerase chain reaction (RT-PCR) were created online (Primer3) using the human Mcl-1 sequence from the NCBI database as a template. The primer sequences are as follows:

- Forward sequence (5'-3'), GAGGAGGAGGAGGACGAGTT (Mcl-1 Ex1F1);
- Reverse sequence (5'-3'), TCCTCTTGCCACTTGCTTTT (Mcl-1 Ex3r1).

All PCR products were separated by 2% agarose gel electrophoresis and visualized with ethidium bromide. The expected sizes were 689 bp for Mcl-1L and 441 bp for Mcl-1S.

6.4 mRNA splicing pattern and protein expression of Mcl-1

HeLa cells were plated onto 35-mm plates. After transfection, total RNA was extracted using the phenol/chloroform method. All steps were performed at 4°C. RNA was quantified with a NanoDrop ND-1000, and protein/solvent contaminations were evaluated (A260/280=1.8; A260/230=2.0). RNA was converted to cDNA and amplified using the Mcl-1 primers via RT-PCR (SuperScript III one-step RT-PCR system with Platinum Taq DNA polymerase, Invitrogen). Proteins were separated by SDS-PAGE on a 4-12% precast gel and detected by Western blotting using polyclonal rabbit anti-Mcl-1 (1:500) for both the L (40 kDa) and S (32 kDa) isoforms (Santa Cruz Biotechnology) and monoclonal mouse anti-β tubulin (1:5000)

(Sigma Aldrich) as the primary antibodies and respective horseradish peroxidase (HRP)-labeled secondary antibodies (1:5000), according to standard protocols.

6.5 Inhibition of proteasomal degradation

HeLa cells were plated onto 35-mm well plates for a time-lapse experiment. Twenty-four hours after plating, cells were treated with 10 μM MG132 (dissolved in dimethyl sulfoxide [DMSO]) for 3, 6, 9, and 12 h. The control cells were treated with DMSO alone. Mcl-1 expression was then detected by Western blotting as described previously.

6.6 Design of ASOs

ASOs were synthesized in collaboration with Dr. Daniela Perrone and co-workers at the Department of Chemical and Pharmaceutical Sciences, University of Ferrara. The putative ESE in Mcl-1 exon 2 was identified using the ESEfinder (*http://rulai.cshl.edu/tools/ESE2/*) program, whereas the secondary structures of the sc-ASOs were analyzed using Sfold (http://sfold.wadsworth.org/cgi-bin/index.pl). The sc-ASOs were designed and then chemically synthesized to contain 2′-O-methyl-modified RNA and a full-length phosphorothioate backbone.

The oligonucleotide sequences were as follows:

- Mcl-1S3 (5'-3'), AACGUCUGUGAUACUUUCUGCUAAU;
- Scramble (5'-3'), AUUAUGCUUUUGACCCGAUUAAUCG.

6.7 Apoptosis assessment

WB − HeLa cells were plated onto 35-mm well plates. After the transfection of ASOs and treatment with Ca^{2+}-dependent (menadione 20 μM for 2 h; ceramide 10 μM for 2; H_2O_2 1 mM for 1 h, thapsigargin 4 μM for 2 h) or Ca^{2+}-independent (etoposide 100 μM for 3 h) apoptotic stimuli, cells were trypsinized, pelleted (1,100 rpm, 5 min, +4°C), re-suspended, and homogenized (EBC buffer with protease/phosphatase inhibitor cocktail, pH 7.4). Proteins were separated by SDS-PAGE on a 4-12% precast gel, and the levels of cleaved PARP (89 kDa), β-tubulin (50 kDa), and cleaved caspase 3 (17 kDa) were estimated by Western blots using polyclonal rabbit anti-PARP (1:1000), polyclonal rabbit anti-caspase 3 (1:1000), and monoclonal mouse anti-β-tubulin (1:5000) primary antibodies according to standard protocols. Antibodies were purchased from Cell Signaling and Sigma-Aldrich. Nitrocellulose membranes were incubated with appropriate horseradish peroxidase-conjugated secondary antibodies (1:5000) (Santa Cruz), and protein bands were then visualized by chemiluminescence.

Annexin V staining – HeLa cells were plated onto 35-mm well plates. After the transfection of ASOs and treatment with Ca^{2+}-dependent apoptotic stimuli, cells were gently harvested, processed with buffers, and incubated with annexin V according to manufacturer's protocols (BioVision). The green fluorescence signal was quantified under all conditions on a Tali image-based cytometer.

6.8 Aequorin measurement

For cytAEQ and mtAEQmut at 24 h post-transfection, the coverslips were incubated with 5 µM coelenterazine for 1.5 h in Krebs-Ringer modified buffer (KRB) supplemented with 1 mM $CaCl_2$ (KRB: 125 mM NaCl, 5 mM KCl, 1 mM Na_3PO_4, 1 mM $MgSO_4$, 5.5 mM glucose, and 20 mM Hepes, pH 7.4, at 37°C). To reconstitute erAEQ with high efficiency, the luminal $[Ca^{2+}]$ of the ER was first reduced by incubating the cells for 45 min at 4°C in KRB supplemented with 5 µM coelenterazine, the Ca^{2+} ionophore ionomycin, and 600 µM EGTA. After incubation, the cells were extensively washed with KRB supplemented with 2% bovine serum albumin (BSA) and 2 mM EGTA before the luminescence measurement was initiated. Aequorin signals were measured in KRB supplemented with either 1 mM $CaCl_2$ or 100 µM EGTA using a purpose-built luminometer. The agonist (histamine at 100 µM) was added to the same medium. The experiments were terminated by lysing the cells with Triton X-100 in a hypotonic Ca^{2+}-rich solution (10 mM $CaCl_2$ in H_2O), thus discharging the remaining aequorin pool. The light signals were collected and calibrated with $[Ca^{2+}]$ values. Further experimental details have been previously described [117].

6.9 Mitochondrial Ca^{2+} concentration measurements with 2mt-GCaMP6m

To test resting mitochondrial Ca^{2+} concentrations with high sensitivity, we used a new Ca^{2+} probe based on the last-generation GCaMP probe [211] targeted to the mitochondrial matrix. We chose the GCaMP6m version because it had the highest Ca^{2+} affinity. To measure the signal independent of variations in basal fluorescence intensity due to the variable expression levels of the probe, we took advantage of the isosbestic point in the GCaMP6m excitation spectrum; exciting GCaMP6m at 406 nm led to fluorescence emission that was not Ca^{2+} dependent. As a consequence, the ratio between the excitation wavelengths of 494 and 406 nm was proportional to the Ca^{2+} concentration and independent of probe expression levels. Cells were imaged with an IX-81 automated epifluorescence microscope (Olympus) equipped with a 40× oil immersion objective (N.A. 1.35, from Olympus) and an ORCA-R2 CCD camera (Hamamatsu Photonics K.K.).

6.10 Microscopic analysis

Mitochondrial morphology was assessed under four conditions: Ctr; Mcl-1S3; Ctr+Drp1; and Mcl-1S3+Drp1. Under each condition, cells were transfected with 1 μg mtDSred (Ex/Em: 556/586) and stained with 1 μM calcein (Ex/Em: 495/515) for 10 min at 37°C to mark the mitochondria and to normalize for cell volume.

Ψ_M was assessed under two conditions: Ctr and Mcl-1S3. Under each condition, cells were incubated with 10 nM TMRM (Ex/Em: 548/573) for 20 min at 37°C. Steady-state and post-stimulation (FCCP 10 μM) dye intensities were quantified.

All of the experiments were performed on a confocal Nikon Eclipse T_i system. Fluorescent images were captured and analyzed using NisElements 3.2 for membrane potential and Imaris 4.0 software for morphology. To improve image resolution, Z-series acquisitions were deconvolved using Huygens Essential 3.3 software.

6.11 Mitochondrial mass and biogenesis

Control and Mcl-1S3-transfected HeLa cells were harvested, washed, and pelleted (1,100 rpm, 5 min, +4°C) in PBS, re-suspended in RIPA buffer supplemented with protease and phosphatase inhibitor cocktail (pH 7.4), and homogenized. After measuring the concentrations, proteins were separated by SDS-PAGE on a 4-12% precast gel, and the levels of two protein markers for each mitochondrial compartment were detected using the primary antibodies rabbit anti-VDAC (1:2500, 31 kDa) and anti-TOM20 (1:5000, 20 kDa) for OMM, rabbit anti-MCU (1:2000, 35 kDa) and mouse anti-TIM23 (1:5000, 23 kDa) for IMM, and mouse anti-HSP60 (1:5000, 60 kDa) and anti-ATP5A (1:5000, 55 kDa) for matrix. Anti-β-tubulin (1:5000, 50kDa) was included as a loading control. After overnight incubation, the nitrocellulose membranes were incubated with appropriate HRP-conjugated secondary antibodies (1:5000) (Santa Cruz), and the proteins were visualized by chemiluminescence. Similarly, for the evaluation of biogenesis, anti-PGC1α antibody (1:1000, 113 kDa) was used. The expression of fusion proteins was detected by anti-MFN1 (1:1000, 60 kDa and 86 kDa), anti-MFN2 (1:1000, 90 kDa), and anti-OPA1 (1:1000, 88 kDa and 93kDa for major isoforms).

6.12 Cell cycle synchronization

T98G cells were synchronized using a double-thymidine block method. Briefly, T98G cells in a 100x20 mm petri dish were treated with 2 mM thymidine (Sigma Chemical Co., St. Louis, Mo.) for 16 h. The cells were washed once in fresh medium to remove the thymidine and were then incubated in fresh complete medium. After 6 h, 2 mM thymidine was added again, and the cells were incubated for an additional 16 h. After the second thymidine treatment, the

cells were washed and re-suspended in fresh complete medium. Cell cycle progression was studied at 2-h intervals using phase-specific markers: Cyclin A for the S and M phases; Cyclin B for the G_2/M checkpoint; p27 for the G_0 cells; and pHH3 for mitotic activity. Skp1 was used as a loading control.

6.13 Subcellular fractionation

Cell fractionation was performed using HeLa cells as described [212]. Cells (10^9) were harvested, washed with PBS (supplemented with 2 mM Na_3VO_4 and 2 mM NaF when the preservation of protein phosphorylation states was required) by centrifugation at 500 g for 5 min, resuspended in homogenization buffer (225 mM mannitol, 75 mM sucrose, 30 mM Tris-HCl pH 7.4, 0.1 mM EGTA, and PMSF), and gently disrupted by Dounce homogenization. The homogenate was centrifuged twice at 600 g for 5 min to remove nuclei and unbroken cells, and the supernatant was then centrifuged at 10,300 g for 10 min to pellet crude mitochondria. The resultant supernatant was centrifuged at 20,000 g for 30 min at 4°C. This pellet consisted of the lysosomal and plasma membrane fractions. Further centrifugation of the obtained supernatant at 100,000 g for 90 min (70-Ti rotor; Beckman, Milan, Italy) at 4°C resulted in the isolation of the ER (pellet) and cytosolic (supernatant) fractions. The crude mitochondrial fraction was resuspended in isolation buffer (250 mM mannitol, 5 mM HEPES pH 7.4 and 0.5 mM EGTA) and then subjected to Percoll gradient centrifugation (Percoll medium: 225 mM mannitol, 25 mM HEPES pH 7.4, 1 mM EGTA and 30% vol/vol Percoll) in a 10-ml polycarbonate ultracentrifuge tube. After centrifugation at 95,000 g for 30 min (SW40 rotor), a dense band containing purified mitochondria was recovered approximately three-quarters of the way down the tube. This was then washed by centrifugation at 6,300 g for 10 min to remove the Percoll and finally resuspended in isolation medium. The mitochondrial-associated membranes (MAMs), which contain the structural contacts between the mitochondria and the ER, were removed from the Percoll gradient as a diffuse white band located above the mitochondria, diluted in isolation buffer, and centrifuged at 6,300 g for 10 min. The supernatant was further centrifuged at 100,000 g for 90 min (70-Ti rotor, Beckman) to pellet the MAM fraction. When the preservation of protein phosphorylation states was required, 2 mM Na_3VO_4 and 2 mM NaF were added to each fraction immediately after the recovery.

6.14 Analysis of protein localization using a digitonin-based fractionation technique.

Twenty-four hours post transfection, confluent HeLa cells were trypsinized and harvested in cold PBS pH 7.4, centrifuged at 750 g for 5 min, washed in PBS, and permeabilized with

digitonin for 20 min on ice after resuspending the cell pellet in 200 μl of buffer I (150 mM NaCl, 50 mM HEPES pH 7.4, 100 μg/ml digitonin) supplemented with protease and phosphatase inhibitors. After incubation on ice, plasma membrane permeabilization of cells was confirmed by staining with a 0.2% trypan blue solution. Cells were then centrifuged at 2,000 g for 5 min. The supernatants (cytosolic fractions) were saved, and the pellets were washed, solubilized in the same volume of buffer II (150 mM NaCl, 50 mM HEPES pH 7.4, 1% NP-40) supplemented with complete protease inhibitor cocktail, vortexed, and incubated for 30 min on ice. After centrifugation at 7,000 g for 5 min to pellet nuclei and debris, the supernatants were kept as the heavy membrane fractions enriched for mitochondria. All steps were performed at 4°C. The soluble and heavy membrane fractions were separated by SDS–PAGE (4-12%) and transferred to a nitrocellulose membrane. After blocking nonspecific sites for 1 h at room temperature with 2.5% nonfat milk in PBS supplemented with 0.1% Tween-20, the nitrocellulose membranes were incubated overnight at 4°C with rabbit anti-Drp-1 (1:1000, Cell Signaling), rabbit anti-Mcl-1 (1:500, Santa Cruz), or β-tubulin (1:5000, Sigma Aldrich) as a loading control. The immunoreactive proteins were then visualized using horseradish peroxidase-conjugated goat anti-mouse or anti-rabbit antibodies (1:5000) and enhanced chemiluminescence.

6.15 Immunoprecipitation

Cells were lysed in CHAPS-based lysis buffer. Whole-cell lysates were obtained, pre-cleared with protein A-Sepharose, and then incubated overnight with a 1:100 dilution of the specific antibody anti-Mcl-1. The immunocomplexes were captured with protein A. Beads were pelleted, washed three times, and boiled in SDS sample buffer. For the reverse IP, Drp1 was overexpressed in HeLa cells and the antibody was crosslinked to protein A agarose by 25 mM DMP (dimethyl pimelimidate). The presence of immune complexes was determined by Western blot analysis.

6.16 Statistical analysis and gel quantification

Statistical analysis was performed using Student's t test. A p value <0.05 was considered significant. All data are reported as the means ± standard errors (S.E.).

Quantification of Western Blots was performed with ImageJ (http://rsb.info.nih.gov/ij/index.html) to compare the density of bands on a gel.

6.17 Study design and study population

This is a single-centre, prospective study conducted in two consecutive phases. The first phase was performed from June 2013 to December 2013 with the aim to investigate if Csub was detectable in serum from patients and controls. Accordingly, we enrolled two groups matched for age, sex and cardiovascular risk factors: i) STEMI patients; ii) controls without documented cardiovascular disease. The second phase was performed from December 2013 to January 2015 with the aim to assess, in STEMI patients, a possible relationship between Csub serum levels and surrogate endpoints of RI. STEMI patients eligible for enrollment were individuals admitted to our centre respecting the following inclusion criteria: age >18 years; typical chest pain lasting at least 20 minutes; ST-segment elevation at J-point ≥0.2 mV in at least two contiguous precordial leads; time from onset of symptoms to balloon within 6 hours; culprit lesion in the proximal or mid portion of left anterior descending (LAD); initial thrombolysis in myocardial infarction (TIMI) flow 0-1; successful PCI procedure with stent implantation (final TIMI flow 3 and residual stenosis <30%). Age and sex matched individuals with cardiovascular risk factors, but without evidence of coronary artery disease, were enrolled from our outpatient department and were considered as controls. Exclusion criteria were: previous history and/or signs of MI, percutaneous or surgical coronary revascularization, prior angina or evidence of ischemic heart disease; cardiac arrest and/or cardiogenic shock; atrial fibrillation; pacemaker; concurrent inflammatory, infectious or malignant disease, liver and/or renal failure; recent significant bleeding and/or major surgery (< 4 weeks); use of oral anticoagulants or contraceptive. PCI procedures were performed according to standard clinical practice. Antithrombotic drugs and all other medications (angiotensin converting enzyme inhibitor, statin, beta-blocker, diuretic, nitrate, proton pump inhibitor) were prescribed according current guidelines [213,214]. This study was approved by the local ethics committee (Comitato Etico Unico della Provincia di Ferrara), and all patients gave written informed consent.

6.18 Blood Sample Collection

In STEMI patients, blood withdrawal was performed 6-18 hours after the end of successful PCI (median 10 [8-13] hours), whereas in controls after overnight fasting. Blood samples were collected from an antecubital vein using a 21-gauge needle. The first 2 to 4 mL of blood were discarded. The remaining blood was collected in empty tubes and, after 45 minutes, centrifuged at 1,700g at 4°C for 15 min. The serum obtained was stored at -20°C.

6.19 F$_o$ ATP synthase C subunit and translocase of the inner membrane (TIM) 14.

Both Csub and mitochondrial import inner membrane translocase subunit (TIM) 14 were measured in serum from patients and controls. TIM 14 is an essential part of the TIM 23 machinery in the IMM [215,216]. We reported Csub and TIM 14 serum levels singularly and as Csub/TIM 14 ratio. Of note, we used the human ATP synthase lipid-binding protein, mitochondrial (ATP5G1) ELISA kit (Cusabio Biotech, China) to measure Csub serum values. The ELISA was performed according to the manufacturer's instructions using strips of microtiter wells with a capture antibody, specific for either Csub of the human FO ATP synthase or human TIM 14 coated onto the wells of microplates. Serum samples were first concentrated for the protein of interest using Amicon Ultra-4 10K Centrifugal Filter Devices at 3000g for 40 min (+ 4°C) to minimize the contamination by proteins of high molecular weight and then diluited 1:5 in phosphate-buffered saline (PBS). The dilution is necessary to be in the kit range. One-hundred μl samples were placed in the wells. After 2 h of incubation at 37°C, the liquid was removed from each well. The strips were again incubated for 1 h at 37°C after adding 100 μl biotin-antibody 1X to each well. The wells were then washed three times with wash buffer and after the last one 100 μl HRP-avidin 1X was added to each well and incubated for 1 h at 37°C. The wells were washed five times as in the previous step and 90 μl TMB substrate was added. If the Csub protein is present, a blue color develops between 15 to 30 min. The blue color changes to yellow with the addition of 50 μl phosphoric acid, which is used to stop the reaction. The result can be read with the aid of a spectrophotometer and compared with the negative control and the calibration curve supplied with the test kit. A spectrophotometer (450 nm) was used to obtain protein concentration duplicate readings. A computer software (MARS) capable of generating a four parameter logistic (4-PL) curve-fit was used to obtain concentrations as pg/ml protein. Finally, pg/ml concentrations were converted into percentages on the basis of the highest value that the calibration curve is able to read. Intra- and inter-assay CV% were <8% and <10%, respectively.

6.20 Definition, clinical follow-up and endpoints.

Markers of myocardial necrosis (troponin T and CK-MB) and ST-segment resolution were used as surrogate endpoints of RI [183,194]. Plasma samples for CK-MB and troponin T were collected on admission and subsequently during the hospitalization every 6-8 hours for 2 days [213,214]. Cardiac markers were measured in the laboratory of our hospital (high-sensitivity troponin T: upper reference limit 0.014 ng/ml; CK-MB: upper reference limit 5 ng/ml; Cobas, Roche Diagnostics, Mannheim, Germany). Their values are reported as peak and as area under the curve (AUC) (expressed in arbitrary units). The cumulative ST-segment resolution,

expressed as the percentage, was calculated by an independent reviewer (RP) blinded to Csub values. It was assessed immediately at the end of primary PCI and 90 min thereafter and categorized as complete (≥70%), partial (<70% to 30%), and no/absent (<30%) [15]. Before hospital discharge (median 5 [4-6] days) and after 6 months [median 190 [170-200] days] all patients received transthoracic echocardiography. To measure left ventricle ejection fraction (LVEF) and wall motion score index (WMSI), images were analyzed by an independent reviewer (SB) blinded to Csub values. The 6-months occurrence of principal ischemic adverse events (death, hospital admission for recurrence of acute coronary syndrome [ACS] and/or HF) was recorded. All adverse events were adjudicated by an independent reviewer (SP) blinded to Csub values.

6.21 Sample size.

Given the lack of prior data assessing Csub in humans, in line with recommendations for pilot studies, an arbitrary sample of 60 patients (at least 30 for groups) was chosen for the first phase of the investigation [217]. The results of the first phase were used for the sample size calculation of the second phase. We supposed that, in STEMI patients with Csub levels below the median, the values of troponin T AUC is 30%lower than in others (above median value). Thus, at least 130 STEMI patients are needed (α=0.05; β=0.2).

6.22 Csub detection in cell lysates

Fibroblasts cells were extracted from skin biopsy and plated onto 35-mm well plates. After 24 h cells were trypsinized, pelleted (1,100 rpm, 5 min, +4°C), re-suspended, and homogenized (modified-RIPA buffer with protease/phosphatase inhibitor cocktail, pH 7.4). Proteins were separated by SDS-PAGE on a 4-20% precast gel, and the levels of C subunit (8 kDa) and ATP5A (55 kDa) were estimated by Western blots using polyclonal primary antibodies according to standard protocols. Antibodies were purchased from Abcam. Nitrocellulose membranes were incubated with appropriate horseradish peroxidase-conjugated secondary antibodies (Santa Cruz), and protein bands were then visualized by chemiluminescence.

6.23 Mitochondrial Permeability Transition Pore assay

Fibroblasts were loaded with 1 μM calcein acetoxymethyl ester and Co^{2+} as instructed by the Image-IT® LIVE Mitochondrial Transition Pore Assay Kit (Molecular Probes-Life Technologies). Cells were then imaged by means of 490 ± 20 nm excitation and 525 nm longpass emission filters on a Axiovert 200M fluorescence microscope equipped with a 40× oil immersion objective (Zeiss). Finally, images were analyzed with MetaMorph® and

quenching rates were determined as the slopes of the fluorescence trace over a period of 60 sec post-stimulation. For details see [220].

6.24 Statistical Analysis.

Categorical variables are reported as counts and percentages. Differences between percentages were assessed by chi-square or Fisher exact tests. Continuous data were tested for normal distribution with the Kolmogorov-Smirnov test. Normally distributed values were presented as mean±SD; otherwise median value [interquartile range] was used. Student t tests and analysis of variance were used for normally distributed continuous variables. Appropriate nonparametric tests (Mann-Whitney, Kruskal-Wallis, and Spearman rank correlation tests) were used for all other variables. To better define the relationship between Csub and endpoints, we described it as continuous marker, as above vs. below median value and as tertiles. The effects between all variables: Csub and endpoints (Troponin I AUC, CK-MB AUC, complete ST-segment resolution) were assessed by logistic regression models. Variables with a probability value <0.1 at univariate analysis (symptom-balloon time, first medical contact-balloon time, Csub serum level, age) and several potential confounding factors (sex, glycoprotein IIb/IIIa administration, manual thrombectomy, proximal LAD) were then entered into a multivariable analysis to identify the independent predictors for adverse events. All tests were 2-sided and the statistical significance was defined as p<0.05. All analyses were performed with *STATISTICA 8* (Statsoft Inc, Tulsa, Okla, USA).

7. References

1. Berridge, M.J., Lipp, P. & Bootman, M.D. The versatility and universality of calcium signalling. *Nature reviews. Molecular cell biology* **1**, 11-21 (2000).
2. Pinton, P., Pozzan, T. & Rizzuto, R. The Golgi apparatus is an inositol 1,4,5-trisphosphate-sensitive Ca2+ store, with functional properties distinct from those of the endoplasmic reticulum. *The EMBO journal* **17**, 5298-5308 (1998).
3. Giorgi, C., De Stefani, D., Bononi, A., Rizzuto, R. & Pinton, P. Structural and functional link between the mitochondrial network and the endoplasmic reticulum. *The international journal of biochemistry & cell biology* **41**, 1817-1827 (2009).
4. Foskett, J.K., White, C., Cheung, K.H. & Mak, D.O. Inositol trisphosphate receptor Ca2+ release channels. *Physiological reviews* **87**, 593-658 (2007).
5. Periasamy, M. & Kalyanasundaram, A. SERCA pump isoforms: their role in calcium transport and disease. *Muscle & nerve* **35**, 430-442 (2007).
6. Lipscombe, D., *et al.* Spatial distribution of calcium channels and cytosolic calcium transients in growth cones and cell bodies of sympathetic neurons. *Proceedings of the National Academy of Sciences of the United States of America* **85**, 2398-2402 (1988).
7. Dubois, C., Prevarskaya, N. & Vanden Abeele, F. The calcium-signaling toolkit: Updates needed. *Biochimica et biophysica acta* (2015).
8. Mishra, P. & Chan, D.C. Mitochondrial dynamics and inheritance during cell division, development and disease. *Nature reviews. Molecular cell biology* **15**, 634-646 (2014).
9. Marchi, S. & Pinton, P. The mitochondrial calcium uniporter complex: molecular components, structure and physiopathological implications. *The Journal of physiology* **592**, 829-839 (2014).
10. Pozzan, T. & Rizzuto, R. The renaissance of mitochondrial calcium transport. *European journal of biochemistry / FEBS* **267**, 5269-5273 (2000).
11. Nicholls, D.G. & Crompton, M. Mitochondrial calcium transport. *FEBS letters* **111**, 261-268 (1980).
12. Jiang, D., Zhao, L. & Clapham, D.E. Genome-wide RNAi screen identifies Letm1 as a mitochondrial Ca2+/H+ antiporter. *Science* **326**, 144-147 (2009).
13. Dimmer, K.S., *et al.* LETM1, deleted in Wolf-Hirschhorn syndrome is required for normal mitochondrial morphology and cellular viability. *Human molecular genetics* **17**, 201-214 (2008).
14. Bononi, A., *et al.* Mitochondria-associated membranes (MAMs) as hotspot Ca(2+) signaling units. *Advances in experimental medicine and biology* **740**, 411-437 (2012).
15. Giorgi, C., Wieckowski, M.R., Pandolfi, P.P. & Pinton, P. Mitochondria associated membranes (MAMs) as critical hubs for apoptosis. *Communicative & integrative biology* **4**, 334-335 (2011).
16. Drago, I., De Stefani, D., Rizzuto, R. & Pozzan, T. Mitochondrial Ca2+ uptake contributes to buffering cytoplasmic Ca2+ peaks in cardiomyocytes. *Proceedings of the National Academy of Sciences of the United States of America* **109**, 12986-12991 (2012).
17. Patergnani, S., *et al.* Calcium signaling around Mitochondria Associated Membranes (MAMs). *Cell communication and signaling : CCS* **9**, 19 (2011).

18. Jouaville, L.S., Ichas, F., Holmuhamedov, E.L., Camacho, P. & Lechleiter, J.D. Synchronization of calcium waves by mitochondrial substrates in Xenopus laevis oocytes. *Nature* **377**, 438-441 (1995).

19. Koppenol, W.H., Bounds, P.L. & Dang, C.V. Otto Warburg's contributions to current concepts of cancer metabolism. *Nature reviews. Cancer* **11**, 325-337 (2011).

20. Gottlieb, E. & Tomlinson, I.P. Mitochondrial tumour suppressors: a genetic and biochemical update. *Nature reviews. Cancer* **5**, 857-866 (2005).

21. Vaughn, A.E. & Deshmukh, M. Glucose metabolism inhibits apoptosis in neurons and cancer cells by redox inactivation of cytochrome c. *Nature cell biology* **10**, 1477-1483 (2008).

22. Chatterjee, A., Dasgupta, S. & Sidransky, D. Mitochondrial subversion in cancer. *Cancer prevention research* **4**, 638-654 (2011).

23. Galluzzi, L., *et al.* Mitochondrial gateways to cancer. *Molecular aspects of medicine* **31**, 1-20 (2010).

24. Polyak, K., *et al.* Somatic mutations of the mitochondrial genome in human colorectal tumours. *Nature genetics* **20**, 291-293 (1998).

25. Hamanaka, R.B. & Chandel, N.S. Mitochondrial reactive oxygen species regulate cellular signaling and dictate biological outcomes. *Trends in biochemical sciences* **35**, 505-513 (2010).

26. Sena, L.A. & Chandel, N.S. Physiological roles of mitochondrial reactive oxygen species. *Molecular cell* **48**, 158-167 (2012).

27. Morciano, G., *et al.* Mcl-1 involvement in mitochondrial dynamics is associated with apoptotic cell death. *Molecular biology of the cell* **27**, 20-34 (2016).

28. Chan, D.C. Mitochondria: dynamic organelles in disease, aging, and development. *Cell* **125**, 1241-1252 (2006).

29. Martinou, J.C. & Youle, R.J. Mitochondria in apoptosis: Bcl-2 family members and mitochondrial dynamics. *Developmental cell* **21**, 92-101 (2011).

30. Al-Mehdi, A.B., *et al.* Perinuclear mitochondrial clustering creates an oxidant-rich nuclear domain required for hypoxia-induced transcription. *Science signaling* **5**, ra47 (2012).

31. Knott, A.B., Perkins, G., Schwarzenbacher, R. & Bossy-Wetzel, E. Mitochondrial fragmentation in neurodegeneration. *Nature reviews. Neuroscience* **9**, 505-518 (2008).

32. Twig, G. & Shirihai, O.S. The interplay between mitochondrial dynamics and mitophagy. *Antioxidants & redox signaling* **14**, 1939-1951 (2011).

33. Otera, H. & Mihara, K. Molecular mechanisms and physiologic functions of mitochondrial dynamics. *Journal of biochemistry* **149**, 241-251 (2011).

34. Otera, H., Ishihara, N. & Mihara, K. New insights into the function and regulation of mitochondrial fission. *Biochimica et biophysica acta* **1833**, 1256-1268 (2013).

35. Otera, H. & Mihara, K. Discovery of the membrane receptor for mitochondrial fission GTPase Drp1. *Small GTPases* **2**, 167-172 (2011).

36. Chang, C.R. & Blackstone, C. Dynamic regulation of mitochondrial fission through modification of the dynamin-related protein Drp1. *Annals of the New York Academy of Sciences* **1201**, 34-39 (2010).

37. Autret, A. & Martin, S.J. Emerging role for members of the Bcl-2 family in mitochondrial morphogenesis. *Molecular cell* **36**, 355-363 (2009).

38. Karbowski, M., Norris, K.L., Cleland, M.M., Jeong, S.Y. & Youle, R.J. Role of Bax and Bak in mitochondrial morphogenesis. *Nature* **443**, 658-662 (2006).

39. Karbowski, M. & Youle, R.J. Dynamics of mitochondrial morphology in healthy cells and during apoptosis. *Cell death and differentiation* **10**, 870-880 (2003).

40.   Lindsten, T., *et al.* The combined functions of proapoptotic Bcl-2 family members bak and bax are essential for normal development of multiple tissues. *Molecular cell* **6**, 1389-1399 (2000).

41.   Wei, M.C., *et al.* Proapoptotic BAX and BAK: a requisite gateway to mitochondrial dysfunction and death. *Science* **292**, 727-730 (2001).

42.   Green, D.R. & Kroemer, G. The pathophysiology of mitochondrial cell death. *Science* **305**, 626-629 (2004).

43.   Hoppins, S., *et al.* The soluble form of Bax regulates mitochondrial fusion via MFN2 homotypic complexes. *Molecular cell* **41**, 150-160 (2011).

44.   Li, H., *et al.* Bcl-xL induces Drp1-dependent synapse formation in cultured hippocampal neurons. *Proceedings of the National Academy of Sciences of the United States of America* **105**, 2169-2174 (2008).

45.   Perciavalle, R.M., *et al.* Anti-apoptotic MCL-1 localizes to the mitochondrial matrix and couples mitochondrial fusion to respiration. *Nature cell biology* **14**, 575-583 (2012).

46.   Schwartz Longacre, L., *et al.* New horizons in cardioprotection: recommendations from the 2010 National Heart, Lung, and Blood Institute Workshop. *Circulation* **124**, 1172-1179 (2011).

47.   McBride, H.M., Neuspiel, M. & Wasiak, S. Mitochondria: more than just a powerhouse. *Current biology : CB* **16**, R551-560 (2006).

48.   Haunstetter, A. & Izumo, S. Apoptosis: basic mechanisms and implications for cardiovascular disease. *Circulation research* **82**, 1111-1129 (1998).

49.   Schaper, J., Elsasser, A. & Kostin, S. The role of cell death in heart failure. *Circulation research* **85**, 867-869 (1999).

50.   Sanada, S., Komuro, I. & Kitakaze, M. Pathophysiology of myocardial reperfusion injury: preconditioning, postconditioning, and translational aspects of protective measures. *American journal of physiology. Heart and circulatory physiology* **301**, H1723-1741 (2011).

51.   Crompton, M., Costi, A. & Hayat, L. Evidence for the presence of a reversible Ca2+-dependent pore activated by oxidative stress in heart mitochondria. *The Biochemical journal* **245**, 915-918 (1987).

52.   Crompton, M., Ellinger, H. & Costi, A. Inhibition by cyclosporin A of a Ca2+-dependent pore in heart mitochondria activated by inorganic phosphate and oxidative stress. *The Biochemical journal* **255**, 357-360 (1988).

53.   Griffiths, E.J. & Halestrap, A.P. Mitochondrial non-specific pores remain closed during cardiac ischaemia, but open upon reperfusion. *The Biochemical journal* **307 (Pt 1)**, 93-98 (1995).

54.   Anversa, P., *et al.* Apoptosis and myocardial infarction. *Basic research in cardiology* **93 Suppl 3**, 8-12 (1998).

55.   Chiari, P., *et al.* Cyclosporine protects the heart during aortic valve surgery. *Anesthesiology* **121**, 232-238 (2014).

56.   Crompton, M. The mitochondrial permeability transition pore and its role in cell death. *The Biochemical journal* **341 (Pt 2)**, 233-249 (1999).

57.   Gateau-Roesch, O., Argaud, L. & Ovize, M. Mitochondrial permeability transition pore and postconditioning. *Cardiovascular research* **70**, 264-273 (2006).

58.   Saraste, A., *et al.* Apoptosis in human acute myocardial infarction. *Circulation* **95**, 320-323 (1997).

59.   Bonora, M., *et al.* Molecular mechanisms of cell death: central implication of ATP synthase in mitochondrial permeability transition. *Oncogene* **34**, 1475-1486 (2015).

60.   Kroemer, G., Galluzzi, L. & Brenner, C. Mitochondrial membrane permeabilization in cell death. *Physiological reviews* **87**, 99-163 (2007).

61.   Jeremias, I., *et al.* Involvement of CD95/Apo1/Fas in cell death after myocardial ischemia. *Circulation* **102**, 915-920 (2000).

62.   Kajstura, J., *et al.* Apoptotic and necrotic myocyte cell deaths are independent contributing variables of infarct size in rats. *Laboratory investigation; a journal of technical methods and pathology* **74**, 86-107 (1996).

63.   Torre-Amione, G., *et al.* Tumor necrosis factor-alpha and tumor necrosis factor receptors in the failing human heart. *Circulation* **93**, 704-711 (1996).

64.   Krown, K.A., *et al.* Tumor necrosis factor alpha-induced apoptosis in cardiac myocytes. Involvement of the sphingolipid signaling cascade in cardiac cell death. *The Journal of clinical investigation* **98**, 2854-2865 (1996).

65.   Bednar, M., Smith, B., Pinto, A. & Mullane, K.M. Nafazatrom-induced salvage of ischemic myocardium in anesthetized dogs is mediated through inhibition of neutrophil function. *Circulation research* **57**, 131-141 (1985).

66.   Mullane, K.M., Read, N., Salmon, J.A. & Moncada, S. Role of leukocytes in acute myocardial infarction in anesthetized dogs: relationship to myocardial salvage by anti-inflammatory drugs. *The Journal of pharmacology and experimental therapeutics* **228**, 510-522 (1984).

67.   Ross, A.M., *et al.* A randomized, double-blinded, placebo-controlled multicenter trial of adenosine as an adjunct to reperfusion in the treatment of acute myocardial infarction (AMISTAD-II). *Journal of the American College of Cardiology* **45**, 1775-1780 (2005).

68.   Kroemer, G. & Reed, J.C. Mitochondrial control of cell death. *Nature medicine* **6**, 513-519 (2000).

69.   Giorgi, C., *et al.* Mitochondrial Ca(2+) and apoptosis. *Cell calcium* **52**, 36-43 (2012).

70.   Bialik, S., *et al.* The mitochondrial apoptotic pathway is activated by serum and glucose deprivation in cardiac myocytes. *Circulation research* **85**, 403-414 (1999).

71.   Gottlieb, R.A., Burleson, K.O., Kloner, R.A., Babior, B.M. & Engler, R.L. Reperfusion injury induces apoptosis in rabbit cardiomyocytes. *The Journal of clinical investigation* **94**, 1621-1628 (1994).

72.   McCully, J.D., Wakiyama, H., Hsieh, Y.J., Jones, M. & Levitsky, S. Differential contribution of necrosis and apoptosis in myocardial ischemia-reperfusion injury. *American journal of physiology. Heart and circulatory physiology* **286**, H1923-1935 (2004).

73.   Yeap, X.Y., Dehn, S., Adelman, J., Lipsitz, J. & Thorp, E.B. Quantitation of acute necrosis after experimental myocardial infarction. *Methods in molecular biology* **1004**, 115-133 (2013).

74.   James, T.N. The variable morphological coexistence of apoptosis and necrosis in human myocardial infarction: significance for understanding its pathogenesis, clinical course, diagnosis and prognosis. *Coronary artery disease* **9**, 291-307 (1998).

75.   Marchi, S., *et al.* Mitochondria-ros crosstalk in the control of cell death and aging. *Journal of signal transduction* **2012**, 329635 (2012).

76.   Zweier, J.L. & Talukder, M.A. The role of oxidants and free radicals in reperfusion injury. *Cardiovascular research* **70**, 181-190 (2006).

77.   Giorgi, C., Romagnoli, A., Pinton, P. & Rizzuto, R. Ca2+ signaling, mitochondria and cell death. *Current molecular medicine* **8**, 119-130 (2008).

78. Saito, S._, et al._ beta-Adrenergic pathway induces apoptosis through calcineurin activation in cardiac myocytes. _The Journal of biological chemistry_ **275**, 34528-34533 (2000).

79. Hanada, M., Delia, D., Aiello, A., Stadtmauer, E. & Reed, J.C. bcl-2 gene hypomethylation and high-level expression in B-cell chronic lymphocytic leukemia. _Blood_ **82**, 1820-1828 (1993).

80. Boise, L.H., Gottschalk, A.R., Quintans, J. & Thompson, C.B. Bcl-2 and Bcl-2-related proteins in apoptosis regulation. _Current topics in microbiology and immunology_ **200**, 107-121 (1995).

81. Kozopas, K.M., Yang, T., Buchan, H.L., Zhou, P. & Craig, R.W. MCL1, a gene expressed in programmed myeloid cell differentiation, has sequence similarity to BCL2. _Proceedings of the National Academy of Sciences of the United States of America_ **90**, 3516-3520 (1993).

82. Yang, T., Kozopas, K.M. & Craig, R.W. The intracellular distribution and pattern of expression of Mcl-1 overlap with, but are not identical to, those of Bcl-2. _The Journal of cell biology_ **128**, 1173-1184 (1995).

83. Clohessy, J.G., Zhuang, J., de Boer, J., Gil-Gomez, G. & Brady, H.J. Mcl-1 interacts with truncated Bid and inhibits its induction of cytochrome c release and its role in receptor-mediated apoptosis. _The Journal of biological chemistry_ **281**, 5750-5759 (2006).

84. Hershko, A. & Ciechanover, A. The ubiquitin system. _Annual review of biochemistry_ **67**, 425-479 (1998).

85. Maurer, U., Charvet, C., Wagman, A.S., Dejardin, E. & Green, D.R. Glycogen synthase kinase-3 regulates mitochondrial outer membrane permeabilization and apoptosis by destabilization of MCL-1. _Molecular cell_ **21**, 749-760 (2006).

86. Opferman, J.T._, et al._ Development and maintenance of B and T lymphocytes requires antiapoptotic MCL-1. _Nature_ **426**, 671-676 (2003).

87. Yin, X.M., Oltvai, Z.N. & Korsmeyer, S.J. BH1 and BH2 domains of Bcl-2 are required for inhibition of apoptosis and heterodimerization with Bax. _Nature_ **369**, 321-323 (1994).

88. Kelekar, A. & Thompson, C.B. Bcl-2-family proteins: the role of the BH3 domain in apoptosis. _Trends in cell biology_ **8**, 324-330 (1998).

89. Bae, J., Leo, C.P., Hsu, S.Y. & Hsueh, A.J. MCL-1S, a splicing variant of the antiapoptotic BCL-2 family member MCL-1, encodes a proapoptotic protein possessing only the BH3 domain. _The Journal of biological chemistry_ **275**, 25255-25261 (2000).

90. Bingle, C.D._, et al._ Exon skipping in Mcl-1 results in a bcl-2 homology domain 3 only gene product that promotes cell death. _The Journal of biological chemistry_ **275**, 22136-22146 (2000).

91. Kim, J.H._, et al._ MCL-1ES, a novel variant of MCL-1, associates with MCL-1L and induces mitochondrial cell death. _FEBS letters_ **583**, 2758-2764 (2009).

92. Derenne, S._, et al._ Antisense strategy shows that Mcl-1 rather than Bcl-2 or Bcl-x(L) is an essential survival protein of human myeloma cells. _Blood_ **100**, 194-199 (2002).

93. Khoury, J.D._, et al._ Expression of Mcl-1 in mantle cell lymphoma is associated with high-grade morphology, a high proliferative state, and p53 overexpression. _The Journal of pathology_ **199**, 90-97 (2003).

94. Perciavalle, R.M. & Opferman, J.T. Delving deeper: MCL-1's contributions to normal and cancer biology. _Trends in cell biology_ **23**, 22-29 (2013).

95. Placzek, W.J., *et al.* A survey of the anti-apoptotic Bcl-2 subfamily expression in cancer types provides a platform to predict the efficacy of Bcl-2 antagonists in cancer therapy. *Cell death & disease* **1**, e40 (2010).

96. Hackenbrock, C.R. Ultrastructural bases for metabolically linked mechanical activity in mitochondria. I. Reversible ultrastructural changes with change in metabolic steady state in isolated liver mitochondria. *The Journal of cell biology* **30**, 269-297 (1966).

97. Scheckhuber, C. Mitochondrial Dynamics in Cell Life and Death. *Science of aging knowledge environment : SAGE KE* **2005**, pe36 (2005).

98. Frezza, C., *et al.* OPA1 controls apoptotic cristae remodeling independently from mitochondrial fusion. *Cell* **126**, 177-189 (2006).

99. James, D.I., Parone, P.A., Mattenberger, Y. & Martinou, J.C. hFis1, a novel component of the mammalian mitochondrial fission machinery. *The Journal of biological chemistry* **278**, 36373-36379 (2003).

100. Frank, S., *et al.* The role of dynamin-related protein 1, a mediator of mitochondrial fission, in apoptosis. *Developmental cell* **1**, 515-525 (2001).

101. Szabadkai, G., *et al.* Drp-1-dependent division of the mitochondrial network blocks intraorganellar Ca2+ waves and protects against Ca2+-mediated apoptosis. *Molecular cell* **16**, 59-68 (2004).

102. Chen, H., Chomyn, A. & Chan, D.C. Disruption of fusion results in mitochondrial heterogeneity and dysfunction. *The Journal of biological chemistry* **280**, 26185-26192 (2005).

103. Westrate, L.M., Sayfie, A.D., Burgenske, D.M. & MacKeigan, J.P. Persistent mitochondrial hyperfusion promotes G2/M accumulation and caspase-dependent cell death. *PloS one* **9**, e91911 (2014).

104. Tondera, D., *et al.* Knockdown of MTP18, a novel phosphatidylinositol 3-kinase-dependent protein, affects mitochondrial morphology and induces apoptosis. *The Journal of biological chemistry* **279**, 31544-31555 (2004).

105. Gleave, M.E. & Monia, B.P. Antisense therapy for cancer. *Nature reviews. Cancer* **5**, 468-479 (2005).

106. Hadaschik, B.A., *et al.* Intravesically administered antisense oligonucleotides targeting heat-shock protein-27 inhibit the growth of non-muscle-invasive bladder cancer. *BJU international* **102**, 610-616 (2008).

107. Skvara, H., *et al.* Mcl-1 blocks radiation-induced apoptosis and inhibits clonogenic cell death. *Anticancer research* **25**, 2697-2703 (2005).

108. Wacheck, V., *et al.* Mcl-1 is a relevant molecular target for antisense oligonucleotide strategies in gastric cancer cells. *Cancer biology & therapy* **5**, 1348-1354 (2006).

109. Sieghart, W., *et al.* Mcl-1 overexpression in hepatocellular carcinoma: a potential target for antisense therapy. *Journal of hepatology* **44**, 151-157 (2006).

110. Skoda, C., *et al.* Down-regulation of Mcl-1 with antisense technology alters the effect of various cytotoxic agents used in treatment of squamous cell carcinoma of the head and neck. *Oncology reports* **19**, 1499-1503 (2008).

111. Spitali, P. & Aartsma-Rus, A. Splice modulating therapies for human disease. *Cell* **148**, 1085-1088 (2012).

112. Koo, T. & Wood, M.J. Clinical trials using antisense oligonucleotides in duchenne muscular dystrophy. *Human gene therapy* **24**, 479-488 (2013).

113. Bauman, J.A., Li, S.D., Yang, A., Huang, L. & Kole, R. Anti-tumor activity of splice-switching oligonucleotides. *Nucleic acids research* **38**, 8348-8356 (2010).

114. Shieh, J.J., Liu, K.T., Huang, S.W., Chen, Y.J. & Hsieh, T.Y. Modification of alternative splicing of Mcl-1 pre-mRNA using antisense morpholino oligonucleotides induces

apoptosis in basal cell carcinoma cells. *The Journal of investigative dermatology* **129**, 2497-2506 (2009).

115. Thomas, L.W., Lam, C. & Edwards, S.W. Mcl-1; the molecular regulation of protein function. *FEBS letters* **584**, 2981-2989 (2010).

116. Galluzzi, L.*, et al.* Essential versus accessory aspects of cell death: recommendations of the NCCD 2015. *Cell death and differentiation* **22**, 58-73 (2015).

117. Bonora, M.*, et al.* Subcellular calcium measurements in mammalian cells using jellyfish photoprotein aequorin-based probes. *Nature protocols* **8**, 2105-2118 (2013).

118. Gunter, T.E. & Pfeiffer, D.R. Mechanisms by which mitochondria transport calcium. *The American journal of physiology* **258**, C755-786 (1990).

119. Scarpa, A. & Azzone, G.F. The mechanism of ion translocation in mitochondria. 4. Coupling of K+ efflux with Ca2+ uptake. *European journal of biochemistry / FEBS* **12**, 328-335 (1970).

120. Suski, J.M.*, et al.* Relation between mitochondrial membrane potential and ROS formation. *Methods in molecular biology* **810**, 183-205 (2012).

121. Vinogradov, A. & Scarpa, A. The initial velocities of calcium uptake by rat liver mitochondria. *The Journal of biological chemistry* **248**, 5527-5531 (1973).

122. Bereiter-Hahn, J. & Voth, M. Dynamics of mitochondria in living cells: shape changes, dislocations, fusion, and fission of mitochondria. *Microscopy research and technique* **27**, 198-219 (1994).

123. Marchi, S., Patergnani, S. & Pinton, P. The endoplasmic reticulum-mitochondria connection: one touch, multiple functions. *Biochimica et biophysica acta* **1837**, 461-469 (2014).

124. Scorrano, L. Keeping mitochondria in shape: a matter of life and death. *European journal of clinical investigation* **43**, 886-893 (2013).

125. van der Bliek, A.M. Functional diversity in the dynamin family. *Trends in cell biology* **9**, 96-102 (1999).

126. Smirnova, E., Griparic, L., Shurland, D.L. & van der Bliek, A.M. Dynamin-related protein Drp1 is required for mitochondrial division in mammalian cells. *Molecular biology of the cell* **12**, 2245-2256 (2001).

127. Mitra, K., Wunder, C., Roysam, B., Lin, G. & Lippincott-Schwartz, J. A hyperfused mitochondrial state achieved at G1-S regulates cyclin E buildup and entry into S phase. *Proceedings of the National Academy of Sciences of the United States of America* **106**, 11960-11965 (2009).

128. Shin, H.W., Shinotsuka, C., Torii, S., Murakami, K. & Nakayama, K. Identification and subcellular localization of a novel mammalian dynamin-related protein homologous to yeast Vps1p and Dnm1p. *Journal of biochemistry* **122**, 525-530 (1997).

129. Fesik, S.W. Promoting apoptosis as a strategy for cancer drug discovery. *Nature reviews. Cancer* **5**, 876-885 (2005).

130. Akl, H.*, et al.* A dual role for the anti-apoptotic Bcl-2 protein in cancer: mitochondria versus endoplasmic reticulum. *Biochimica et biophysica acta* **1843**, 2240-2252 (2014).

131. Hardwick, J.M. & Youle, R.J. SnapShot: BCL-2 proteins. *Cell* **138**, 404, 404 e401 (2009).

132. Hajnoczky, G.*, et al.* Mitochondrial calcium signalling and cell death: approaches for assessing the role of mitochondrial Ca2+ uptake in apoptosis. *Cell calcium* **40**, 553-560 (2006).

133. Bonora, M.*, et al.* Role of the c subunit of the FO ATP synthase in mitochondrial permeability transition. *Cell cycle* **12**, 674-683 (2013).

134. Minagawa, N.*, et al.* The anti-apoptotic protein Mcl-1 inhibits mitochondrial Ca2+ signals. *The Journal of biological chemistry* **280**, 33637-33644 (2005).

135. Eckenrode, E.F., Yang, J., Velmurugan, G.V., Foskett, J.K. & White, C. Apoptosis protection by Mcl-1 and Bcl-2 modulation of inositol 1,4,5-trisphosphate receptor-dependent Ca2+ signaling. *The Journal of biological chemistry* **285**, 13678-13684 (2010).

136. Varadarajan, S.*, et al.* Sabutoclax (BI97C1) and BI112D1, putative inhibitors of MCL-1, induce mitochondrial fragmentation either upstream of or independent of apoptosis. *Neoplasia* **15**, 568-578 (2013).

137. Laslett, L.J.*, et al.* The worldwide environment of cardiovascular disease: prevalence, diagnosis, therapy, and policy issues: a report from the American College of Cardiology. *Journal of the American College of Cardiology* **60**, S1-49 (2012).

138. Campo, G.*, et al.* Prognostic impact of hospital readmissions after primary percutaneous coronary intervention. *Archives of internal medicine* **171**, 1948-1949 (2011).

139. Yetgin, T., Manintveld, O.C., Duncker, D.J. & van der Giessen, W.J. Postconditioning against ischaemia-reperfusion injury: ready for wide application in patients? *Netherlands heart journal : monthly journal of the Netherlands Society of Cardiology and the Netherlands Heart Foundation* **18**, 389-392 (2010).

140. Yellon, D.M. & Hausenloy, D.J. Myocardial reperfusion injury. *The New England journal of medicine* **357**, 1121-1135 (2007).

141. Kloner, R.A., Bolli, R., Marban, E., Reinlib, L. & Braunwald, E. Medical and cellular implications of stunning, hibernation, and preconditioning: an NHLBI workshop. *Circulation* **97**, 1848-1867 (1998).

142. Morciano, G.*, et al.* Molecular identity of the mitochondrial permeability transition pore and its role in ischemia-reperfusion injury. *Journal of molecular and cellular cardiology* **78**, 142-153 (2015).

143. Halestrap, A.P., Connern, C.P., Griffiths, E.J. & Kerr, P.M. Cyclosporin A binding to mitochondrial cyclophilin inhibits the permeability transition pore and protects hearts from ischaemia/reperfusion injury. *Molecular and cellular biochemistry* **174**, 167-172 (1997).

144. Haworth, R.A. & Hunter, D.R. The Ca2+-induced membrane transition in mitochondria. II. Nature of the Ca2+ trigger site. *Archives of biochemistry and biophysics* **195**, 460-467 (1979).

145. Crompton, M. & Costi, A. A heart mitochondrial Ca2(+)-dependent pore of possible relevance to re-perfusion-induced injury. Evidence that ADP facilitates pore interconversion between the closed and open states. *The Biochemical journal* **266**, 33-39 (1990).

146. Szabo, I., De Pinto, V. & Zoratti, M. The mitochondrial permeability transition pore may comprise VDAC molecules. II. The electrophysiological properties of VDAC are compatible with those of the mitochondrial megachannel. *FEBS letters* **330**, 206-210 (1993).

147. Szabo, I. & Zoratti, M. The mitochondrial permeability transition pore may comprise VDAC molecules. I. Binary structure and voltage dependence of the pore. *FEBS letters* **330**, 201-205 (1993).

148. Harris, E.J. Modulation of Ca2+ efflux from heart mitochondria. *The Biochemical journal* **178**, 673-680 (1979).

149. Brustovetsky, N. & Klingenberg, M. Mitochondrial ADP/ATP carrier can be reversibly converted into a large channel by Ca2+. *Biochemistry* **35**, 8483-8488 (1996).

150. Beutner, G., Ruck, A., Riede, B. & Brdiczka, D. Complexes between porin, hexokinase, mitochondrial creatine kinase and adenylate translocator display properties of the permeability transition pore. Implication for regulation of permeability transition by the kinases. *Biochimica et biophysica acta* **1368**, 7-18 (1998).

151. Crompton, M., Virji, S. & Ward, J.M. Cyclophilin-D binds strongly to complexes of the voltage-dependent anion channel and the adenine nucleotide translocase to form the permeability transition pore. *European journal of biochemistry / FEBS* **258**, 729-735 (1998).

152. Basso, E., *et al.* Properties of the permeability transition pore in mitochondria devoid of Cyclophilin D. *The Journal of biological chemistry* **280**, 18558-18561 (2005).

153. Baines, C.P., *et al.* Loss of cyclophilin D reveals a critical role for mitochondrial permeability transition in cell death. *Nature* **434**, 658-662 (2005).

154. Kokoszka, J.E., *et al.* The ADP/ATP translocator is not essential for the mitochondrial permeability transition pore. *Nature* **427**, 461-465 (2004).

155. Baines, C.P., Kaiser, R.A., Sheiko, T., Craigen, W.J. & Molkentin, J.D. Voltage-dependent anion channels are dispensable for mitochondrial-dependent cell death. *Nature cell biology* **9**, 550-555 (2007).

156. Leung, A.W., Varanyuwatana, P. & Halestrap, A.P. The mitochondrial phosphate carrier interacts with cyclophilin D and may play a key role in the permeability transition. *The Journal of biological chemistry* **283**, 26312-26323 (2008).

157. Alcala, S., Klee, M., Fernandez, J., Fleischer, A. & Pimentel-Muinos, F.X. A high-throughput screening for mammalian cell death effectors identifies the mitochondrial phosphate carrier as a regulator of cytochrome c release. *Oncogene* **27**, 44-54 (2008).

158. Varanyuwatana, P. & Halestrap, A.P. The roles of phosphate and the phosphate carrier in the mitochondrial permeability transition pore. *Mitochondrion* **12**, 120-125 (2012).

159. Sileikyte, J., *et al.* Regulation of the inner membrane mitochondrial permeability transition by the outer membrane translocator protein (peripheral benzodiazepine receptor). *The Journal of biological chemistry* **286**, 1046-1053 (2011).

160. Krestinina, O.V., *et al.* Effect of peripheral benzodiazepine receptor (PBR/TSPO) ligands on opening of Ca2+-induced pore and phosphorylation of 3.5-kDa polypeptide in rat brain mitochondria. *Biochemistry. Biokhimiia* **74**, 421-429 (2009).

161. Li, J., Wang, J. & Zeng, Y. Peripheral benzodiazepine receptor ligand, PK11195 induces mitochondria cytochrome c release and dissipation of mitochondria potential via induction of mitochondria permeability transition. *European journal of pharmacology* **560**, 117-122 (2007).

162. Sileikyte, J., *et al.* Regulation of the mitochondrial permeability transition pore by the outer membrane does not involve the peripheral benzodiazepine receptor (Translocator Protein of 18 kDa (TSPO)). *The Journal of biological chemistry* **289**, 13769-13781 (2014).

163. Marzo, I., *et al.* Bax and adenine nucleotide translocator cooperate in the mitochondrial control of apoptosis. *Science* **281**, 2027-2031 (1998).

164. Narita, M., *et al.* Bax interacts with the permeability transition pore to induce permeability transition and cytochrome c release in isolated mitochondria. *Proceedings of the National Academy of Sciences of the United States of America* **95**, 14681-14686 (1998).

165. Karch, J., *et al.* Bax and Bak function as the outer membrane component of the mitochondrial permeability pore in regulating necrotic cell death in mice. *eLife* **2**, e00772 (2013).

166. Roy, S.S., *et al.* Bad targets the permeability transition pore independent of Bax or Bak to switch between Ca2+-dependent cell survival and death. *Molecular cell* **33**, 377-388 (2009).

167. Arbel, N., Ben-Hail, D. & Shoshan-Barmatz, V. Mediation of the antiapoptotic activity of Bcl-xL protein upon interaction with VDAC1 protein. *The Journal of biological chemistry* **287**, 23152-23161 (2012).

168. Brenner, C., *et al.* Bcl-2 and Bax regulate the channel activity of the mitochondrial adenine nucleotide translocator. *Oncogene* **19**, 329-336 (2000).

169. Wang, S.B., Murray, C.I., Chung, H.S. & Van Eyk, J.E. Redox regulation of mitochondrial ATP synthase. *Trends in cardiovascular medicine* **23**, 14-18 (2013).

170. Ko, Y.H., Delannoy, M., Hullihen, J., Chiu, W. & Pedersen, P.L. Mitochondrial ATP synthasome. Cristae-enriched membranes and a multiwell detergent screening assay yield dispersed single complexes containing the ATP synthase and carriers for Pi and ADP/ATP. *The Journal of biological chemistry* **278**, 12305-12309 (2003).

171. Giorgio, V., *et al.* Cyclophilin D modulates mitochondrial F0F1-ATP synthase by interacting with the lateral stalk of the complex. *The Journal of biological chemistry* **284**, 33982-33988 (2009).

172. Alavian, K.N., *et al.* Bcl-xL regulates metabolic efficiency of neurons through interaction with the mitochondrial F1FO ATP synthase. *Nature cell biology* **13**, 1224-1233 (2011).

173. De Marchi, E., Bonora, M., Giorgi, C. & Pinton, P. The mitochondrial permeability transition pore is a dispensable element for mitochondrial calcium efflux. *Cell calcium* **56**, 1-13 (2014).

174. Masgras, I., Rasola, A. & Bernardi, P. Induction of the permeability transition pore in cells depleted of mitochondrial DNA. *Biochimica et biophysica acta* **1817**, 1860-1866 (2012).

175. McGeoch, J.E. & Guidotti, G. A 0.1-700 Hz current through a voltage-clamped pore: candidate protein for initiator of neural oscillations. *Brain research* **766**, 188-194 (1997).

176. Azarashvili, T., *et al.* Potential role of subunit c of F0F1-ATPase and subunit c of storage body in the mitochondrial permeability transition. Effect of the phosphorylation status of subunit c on pore opening. *Cell calcium* **55**, 69-77 (2014).

177. Wong, R., Steenbergen, C. & Murphy, E. Mitochondrial permeability transition pore and calcium handling. *Methods in molecular biology* **810**, 235-242 (2012).

178. Weiss, J.N., Korge, P., Honda, H.M. & Ping, P. Role of the mitochondrial permeability transition in myocardial disease. *Circulation research* **93**, 292-301 (2003).

179. Baines, C.P. The mitochondrial permeability transition pore and ischemia-reperfusion injury. *Basic research in cardiology* **104**, 181-188 (2009).

180. Halestrap, A.P., Clarke, S.J. & Javadov, S.A. Mitochondrial permeability transition pore opening during myocardial reperfusion--a target for cardioprotection. *Cardiovascular research* **61**, 372-385 (2004).

181. Murphy, E. & Steenbergen, C. What makes the mitochondria a killer? Can we condition them to be less destructive? *Biochimica et biophysica acta* **1813**, 1302-1308 (2011).

182. Gerczuk, P.Z. & Kloner, R.A. An update on cardioprotection: a review of the latest adjunctive therapies to limit myocardial infarction size in clinical trials. *Journal of the American College of Cardiology* **59**, 969-978 (2012).

183. Piot, C., *et al.* Effect of cyclosporine on reperfusion injury in acute myocardial infarction. *The New England journal of medicine* **359**, 473-481 (2008).

184. Cung, T.T., *et al.* Cyclosporine before PCI in Patients with Acute Myocardial Infarction. *The New England journal of medicine* **373**, 1021-1031 (2015).

185. Ottani, F., *et al.* Cyclosporine A in Reperfused Myocardial Infarction: The Multicenter, Controlled, Open-Label CYCLE Trial. *Journal of the American College of Cardiology* **67**, 365-374 (2016).

186. Bernardi, P. & Di Lisa, F. Cyclosporine before PCI in Acute Myocardial Infarction. *The New England journal of medicine* **374**, 89-90 (2016).

187. Mewton, N., Bergerot, C. & Ovize, M. Cyclosporine before PCI in Acute Myocardial Infarction. *The New England journal of medicine* **374**, 90 (2016).

188. Pottecher, J., Diemunsch, P. & Geny, B. Cyclosporine before PCI in Acute Myocardial Infarction. *The New England journal of medicine* **374**, 88-89 (2016).

189. Santos-Gallego, C.G. & Badimon, J.J. Cyclosporine before PCI in Acute Myocardial Infarction. *The New England journal of medicine* **374**, 88 (2016).

190. Zografos, T.A. & Katritsis, D.G. Cyclosporine before PCI in Acute Myocardial Infarction. *The New England journal of medicine* **374**, 89 (2016).

191. Hausenloy, D., *et al.* The effect of cyclosporin-A on peri-operative myocardial injury in adult patients undergoing coronary artery bypass graft surgery: a randomised controlled clinical trial. *Heart* **100**, 544-549 (2014).

192. Schaller, S., *et al.* TRO40303, a new cardioprotective compound, inhibits mitochondrial permeability transition. *The Journal of pharmacology and experimental therapeutics* **333**, 696-706 (2010).

193. Group, M.S. Rationale and design of the 'MITOCARE' Study: a phase II, multicenter, randomized, double-blind, placebo-controlled study to assess the safety and efficacy of TRO40303 for the reduction of reperfusion injury in patients undergoing percutaneous coronary intervention for acute myocardial infarction. *Cardiology* **123**, 201-207 (2012).

194. Atar, D., *et al.* Effect of intravenous TRO40303 as an adjunct to primary percutaneous coronary intervention for acute ST-elevation myocardial infarction: MITOCARE study results. *European heart journal* **36**, 112-119 (2015).

195. Lonborg, J., *et al.* Exenatide reduces final infarct size in patients with ST-segment-elevation myocardial infarction and short-duration of ischemia. *Circulation. Cardiovascular interventions* **5**, 288-295 (2012).

196. Hong, L., *et al.* Atrial natriuretic peptide prevents the mitochondrial permeability transition pore opening by inactivating glycogen synthase kinase 3beta via PKG and PI3K in cardiac H9c2 cells. *European journal of pharmacology* **695**, 13-19 (2012).

197. Hausenloy, D.J., Lecour, S. & Yellon, D.M. Reperfusion injury salvage kinase and survivor activating factor enhancement prosurvival signaling pathways in ischemic postconditioning: two sides of the same coin. *Antioxidants & redox signaling* **14**, 893-907 (2011).

198. Clarke, S.J., McCormick, L.M. & Dutka, D.P. Optimising cardioprotection during myocardial ischaemia: targeting potential intracellular pathways with glucagon-like peptide-1. *Cardiovascular diabetology* **13**, 12 (2014).

199. Selker, H.P.*, et al.* Out-of-hospital administration of intravenous glucose-insulin-potassium in patients with suspected acute coronary syndromes: the IMMEDIATE randomized controlled trial. *Jama* **307**, 1925-1933 (2012).

200. Chakrabarti, A.K.*, et al.* Rationale and design of the EMBRACE STEMI study: a phase 2a, randomized, double-blind, placebo-controlled trial to evaluate the safety, tolerability and efficacy of intravenous Bendavia on reperfusion injury in patients treated with standard therapy including primary percutaneous coronary intervention and stenting for ST-segment elevation myocardial infarction. *American heart journal* **165**, 509-514 e507 (2013).

201. Gibson, C.M.*, et al.* EMBRACE STEMI study: a Phase 2a trial to evaluate the safety, tolerability, and efficacy of intravenous MTP-131 on reperfusion injury in patients undergoing primary percutaneous coronary intervention. *European heart journal* (2015).

202. Friedrich, M.G.*, et al.* The salvaged area at risk in reperfused acute myocardial infarction as visualized by cardiovascular magnetic resonance. *Journal of the American College of Cardiology* **51**, 1581-1587 (2008).

203. Kim, R.J.*, et al.* The use of contrast-enhanced magnetic resonance imaging to identify reversible myocardial dysfunction. *The New England journal of medicine* **343**, 1445-1453 (2000).

204. Alavian, K.N.*, et al.* An uncoupling channel within the c-subunit ring of the F1FO ATP synthase is the mitochondrial permeability transition pore. *Proceedings of the National Academy of Sciences of the United States of America* **111**, 10580-10585 (2014).

205. Halestrap, A.P. & Richardson, A.P. The mitochondrial permeability transition: a current perspective on its identity and role in ischaemia/reperfusion injury. *Journal of molecular and cellular cardiology* **78**, 129-141 (2015).

206. Frohlich, G.M., Meier, P., White, S.K., Yellon, D.M. & Hausenloy, D.J. Myocardial reperfusion injury: looking beyond primary PCI. *European heart journal* **34**, 1714-1722 (2013).

207. Hausenloy, D.J.*, et al.* Translating cardioprotection for patient benefit: position paper from the Working Group of Cellular Biology of the Heart of the European Society of Cardiology. *Cardiovascular research* **98**, 7-27 (2013).

208. Lecour, S.*, et al.* ESC working group cellular biology of the heart: position paper: improving the preclinical assessment of novel cardioprotective therapies. *Cardiovascular research* **104**, 399-411 (2014).

209. Fernandez-Sanz, C.*, et al.* Altered FoF1 ATP synthase and susceptibility to mitochondrial permeability transition pore during ischaemia and reperfusion in aging cardiomyocytes. *Thrombosis and haemostasis* **113**, 441-451 (2015).

210. Karunakaran, D.*, et al.* Macrophage Mitochondrial Energy Status Regulates Cholesterol Efflux and Is Enhanced by Anti-miR33 in Atherosclerosis. *Circulation research* **117**, 266-278 (2015).

211. Chen, T.W.*, et al.* Ultrasensitive fluorescent proteins for imaging neuronal activity. *Nature* **499**, 295-300 (2013).

212. Wieckowski, M.R., Giorgi, C., Lebiedzinska, M., Duszynski, J. & Pinton, P. Isolation of mitochondria-associated membranes and mitochondria from animal tissues and cells. *Nature protocols* **4**, 1582-1590 (2009).

213. Authors/Task Force, m.*, et al.* 2014 ESC/EACTS Guidelines on myocardial revascularization: The Task Force on Myocardial Revascularization of the European Society of Cardiology (ESC) and the European Association for Cardio-Thoracic Surgery (EACTS)Developed with the special contribution of the

European Association of Percutaneous Cardiovascular Interventions (EAPCI). *European heart journal* **35**, 2541-2619 (2014).

214. O'Gara, P.T.*, et al.* 2013 ACCF/AHA guideline for the management of ST-elevation myocardial infarction: executive summary: a report of the American College of Cardiology Foundation/American Heart Association Task Force on Practice Guidelines: developed in collaboration with the American College of Emergency Physicians and Society for Cardiovascular Angiography and Interventions. *Catheterization and cardiovascular interventions : official journal of the Society for Cardiac Angiography & Interventions* **82**, E1-27 (2013).

215. Milisav, I., Moro, F., Neupert, W. & Brunner, M. Modular structure of the TIM23 preprotein translocase of mitochondria. *The Journal of biological chemistry* **276**, 25856-25861 (2001).

216. Mokranjac, D., Sichting, M., Neupert, W. & Hell, K. Tim14, a novel key component of the import motor of the TIM23 protein translocase of mitochondria. *The EMBO journal* **22**, 4945-4956 (2003).

217. Lancaster, G.A., Dodd, S. & Williamson, P.R. Design and analysis of pilot studies: recommendations for good practice. *Journal of evaluation in clinical practice* **10**, 307-312 (2004).

218. Kitakaze, M.*, et al.* Human atrial natriuretic peptide and nicorandil as adjuncts to reperfusion treatment for acute myocardial infarction (J-WIND): two randomised trials. *Lancet* **370**, 1483-1493 (2007).

219. Kim, J.S.*, et al.* Efficacy of high-dose atorvastatin loading before primary percutaneous coronary intervention in ST-segment elevation myocardial infarction: the STATIN STEMI trial. *JACC. Cardiovascular interventions* **3**, 332-339 (2010).

220. Bonora, M., Morganti, M. & Morciano, G. Comprehensive analysis of mitochondrial permeability transition pore activity in living cells using imaging techniques. *Nature Protocols* (2016).

Study	Ref.	Pts.	Therapeutic substance	Therapeutic protocol	Outcome
Agents directly targeting mPTP					
Piot et al.	[183]	58	*Cyclosporin A*: Inhibitor of cyclophilin D, directly blocks mPTP opening.	Cyclosporin A (2.5 mg/kg iv) 10 min prior to primary PCI.	44% reduction of MI size (72-h AUC total CK), 20% reduction of MI size (MRI in a subset of 27 patients), 28% reduction of MI size and smaller LVESV on MRI at 6 months.
Hausenloy et al.	[191]	78	*Cyclosporin A*	Cyclosporin A (2.5 mg/kg iv) after induction of anesthesia but prior to sternotomy.	Reduction in perioperative myocardial injury with CsA (p=0.049) with the postoperative cardiac troponin T rise reduced by 0.03 ng/ml for every 10 min. No differences in mean peak cardiac troponin T between control and CsA treatment.
Chiari et al.	[55]	61	*Cyclosporin A*	Cyclosporin A (2.5 mg/kg iv) less than 10 min before aortic clamping.	35% reduction in AUC for cardiac troponin I in the CsA group compared with the control.
Ottani et al.	[185]	410	*Cyclosporin A*	Cyclosporine A (2.5 mg/kg) 5 min before PCI.	A single intravenous CsA bolus just before primary percutaneous coronary intervention had no effect on ST-segment resolution or hs-cTnT, and did not improve clinical outcomes or LV remodeling up to 6 months.
Mitocare group	[193]	163	*TRO40303*: Binds mitochondrial translocator protein at the cholesterol site, modulates mPTP.	TRO40303 (35 ml/min iv) injection of TRO40303 15 min before balloon inflation and stenting.	This study in STEMI patients treated with contemporary mechanical revascularization principles did not show any effect of TRO40303 in limiting reperfusion injury of the ischaemic myocardium.

Agents indirectly targeting mPTP					
Lønborg et al.	[195]	107	***Exenatide***: Analog of GLP-1.	Exenatide (25 mg in 250 ml saline, iv) 15 min prior to primary PCI and continued for 6 h.	23% reduction in MI size by AAR at 90 days by MRI (from 0.30 to 0.39), Increased myocardial salvage index (from 0.62 to 0.71), Reduced size in patients presenting with ischemic tim <132 min (8% vs 11%).
Kitakaze et al.	[218]	569	***Atrial natriuretic peptide:*** Inactivation of GSK3-β, indirectly blocks mPTP.	Carperitide (0.025μg/kg/min iv) for 72 h after reperfusion.	14% reduction in MI size (total CK AUC), 2% increase in LVEF at 6-12 months.
Ross et al.	[67]	2118	***Adenosine***: Anti-inflammatory effect, reduction of oxygen-free radicals.	Adenosine (50-70 μg/kg/min iv) for 3 h after PCI.	No difference in death or HF at 6 months.
Kim et al.	[219]	171	***Atorvastatin***: Reduction of oxygen-free radicals.	Atorvastatin (80 mg oral) vs atorvastatin (10 mg oral) prior to primary PCI	No difference in death, MI size, revascularization, MI recurrence.
Selker et al.	[199]	357	***Glucose insulin potassium*** (GIK): Prevention of oxygen-free radical production.	GIK (iv) begun in the ambulance for suspected STEMI.	No difference in progression to MI, reduction of composite endpoint of cardiac arrest or in-hospital mortality (6.1% vs 14.1%).
Chakrabarti et al.	[200]	300	***Bendavia***: Interaction with cardiolipin, reduces ROS production.	Bendavia (0.05 mg/kg iv) between 15-60 min before PCI and continued for 1 h after revascularization.	Ongoing trials to investigate the reduction of MI size (total CK AUC and late-enhancement on MRI).

Table 1 – Pharmacological approaches for cardioprotection in humans.
Ref: reference. Pts: number of patients. CK: creatine kinase. AUC: area under the curve. MRI: magnetic resonance imaging. h: hours. AAR: area at risk. min: minutes.